Protein-protein interactions that mediate the role of AAA-ATPase p97/VCP/Cdc48 in protein aggregation and degradation

Chia, Wei Sheng

2013

Chia, W. S. (2013). Protein-protein interactions that mediate the role of AAA-ATPase p97/VCP/Cdc48 in protein aggregation and degradation. Doctoral thesis, Nanyang Technological University, Singapore.

https://hdl.handle.net/10356/54954

https://doi.org/10.32657/10356/54954

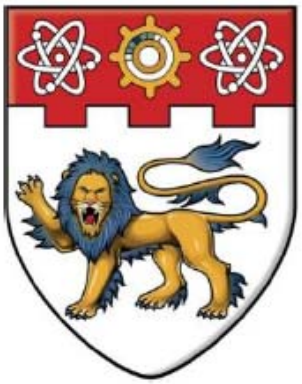

NANYANG TECHNOLOGICAL UNIVERSITY

Protein-protein interactions that mediate the role of AAA-ATPase p97/VCP/Cdc48 in protein aggregation and degradation

CHIA WEI SHENG

SCHOOL OF BIOLOGICAL SCIENCES

2013

Protein-protein interactions that mediate the role of AAA-ATPase p97/VCP/Cdc48 in protein aggregation and degradation

CHIA WEI SHENG

SCHOOL OF BIOLOGICAL SCIENCES

A thesis submitted to the Nanyang Technological University in partial fulfillment of the requirement for the degree of Doctor of Philosophy

2013

Acknowledgements

7.5 years in NTU is a long time indeed (3.5 years Bachelor's, 4 years PhD).

I would like to thank the following people that had made this long stay, seem shorter than it actually was.

My parents whom had always been supportive in whatever I choose to do, and never imposing a financial burden on me, I hope I will be able to provide them a comfortable retirement one day. (if only post docs had higher salaries!!)

My wife, whom I met in NTU during my undergraduate, for being always supportive, patient and kind especially when time to be spent with her was regularly sacrificed on experiments and work.

My supervisors, A/P Susana Geifman & Prof Shoshana Bar-nun for the opportunity to do a PhD. Especially to A/P Susana Geifman whom had provided an open environment for work to be done, the fights that we had, and the triumphs. She was not only a supervisor, but a mentor in life and a friend.

My thesis advisory committee, Asst Prof Andrew Tan and A/P Liang Zhaoxun, for their advice and guidances during the course of my PhD.

The many FYP and attachment students that I had been involved in guiding for their final year project in the past 4 years, especially Diana, Yongchuan, Elaine, Jim, etc, for allowing me to experience the synergy of research when multiple people work towards similar goals, making work seem less mundane than usual.

Last but not least the countless colleagues and friends that I've met over the years in NTU, too many to name here, whom had always been helpful in all ways imaginable and unimaginable.

Table of Contents

List of figures

Chapter 1

Introduction

Material Methods

Results

Chapter 2

Introduction

Results

Chapter 3

Introduction

Results

Chapter 4

List of tables

Abbreviations

AAA-ATPase – ATPases associated with various cellular activities

ADP – Adenosine Di-phosphate

AIRAPL - Arsenic-inducible proteasomal 19S regulatory particle associated protein-like protein

AMP-PNP - Adenylyl-imidodiphosphate

ATP – Adenosine Tri-phosphate

ATPγS - Adenosine 5′ -O-(3-thio)triphosphate

ATPase – ATP-hydrolase

BSA – Bovine Serum Albumin

cDNA – Complimentary DNA

CMD – Carboxy-methyl-dextran

CFP – Cyan fluorescent protein

CFTR – Cystic fibrosis transmembrane receptor

CPT – Cationic-polythiopene

DSF – Differential Scanning Fluorimetry

DLS – Dynamic Light Scattering

DNA – Deoxyribonucleic acid

DUB – Deubiquitinating enzyme

ECL – enhanced chemiluminiscent

EDC – Ethyl-carbodi-imide

EDTA – Ethylene-diamine-tetraacetic acid

ER – Endoplasmic Reticulum

ERAD – Endoplasmic Reticulum Associated Degradation

FRET – Fluorescence resonance energy transfer

GST – Glutathione-S-transferrase

HIF1α – hypoxia inducible factor 1 alpha

HPLC – High performance liquid chromatography

HSP – Heatshock protein

Htt – Huntingtin protein

IBMPFD – Inclusion body myopathy and Paget's disease of the bone

IGG – Immunoglobulin G

Iκβα - inhibitor alpha of Nfκβ

IMAC – immobilized metal-ion affinity chromatography

IPTG - Isopropyl β-D-1-thiogalactopyranoside

kDa – Kilodalton

LB – Luria Bertani

MESG – 2-amino-6-mercapto-7-methylpurine riboside

NAD – Nicotinamide adenine dinucleotide

NF1 – neurofibrinomin-1

Nfκβ – nuclear factor kappa-light-chain-enhancer of activated B cells

NHS – n-hydroxysuccinimide

Npl4 – Nuclear localization protein 4

NZF – Npl4 Zinc Finger

PBS – Phosphate Buffered Saline

PBST – Phosphate Buffered Saline with 1% Tween

PEP - Phosphoenolpyruvate

PMMA – Poly-methyl-methyl-acrylate

PNP – purine nucleoside phosphorylase

PT – Polythiopene

PTQ – poly 1-(3-((4-methylthiophen-3-yl)oxy)propyl)quinuclidin-1-ium

PVDF – polyvinylidene fluoride

RCF – Relative Centrifugal Force

RU – Response unit

SDS-PAGE - Sodium-dodecyl sulphate – Polyacrylamide gel electrophoresis

SRP – Signal Recognition Particle

SPR – Surface Plasmon resonance

SVIP – Small VCP interacting protein

TAE – Tris-Acetate-EDTA

TER94 – Transitional endoplasmic reticulum ATPase 94

Ufd1 – Ubiquitin fusion degradation protein 1

UIM – Ubiquitin interacting motif

UN – Ufd1/Npl4

VAT – VCP-like ATPase

VCP – Valosin Containing Protein

VIM – VCP-interacting motif

YFP – Yellow fluorescent protein

Abstract :

p97/VCP is a multifunctional AAA-ATPase that is directed into many different cellular processes by adaptor proteins that bind to it. With the use of SPR biosensor technology, we demonstrated the role of ATP binding to the D1 ATPase domain in p97/VCP in regulating adaptor protein competition between Ufd1/Npl4 and p47, two major adaptor proteins of p97/VCP that direct it to this AAA-ATPase to different core-complexes for executing different cellular functions. A novel p97/VCP adaptor protein, AIRAPL was also characterized for its binding to p97/VCP via AIRAPL's VIM domain and to substrates such as K48-tetraubiquitin chains via its tandem double-sided UIMs. We speculate possible roles of AIRAPL in regulating ubiquitin chain lengths and consequently ubiquitin-dependent processes by affecting deubiquitinase activity. In an attempt to develop a system for studying metabolic fluxes in correlation with p97/VCP functions and activities in the cell, we validated a new group of chemical ATP sensors known as cationic poly-thiophene polymers. Using these sensors, a real-time ATPase assay was developed and authenticated.

Chapter 1

Regulation of p97/VCP adaptor protein preference by ATP

1. 1 Introduction

1.1.1 p97/VCP History

Valosin-containing protein, otherwise known by its popular abbreviated name VCP or p97, was first serendipitously identified by Koller & Brownstein in 1987 (Koller and Brownstein, 1987). p97/VCP,a protein with unknown function then, turned out to be an essential protein e in all eukaryotic cells. Just two years earlier, in 1985, Schmidt *et al*. purified chromatographically and sequenced through Edman degradation, a 25-mer peptide from the gastrointestinal tracts of pigs (Schmidt *et al*., 1985). Not finding any sequence homologies in then the state of the art reference, Dayhoff's Protein Segment dictionary, this novel peptide was named Valosin, and was found to possess certain biological activities in regulating pancreatic secretions and gastrointestinal movements in animals tested (dogs).

In a bid to determine precursor proteins of valosin, Koller & Brownstein used a 36-mer nucleotide probe with the sequence coding for the first 12 amino acids of valosin. In a porcine complimentary DNA (cDNA) library they identified a2,466 nucleotide long cDNA. Northern blot analysis showed the presence of the valosin "message" in all tissues tested, ranging from neurological tissues to liver and intestinal materials. p97/VCP has now been found to be highly abundant in all cells, comprising up to 1% of a cell's total protein. The cDNA pulled out from the library codes for a 806 amino acid protein that the authors named Valosin-containing protein (VCP), which

includes the 25-mer valosin sequence of V Q Y P V E H P D K F L K F G M T P S K G V L F Y between amino acids 493 and 517.

To date, the focus on valosin, the gastrointestinal peptide, is highly over-shadowed by the attention given to p97/VCP. No one has yet discovered additional functions of valosin, nor identified its precursor, and why this peptide sequence was embedded within a big and important protein such as p97/VCP is not understood. It remains unknown whether it was a gene duplication or transpositions that led to the insertion of the valosin sequence into the VCP gene.

One might argue that in fact p97/VCP was not first discovered by Koller & Brownstein as the yeast homologue, *CDC48*, was identified already in 1982 by Moir *et al*. in a cold-sensitive yeast screen for cell cycle-dependent genes (Moir *et al*., 1982). A cold-sensitive mutant of the *CDC48* gene, otherwise known as the *cdc48-1* allele, arrested cell division at the 17 °C non permissive temperature. Sequence homology studies carried out in 1991 by Frolich *et al*., showed that p97/VCP was 70% homologous to *CDC48*, with the latter being longer by 50 amino acids (Frohlich *et al*., 1991). In the same paper, the authors also demonstrated that mutations in *CDC48* resulted in cell cycle arrest before anaphase, suggesting an important role for Cdc48 in the process of mitosis.

In the same decade, many other VCP homologues were identified: Transitional endoplasmic reticulum ATPase 94 (TER94) in *Drosophila melanogaster*, VCP-like ATPase or VAT in the thermophillic archaeabacteria *Thermoplasma acidophilum*, and Cdc48.1 in *Caenorhabditis elegans (C. elegans)*. One intriguing fact surfaces when the amino acid sequence of

p97/VCP is analysed for sequence homology in protein databases such as UNIPROT (Consortium, 1998; Leon and McKearin, 1999; Pamnani *et al*., 1997). As shown in Table 1.1.1, complete conservation of the p97/VCP amino acid sequence is seen across many higher organisms and mammals ranging from mouse to monkey to human. Such data can only suggest the functional essentiality of p97/VCP, with minimal tolerance to mutations in more complex life forms. Accordingly, some mutations in seemingly benign linker regions of p97/VCP, , result in debilitating neuronal and muscle degeneration or pre-disposition to amyotrophic lateral sclerosis (ALS) and other neurodegenerative diseases (Johnson *et al*., 2010; Kimonis *et al*., 1993). More severe mutations might have been embryonic lethal, just like a p97/VCP knockout, and thus no hereditary records have emerged.

Entry	Entry name	Organism	Length	Identity	Score	Gene name
H0VKG1	H0VKG1_CAVPO	Cavia porcellus (**Guinea pig**)	806	**100.0%**	4,111	**VCP**
G1SR03	G1SR03_RABIT	Oryctolagus cuniculus (**Rabbit**)	806	**100.0%**	4,140	**VCP**
G3QL07	G3QL07_GORGO	Gorilla gorilla gorilla (**Lowland gorilla**)	806	**100.0%**	4,140	**VCP**
H2PRU6	H2PRU6_PONAB	Pongo abelii (**Sumatran orangutan**)	806	**100.0%**	4,140	**VCP**
H2QX75	H2QX75_PANTR	Pan troglodytes (**Chimpanzee**)	806	**100.0%**	4,140	**ENSG00000165280**
H9EPW4	H9EPW4_MACMU	Macaca mulatta (**Rhesus macaque**)	806	**100.0%**	4,140	**VCP**
P55072	TERA_HUMAN	Homo sapiens (**Human**)	806	**100.0%**	4,140	**VCP**
Q01853	TERA_MOUSE	Mus musculus (**Mouse**)	806	**100.0%**	4,140	**Vcp**
F7BWW6	F7BWW6_HORSE	Equus caballus (**Horse**)	803	99.0%	4,068	**LOC100068225**
G5BXB9	G5BXB9_HETGA	Heterocephalus glaber (**Naked mole rat**)	799	99.0%	4,089	GW7_03434
G3WW22	G3WW22_SARHA	Sarcophilus harrisii (**Tasmanian devil**)	802	99.0%	4,094	**VCP**
Q5ZMU9	Q5ZMU9_CHICK	Gallus gallus (**Chicken**)	806	99.0%	4,106	**vcp** RCJMB04_1c3
F7A525	F7A525_CALJA	Callithrix jacchus (**White-tufted-ear marmoset**)	805	99.0%	4,107	**LOC100403131**
G1MAF6	G1MAF6_AILME	Ailuropoda melanoleuca (**Giant panda**)	806	99.0%	4,107	**VCP**
G1QXS1	G1QXS1_NOMLE	Nomascus leucogenys (**White-cheeked gibbon**)	802	99.0%	4,112	**VCP**
G3SZQ9	G3SZQ9_LOXAF	Loxodonta africana (**African elephant**)	802	99.0%	4,112	**VCP**
G7PS17	G7PS17_MACFA	Macaca fascicularis (**Crab-eating macaque**)	803	99.0%	4,112	EGM_06879
H0WYU3	H0WYU3_OTOGA	Otolemur garnettii (**Small-eared galago**)	804	99.0%	4,116	**VCP**
F6ZIF4	F6ZIF4_MONDO	Monodelphis domestica (**Gray opossum**)	806	99.0%	4,119	**VCP**
F1SIH8	F1SIH8_PIG	Sus scrofa (**Pig**)	808	99.0%	4,122	**VCP**
I3MPB2	I3MPB2_SPETR	Spermophilus tridecemlineatus (**Squirrel**)	808	99.0%	4,127	**VCP**

Table 1.1.1 – An Analysis of human p97/VCP amino acid sequence in UNIPROT KB.
Almost total conservation of p97/VCP amino acid sequence is seen across many species.

1.1.2 p97/VCP, a homo hexameric AAA-ATPase

p97/VCP belongs to the family of ATPases associated with various cellular activities, otherwise known as the AAA family. In a cell, p97/VCP performs functions ranging from protein quality control, substrate and protein dislocation/segregation, deoxyribonucleic acid (DNA) repair processes, mitosis processes, mitochondrial protein quality control, etc. p97/VCP is directed to its different functions through its interaction with specific adaptor proteins. Table 1.1.2 summarizes the functions of p97/VCP, and indicates the possible adaptor proteins involved (Boyault *et al*., 2006; Cao *et al*., 2003; Dreveny *et al*., 2004b; Ernst *et al*., 2009; Latterich *et al*., 1995; Nagahama *et al*., 2003; Park *et al*., 2007; Partridge *et al*., 2003; Pleasure *et al*., 1993; Schwieger *et al*., 2008; Uchiyama *et al*., 2002; Ye *et al*., 2005; Yeung *et al*., 2008; Zhang *et al*., 2000a; Zhong and Pittman, 2006; Zhong *et al*., 2004).

p97/VCP Adaptor Protein	**Function**
Ufd1/Npl4	ERAD/Protein degradation, protein segregation,
p47, p37	Membrane fusion, Autophagosome maturation
Faf1 (Fas-associated protein 1)	NFKB-regulation
VCIP135	Works with p97-p47 complex for membrane fusion/transport
Otu1/Yod1	Protein degradation
Ataxin-3	ERAD regulation
SVIP, Clathrin	Autophagic processes, membrane trafficking
VIMP, Derlin 1	ERAD
Hrd1, gp78	ERAD
BRCA1, TB-RBP, WRN	DNA Repair
HDAC6	autophagy
Ase1, Cdc5	Mitosis

Table 1.1.2 – **p97/VCP Adaptor proteins**
Binding of p97/VCP to respective adaptor proteins directs it into various cellular processes.

First predicted to be an oligomer in 1994 by centrifugation experiments demonstrating that p97/VCP sedimented at a rate similar to the 19.2S, 660 kilodalton (kDa) thyroglobulin (Egerton and Samelson, 1994), p97/VCP, like many other AAA-ATPases, is indeed a functional homohexamer. Six 90 kDa monomers assemble into a hexamer, adopting the toroidal shape of a donut with a diameter of 160 Å and 80 Å in height (Zhang *et al*., 2000b) (Figure 1.1.1). Each monomer consists of an N-terminal N-domain, followed by a flexible linker connecting to two tandem ATPase domains, D1 and D2, each containing the Walker A (p-loop) and Walker B (DEXX) motifs, and the SRH (second region of homology) that makes AAA-ATPases unique, separating them from other ATPases with Walker motifs (Figure 1.1.2).

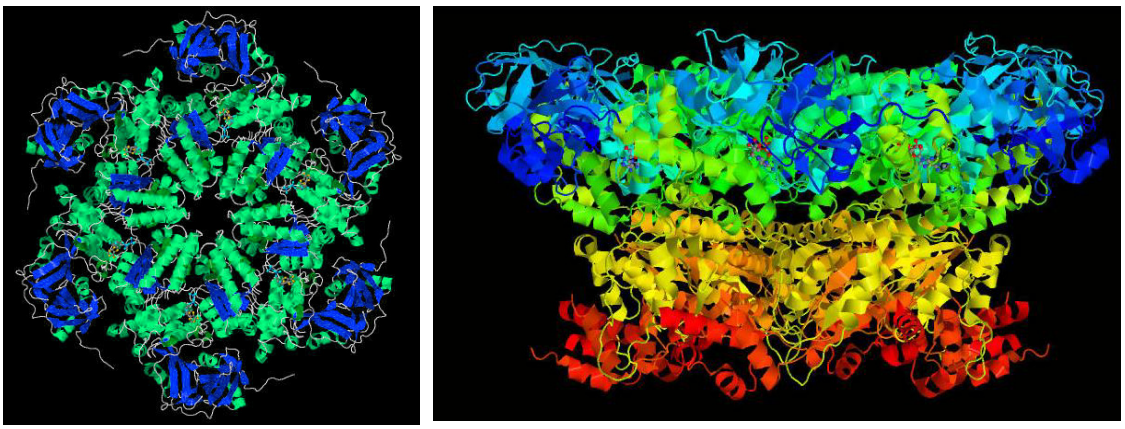

Figure 1.1.1 – Structure of p97/VCP.
First solved in 2000 by Zhang *et al.,* and further refined by several other groups. Structure shown here is taken from the protein data bank structure (3HU1)

In the functional hexamer of p97/VCP, the D1 domain of each monomer is stacked on top of the D2 domain in a head to tail packing, resulting in a D1 "disc" on top of a D2 "disc" having 2 faces with six ATP binding sites each (DeLaBarre and Brunger, 2003; Huyton *et al*., 2003; Zhang *et al*., 2000b). The N-domain of each monomer forms the edge of the "mushroom", sticking out at

the sides (Figure 1.1.1, left panel, blue protrusions), serving as binding site to the majority of the p97/VCP adaptor proteins. The C-terminus region of p97/VCP serves as a minor adaptor protein recruitment region (Madsen *et al*., 2009).

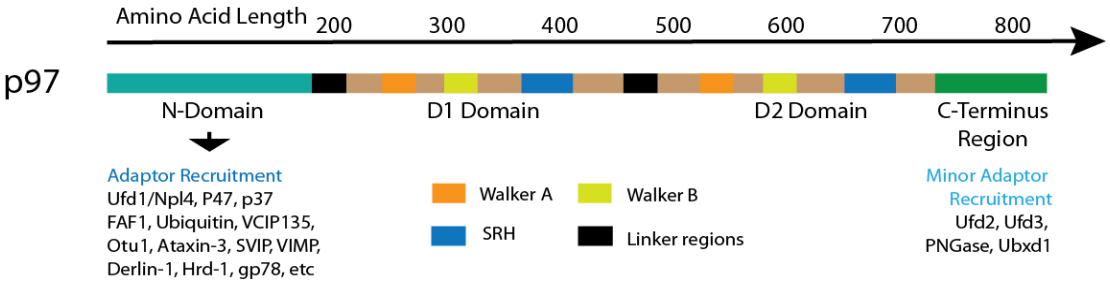

Figure 1.1.2 – Domain arrangements in p97/VCP
p97/VCP is a hexamer made up of 806 amino acid long monomers. In each monomer, there are 4 distinct regions, the N-Domain connected by a linker region to the D1 domain, followed by another linker to the D2 domain, and finally the C-terminus region. The N-Domain serves as a major adaptor protein recruitment region, where the majority of p97/VCP adaptors bind, whereas the C-terminus region functions as a minor adaptor protein binding zone. In the D1 and D2 domains, there are the respective ATP binding and hydrolyzing Walker A and Walker B motifs, and a highly conserved second region of homology (SRH) characteristic of AAA-ATPases.

Within p97/VCP, both ATP hydrolase (ATPase) domains, D1 and D2, are capable of binding and hydrolysing ATP, with D2 contributing to the bulk of p97/VCP's hydrolytic activities, despite both domains having similar affinities to either adenosine tri-phosphate (ATP) or adenosine di-phosphate (ADP) at approximately 1-2 micromolar (Briggs *et al*., 2008; Tang *et al*., 2010). It was reported that ATP binding to D1 was important for accelerating the hexamerization of p97/VCP, whereas the D2 ATPase domain‘s hydrolytic activitiy is believed to provide the mechanical energy needed for p97/VCP functions (Wang *et al*., 2003b).

1.1.3 p97/VCP and its adaptor proteins

1.1.3.1 The Core complex model: p97-Ufd1/Npl4 and p97-p47 form distinct core-complexes

p97/VCP is promiscuous in nature as it binds many different adaptor proteins to achieve its different functions. Among these adaptor proteins, two major ones are responsible for a large proportion of p97/VCP's essential function in living organisms, the heterodimer of ubiquitin-fusion degradation protein 1 (Ufd1) and nuclear localization protein 4 (Npl4), and the homotrimeric p47. A mass spectrometric study of proteins that immunoprecipitated with p97/VCP-myc from human 293T showed that protein complexes containing p97/VCP and Ufd1/Npl4 (UN) were distinct from complexes containing p97/VCP-p47. It suggests that these p97/VCP adaptors form separate signal integration hubs, directing p97/VCP to distinct separate pathways (Alexandru *et al*., 2008; Meyer, 2012; Meyer *et al*., 2012). Hence, the regulation of adaptor protein preference of p97/VCP, between p47 and UN, can be a rate limiting step that affects the equilibrium of ongoing cellular processes (Figure 1.1.3).

1.1.3.2 Ufd1/Npl4, a heterodimeric adaptor of p97/VCP

Ufd1 and Npl4 are p97/VCP adaptor proteins that direct this AAA-ATPase towards many ubiquitin-dependent functions in a cell, including endoplasmic-reticulum (ER)-associated protein degradation (ERAD) processes (Braun *et al*., 2002). In vivo, Ufd1 and Npl4 interact in a 1:1 ratio, forming an elongated 110 kDa heterodimer (UN) that adopts a bi-lobed structure of 80 Å by 30 Å wide (Pye *et al*., 2007). Structurally, Ufd1 has a UT3 domain in its N-terminus that is responsible for ubiquitin binding, while its C-terminal UT6 region binds

both p97/VCP and Npl4 (Hetzer *et al*., 2001) (Figure 1.1.4). The N-terminus of Npl4 mediates p97/VCP binding, but this does not occur if Ufd1is not bound to Npl4 (Bruderer *et al*., 2004). The C-terminus of Npl4 contains a conserved RanBP2/Nup358 zinc finger motif that is now commonly referred to as the Npl4 zinc finger (NZF). This NZF domain binds ubiquitin weakly, and binding to polyubiquitin of various linkage types has yet to be characterized (Wang *et al*., 2003a). A core p97/VCP-UN complex is formed and is responsible for many of p97/VCP's core activities such as ERAD, DNA repair, essential regulatory functions in mitosis and protein segregation, and it is also the backbone for many other interactants to bind for downstream function.

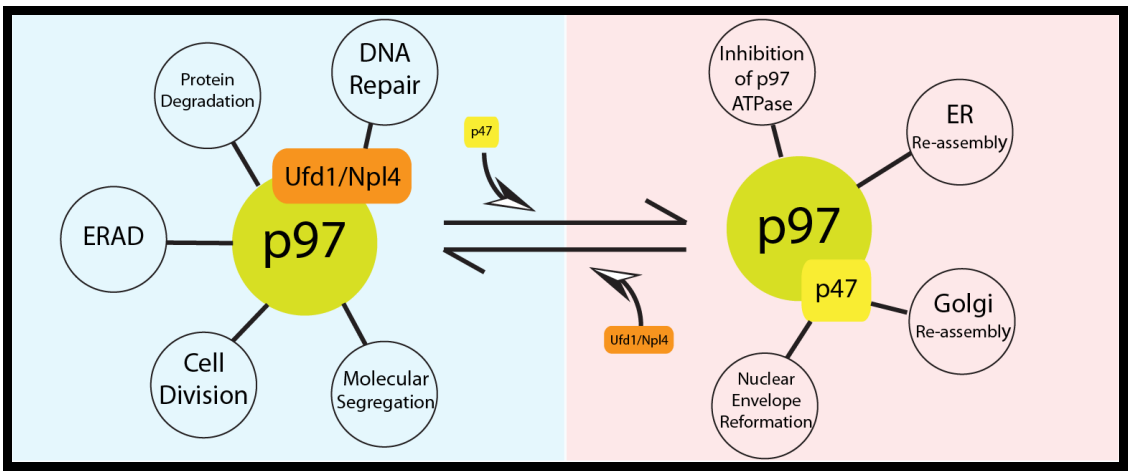

Figure 1.1.3 – The p97/VCP Core complex model.
In the core complex model, p97's diversion into various cellular processes is controlled by the equilibrium between mutually exclusive adaptor proteins that bind to p97.

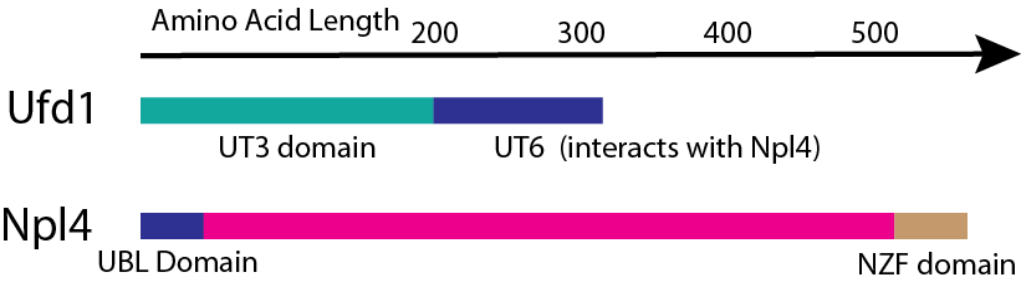

Figure 1.1.4 – The arrangement of various domains in Ufd1 & Npl4.

1.1.3.3 The p97/VCP-UN complex in ERAD

One third of all proteins in a cell are secretory or membrane proteins that undergo in the ER a quality control process known as ERAD. In this process, ribosomes docked on the ER through signal sequence and signal recognition particle (SRP) synthesize nascent chains that cross the Sec61 translocon to be inserted into the ER membrane or released to the ER lumen. In the ER, folding is assisted by chaperones (Guerriero and Brodsky, 2012).

If a protein is irreversibly misfolded, a chain of events occur at the interface between the ER and the cytoplasm: misfolded protein recognition, retro-translocation across the ER membrane back to the cytosol, ubiquitination and delivery to the 26S proteasome for degradation (Smith *et al*., 2011). Protein recognition as the initiating process involves luminal chaperones such as BIP and other members of the Heat Shock Protein (HSP) 70, HSP40 and HSP90 families, that recognize and bind the misfolded proteins and bring them close to the ER membrane. Targeting for retro-translocation then proceeds, mediated by as yet undiscovered channel and assisted by ER proteins such as mannose-6-phosphate-like protein OS9 (Araki and Nagata, 2011).

Retro-translocation, at least of luminal ERAD substrates, is initiated before ubiquitination, as ubiquitination requires the cytoplasmic ubiquitination system. It includes the ubiquitin-activating enzyme UBE1, dedicated ubiquitin-conjugating enzymes (E2) and specific ubiquitin ligases (E3) that function in the cytosol, although they can be transmembrane or membrane-associated and not necessarily soluble in the cytosol (Bernasconi and Molinari, 2011). The nature of the retrotranslocon remains unknown, although some membrane proteins such as Derlin-1 may facilitate retro-translocation.

The involvement of p97/VCP in ERAD was first discovered in early 2000, where p97/VCP and its yeast homologue Cdc48 were found to be in association with the ERAD substrate secretory immunoglobulin M in B cells and Hmg2p in yeast, suggesting a cytosolic chaperone function in ERAD (Rabinovich *et al*., 2002). Mutations in Cdc48 resulted in stabilization of ERAD substrates Hmg2p and CPY* and accumulation of CPY* in the ER lumen, indicating the role of this AAA-ATPase in retro-translocation of ERAD substrates (Rabinovich *et al*., 2002). Around the same time, Ye *et al.*, observed that the retro-translocation of misfolded proteins is not only p97/VCP-dependent, but also involves adaptor proteins UN (Ye *et al*., 2001). The p97/VCP-UN complex, using energy from ATP hydrolysis at the D2 domain, drives the retro-translocation process to deliver substrates to the 26S proteasome ((Bruderer *et al*., 2004; Rabinovich *et al*., 2002; Ye *et al*., 2001). This is an essential step linking a misfolded protein from the ER and the cytosolic 26S proteasome degradation machinery (Figure 1.1.5).

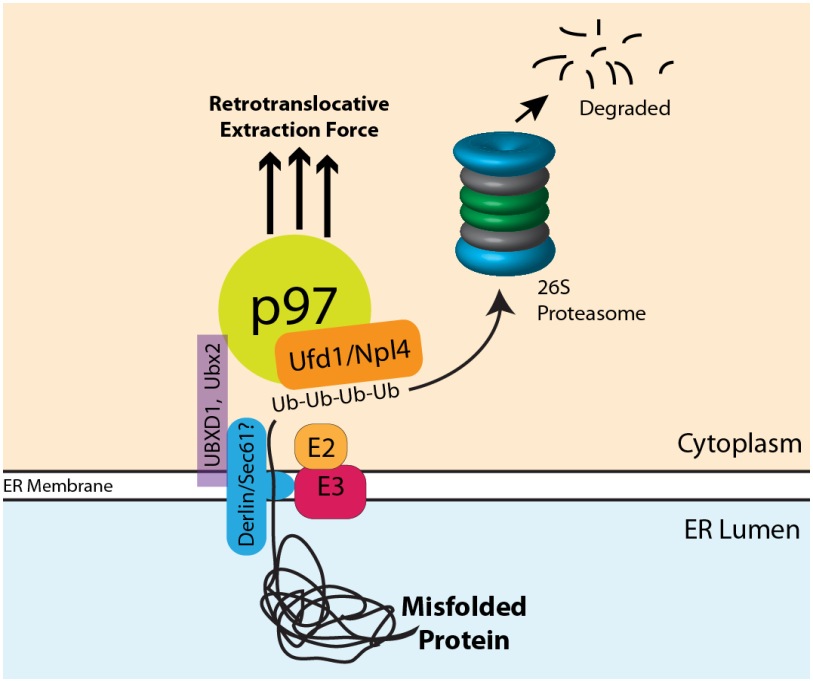

Figure 1.1.5 – Cytoplasmic events of ERAD.
In the ERAD process, misfolded proteins are recognized and targeted for retro-translocation with ubiquitination, followed by terminal degradation by the 26S proteasome. The activity of p97-UN is necessary for proteins' retro-translocation.

1.1.3.4 p97/VCP-UN segregase functions in DNA repair

The p97/VCP-UN complex, which drives the retro-translocation of ERAD substrates, also functions in extracting processes that involve ubiquitin where the final destination of the protein extracted is not degradation. Then p97/VCP-UN functions as a segregase, separating components from larger complexes. One example of the important roles of p97/VCP-UN as a segregase is in DNA repair (Figure 1.1.6).

The recruitment of p97/VCP-UN to sites of DNA damage has been shown to be essential for the DNA repair process (Meerang *et al.*, 2011). Blocking of p97-UN function results in accumulation of damaged DNA upon ionizing radiation treatment in *C. elegans*, affecting genome stability and increasing cell death. At the sites of DNA damage or DNA double stranded

breaks, ubiquitin ligases RNF8 and RNF68 conjugate K48-linked polyubiquitin chains onto substrates such as L3MBTL1, a polycomb protein bound to DNA chromatin (Acs *et al.*, 2011). These poly-ubiquitinated proteins are then recognized by p97-UN complex, via the conjugated K48-polyubiquitin chains, and are extracted from DNA chromatin at the DNA lesion to allow binding of DNA repair factors such as RAD51, BRCA1 and 53BP1. This process is ubiquitin-dependent with p97/VCP-UN functioning to segregate proteins from DNA (Ramadan, 2012). It occurs usually during the interphase state of mitosis, but p97VCP-UN also plays an important role throughout most phases of the mitotic process, i.e. metaphase, anaphase and cytokinesis.

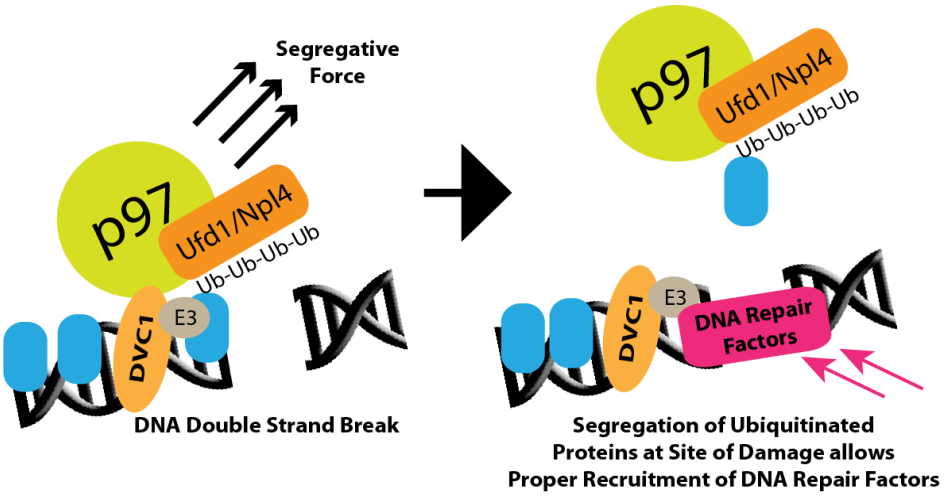

Figure 1.1.6 – p97-UN in molecular segregation
Similar to p97-UN's role in ERAD, instead of extracting proteins from the ER, here p97-UN functions to separate proteins bound to DNA in a ubiquitin-dependent manner to facilitate the association of repair factors.

1.1.3.5 p97/VCP-UN in cell division

In metaphase, p97-UN function is essential for the proper alignment and positioning of chromosomes at the metaphase plate (Figure 1.1.7). This is achieved by regulating aurora B's activities through the extraction of aurora B

from chromatin. It allows proper and efficient alignment of chromosomes at metaphase, without which, abnormal segregation occurs (Dobrynin *et al*., 2011; Ramadan *et al*., 2007). During anaphase, p97/VCP-UN functions to stabilize securin inhibition of separase, to prevent premature cleavage of anaphase cohesins leading to anaphase onset (Ikai and Yanagida, 2006).

Towards the completion of mitosis, the core complex of p97/VCP-UN extracts several microtubule-associated proteins, such as the microtubule polymerases Tpx2, XMAP215, segregating them from microtubules to allow proper microtubule disassembly. Inhibition of p97/VCP-UN's essential role in the maintenance of proper mitotic spindle formations and disassembly in cell division results in cell cycle arrest (Cao *et al*., 2003).

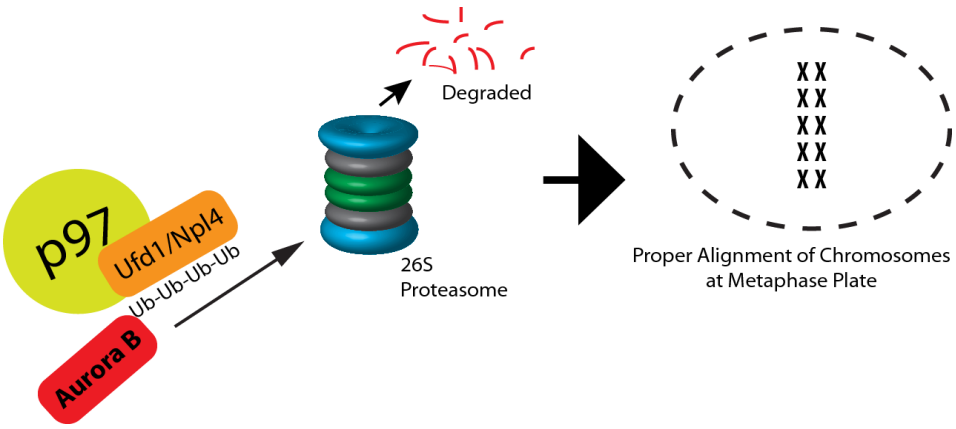

Figure 1.1.7 – Role of p97/VCP-UN in cell division
The timing at which p97-UN extracts and regulates the levels of Aurora B is crucial for the maintenance of chromosomal alignment integrity

1.1.4 p47

p47 is a homotrimeric protein that interacts with homohexameric p97/VCP in a 3:6 stoichiometry (Beuron *et al*., 2006). The p47 monomer (Figure 1.1.8, upper panel), a 370 amino acid protein, contains a SEP domain between amino

acids 179 to 244, which precedes a 78 amino acid UBX domain stretch (Yuan *et al*., 2004). Functionally, the UBX domain serves for recognition and binding of ubiquitin, while the SEP domain has no known function associated with it. The p97/VCP-p47 complex acts as a core complex recruiting other proteins involved in disassembly and re-assembly of the Golgi complex, transitional ER and nuclear envelope (Figure 1.1.8, middle panel) (Kondo *et al*., 1997; Latterich, 2006). The interaction between p97/VCP-p47 with Atg8, an autophagy-related protein, is necessary for the maturation of autophagosomes in yeast (Figure 1.1.8, lower panel). Impediment of this interaction prevents autophagosomes maturation and limits lysosomal fusion, resulting in undesirable accumulations (Krick *et al*., 2010).

1.1.5 Aims

The adaptor protein preference of p97/VCP for UN and p47, which are mutually exclusive adaptor proteins, determines the equilibrium of p97/VCP-dependent cellular activities. Using SPR biosensor technology, we aim to characterize the interaction between p97/VCP with either of these adaptor proteins, in an attempt to understand how adaptor protein preference can be regulated. The study performed through binding assays or via a qualitative competition assay allowed us to observe adaptor protein competition in real time. With p97/VCP being an ATPase, we also performed binding assays in the presence or absence of ATP or its analogs at physiological concentrations, to determine whether nucleotides have any effect on
adaptor protein binding.

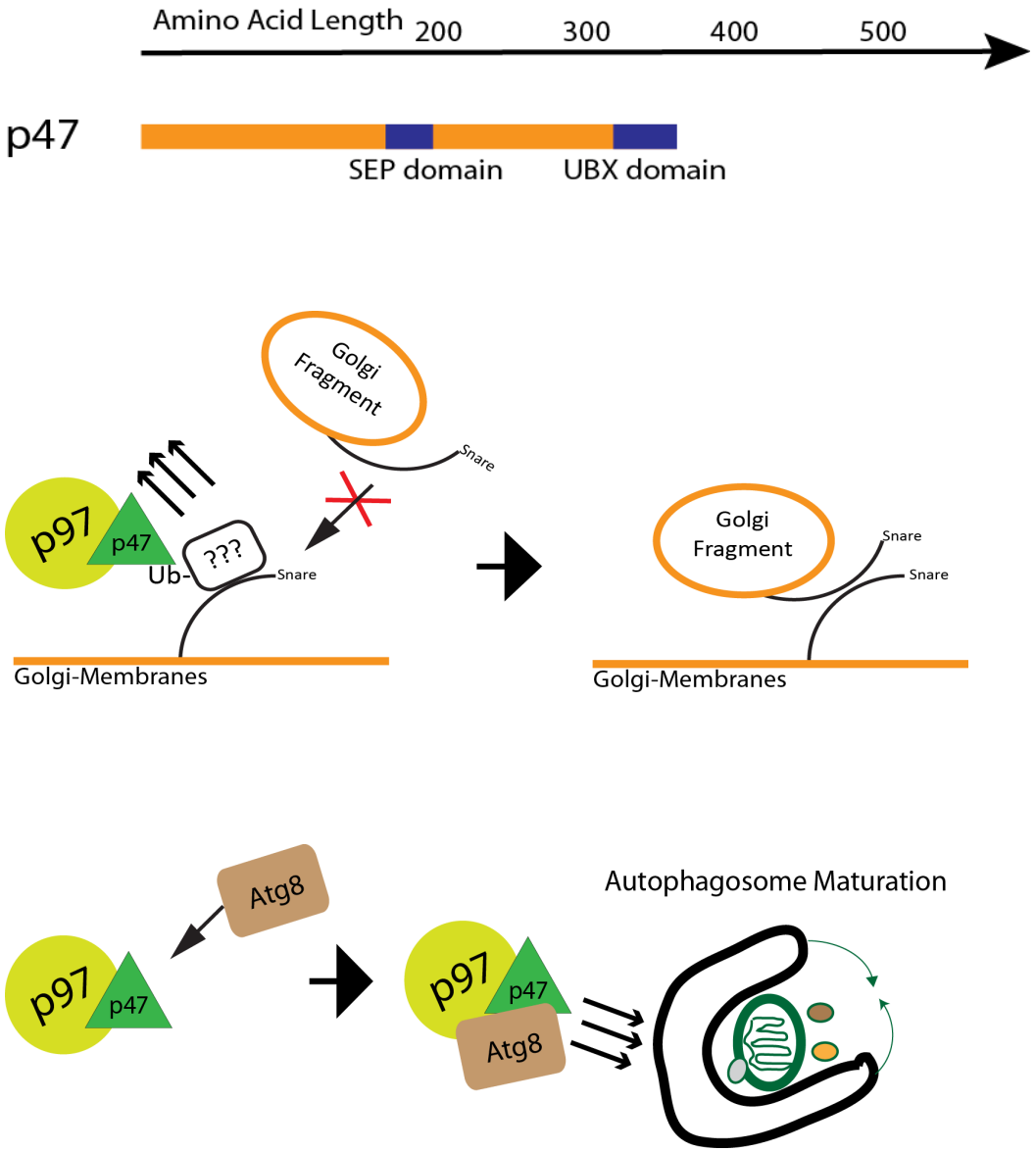

Figure 1.1.8 – p97/VCP-p47 functions
Domains of p47 are depicted. A key role of p97/VCP-p47 is to extract a mono-ubiquitinated substrate from Snare proteins to facilitate Snare-Snare pairings and subsequently membrane fusion. The exact identity of the mono-ubiquitinated substrate has yet to be determined. p97/VCP-p47 is involved also in the maturation of autophagosomes.

1.1.4 Surface Plasmon Resonance

In the late 1960s, physicists Otto and Kretschmann observed a phenomenon of total internal reflection when incident polarized light hits a thin metal film at certain angles (Kretschmann and Raether, 1968; Otto, 1968). This phenomenon, known today as surface plasmon resonance (SPR), is the result of resonance when plasmons absorb the energy from the polarized light, and oscillate locally, resulting in a propagation of an evanescent wave (plasmon) perpendicular to the plane of oscillation (Figure 1.1.9). This phenomenon proved useful for analysis of thin films and surfaces as the angle of total internal reflection is dependent on the mass on the surface of the thin film, and was used by material scientists and physicists for surface analysis for several decades. The idea and application of SPR into biosensing, detecting molecular interactions and observing the binding kinetics in real time was pioneered by Liedberg *et al.*, in 1983.

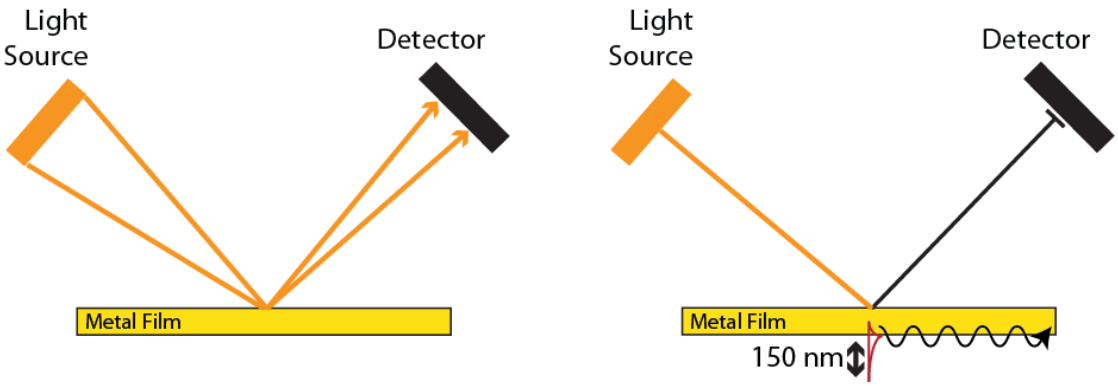

Figure – 1.1.9 The SPR phenomenon
Incident light from a light source at non-SPR angles is reflected by the metal film towards the detector. However, when light is beamed at the angle where SPR occurs, energy from the light source is absorbed in resonance by the plasmons on the surface of the metal film, resulting in little or no light reflected to the detector. An evanescent wave propagates perpendicular to the plane of electron oscillation with the amplitude of the wave diminishing exponentially with increasing distance from the surface, limiting biosensing to within 150 nm from the surface.

In the original manuscript based on Liedberg's MSc thesis, it was demonstrated that the binding kinetics of immunoglobulin G (IGG) to anti-IGG at different concentrations could be monitored by the change in “resonance angle”, the change in angle of incidence where SPR occurs (Liedberg *et al*., 1983). This allowed sensing in both liquid and gases, and the idea resulted in the eventual birth of Biacore under Pharmacia/Amersham, pioneers of SPR-based biosensors, which was finally acquired by GE Healthcare in 2008. The basis of SPR bio-sensing starts with the presence of a thin film of metal, gold, silver, titanium etc. Gold was the predominant metal of choice due to its chemical inertness, high sensitivity and good signal-to-noise ratio, and the possibility of gold-thiol bond that facilitates immobilization of molecules as self-assembled monolayers (matrix) on the gold surface, allowing useful derivatizations (Hakkinen, 2012). As pure gold itself easily adsorbs random molecules, a surface coating or matrix was necessary to block all available sites on the gold surface to prevent non-specific interactions of molecules. At the same time, the surface coating must be selectively chemo-reactive, for the specific conjugation of ligands of interest.

In the Biacore instruments, carboxylated methyl dextran (CMD) is the matrix of choice (Lofas, 1995). Apart from having rapid hydration/dehydration properties, chemical stability, and low non-specific bindings to proteins, CMD is structured like little bushes on the gold surface, with its long mesh-like multi-stranded structure greatly increasing the amount of ligand that can be coupled as compared to a simple alkane-thiol monolayer (Figure 1.1.10).

50 nm of gold is sputtered onto optical glass, which is then coated with a self-assembled monolayer of carboxylated methyl-dextran (CMD). Carboxyl

groups present on the CMD allow for easy amine-reactive chemistry, using n-hydroxysuccinimide (NHS)/ethyl-carbo-diimide (EDC) activation and either blocking with ethanolamine or further modifying with 2-(2-pyridinyldithio) ethaneamine hydrochloride to derivatize the surface for thiol-coupling (Figure 1.1.11).

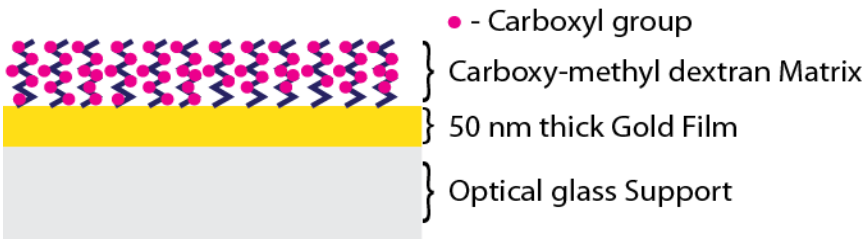

Figure 1.1.10 – The SPR-Biosensor Sensorchip design

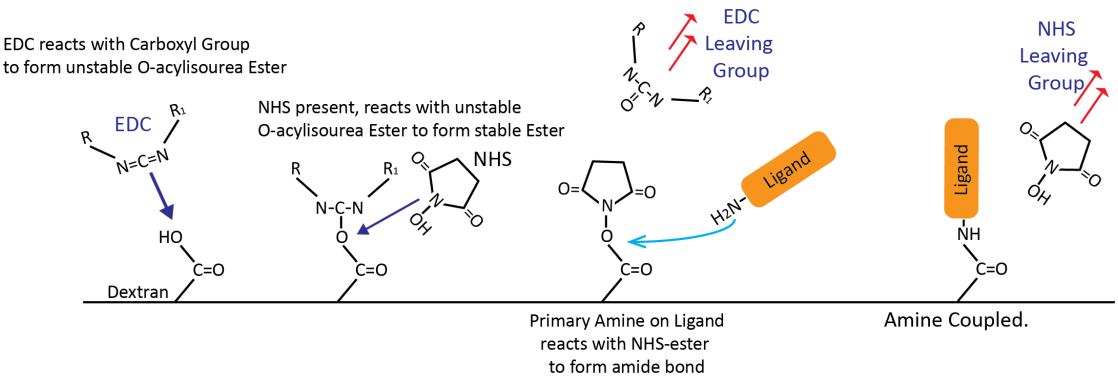

Figure 1.1.11 - Amine coupling mechanism
Carboxyl groups on CMD are activated with a 1:1 mixture of ethyl-carbo-diimide (EDC) and n-hydroxysuccinimide (NHS) to form a stable amine-reactive ester on dextran before application of the ligand to be immobilized. Primary amines on the ligand react with the NHS-ester to form a covalent amide bond to the dextran matrix.

By varying the angles of incident light on the film, it is possible to excite plasmons at a particular angle known as the SPR angle, at which light energy is absorbed and minimally reflected to a detector. When a binding event occurs on the surface of the gold film, the change in mass brings about a

change in the angle where SPR occurs. By monitoring the shift in SPR angle over time, one can observe the binding event, and the dissociation from the surface in real time Figure 1.1.12). This shift in SPR angle is commonly referred to as a response signal, and is given as Response Units (RUs) where 1000 RUs is equivalent to 1 nanogram of mass change, and a 0.1 degree shift in angle.

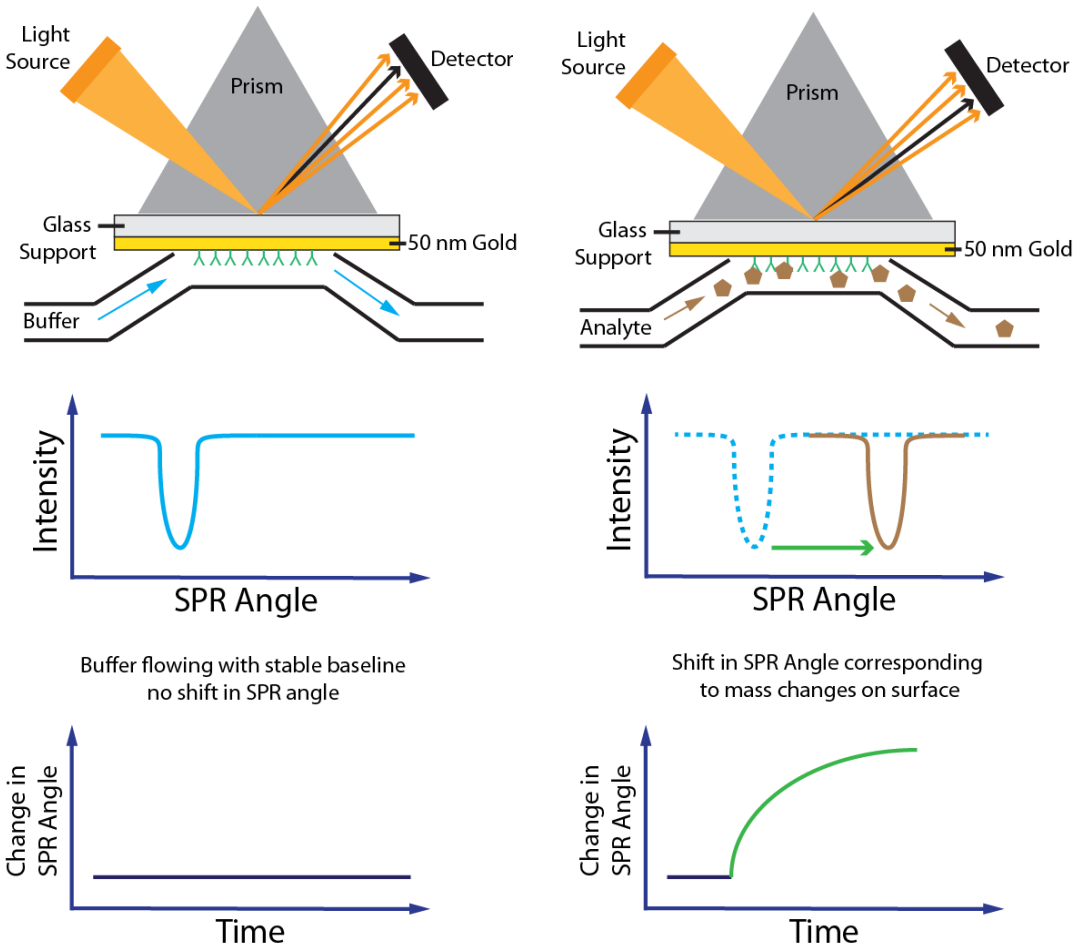

Figure 1.1.12 – Real-time observation of binding through monitoring changes in SPR angle
A fixed SPR angle is seen when buffer flows with nothing binding to the ligand on the surface, no mass changing. When an analyte is injected, it binds to the ligand and increases the mass on the surface, resulting in a shift in angle to the right. With increased binding, the SPR angle will shift to the right even more.

In a SPR binding assay, one of the interactants, termed as the analyte, is injected across immobilized ligand on a flow cell of a sensorchip. Binding events are observed as a rising exponential, with the curve tapering off towards equilibrium, when association and dissociation rates are equal. Equilibrium may not be achievable for low affinity interactants or low sample concentrations. At the end of analyte injection, only buffer flows across the surface with the bound analyte falling off at a rate known as a dissociation rate. Alternatively, when a co-injection method is used, a second solution, or analyte is injected in the dissociation to allow one to observe competition. When all bound analyte has fallen off the surface, the surface is considered "regenerated" and the signal will be back to baseline ready for the next analyte injection (Figure 1.1.13).

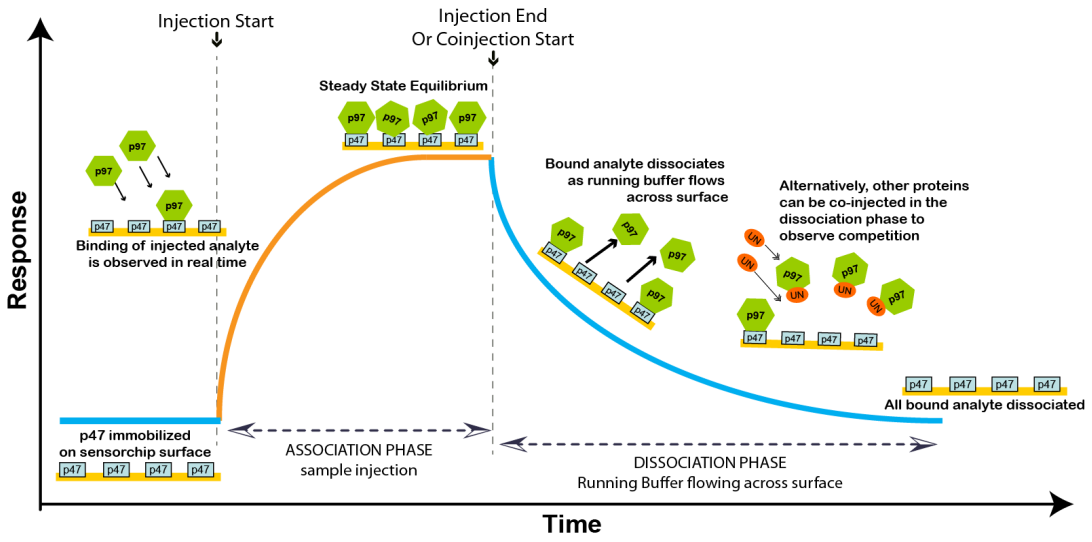

Figure 1.1.13 – Typical events on the surface of a sensorchip
Both association and dissociation events on the surface are monitored in real time.

In our SPR studies, we used the commercial Biacore 3000 Instrument where the built-in microfluidic system creates on the carboxymethylated surface of a sensorchip four flow cell channels in serial flow design. For typical binding

experiments, active referencing is achieved when two channels are used and samples are serially injected across the reference flow cell followed by the ligand flow cell. The sensorgrams obtained from both flow cells are then subtracted to give the specific binding curves that describe the kinetic parameters of the interaction studied. With the advanced microfluidics for sample delivery on the Biacore 3000, in the dissociation phase one can choose whether to have running buffer or a different buffer/solution/sample injected immediately in this phase by selecting the appropriate injection methods (Figure 1.1.14).

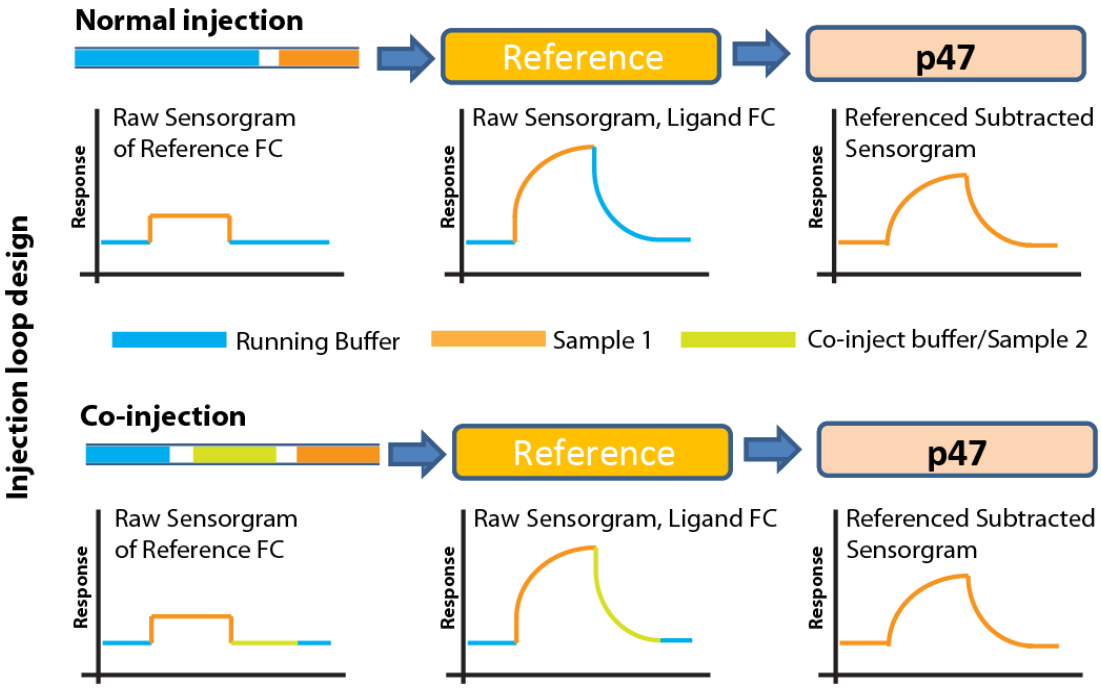

Figure 1.1.14 – Active referencing of both normal injection and co-injection methods
Serial injection across reference surfaces before the ligand flow cell. In a typical scenario, where running buffer is matched with the sample buffer, upon injection of the analyte without non-specific bindings occuring, the reference flow cell sensorgram is flat or a small box shape, whereas in the ligand flow cell, the binding curve is seen. The two curves can then be subtracted to give a final referenced subtracted sensorgram.

1.2 Materials & Methods

1.2.1 LB broth

The Luria Bertani (LB) broth formula used for all bacterial cultures is the Miller Formula mix from Novagen, containing 5 g yeast extract, 10 g NaCl, 10 g tryptone in 1 litre water, sterilized by autoclaving at 121 °C for 20 minutes.

1.2.2 Competent bacteria for protein expression

Escherichia coli (E.coli) Rosetta DE3 (P.Lyss) from Novagen was kindly provided by Asst. Professor Andrew Tan's Lab in NTU School of Biological Sciences. An innoculum was grown in LB broth to 0.7 A_{600} and cells were pelleted by centrifugation (5000 x g, fixed angle Eppendorf Centrifuge, 4°C). In all subsequent steps, all buffers used were ice-cold. Cells pellet was re-suspended in ice cold RF1 (50ml to pellet from 100ml culture; Table 2), incubated on ice for one hour, pelleted by centrifugation and re-suspended in ice-cold RF2 (5ml to pellet from 200ml culture; Table 3). After incubation for one hour on ice, the resuspended cells were divided on ice into 50 aliquots of 100 μl, snap frozen with liquid nitrogen and stored at -80°C.

1.2.3 Plasmids and transformation of bacteria

Plasmids for expressing the various proteins of interests were obtained from Professor Hemmo Meyer through the Addgene database. The plasmid pQe-p97 for the expression of p97/VCP with N-terminal His-tag did not yield homogenous protein and its purification was unsatisfactory. Therefore, p97/VCP was re-cloned at *Nde*I and *Xho*I sites into pET-26B (Novagen),

generating p97/VCP with C-terminal His-tag. Plasmids for recombinant protein expression were introduced into competent *E. coli* Rosetta DE3 bacterial cells via heat-shock transformation.

RF1 Buffer	
Rubidium Chloride	100 mM
Calcium Chloride.$2H_2O$	10 mM
Manganese Chloride.$4H_2O$	80 mM
Potassium Acetate	60 mM
Glycerol	15 %
Adjust to pH 5.8 with acetic acid and 0.2uM filter	

RF2 Buffer	
Rubidium Chloride	10 mM
Calcium Chloride.$2H_2O$	100 mM
MOPS	10 mM
Glycerol	15 %
Adjust to pH 6.5 with NaOH and 0.2uM filter	

Table 1.2.1 – Recipe for the rubidium chloride-based solutions for preparing competent *E. coli (Renzette, 2005)*.
Solutions prepared were sterilized by filtration and stored at 4°C. Prior to usage, bottles were chilled on ice for 1 hour.

Purified plasmid DNA (5-10 ng) was added to 100 μl of competent bacteria, incubated on ice for 1 hour and subjected to a 60 second heat-shock at 42 °C. Cells were placed on ice for 5 minutes, 1 ml of LB broth was added and bacteria were incubated with shaking at 37 °C for expression of antibiotic-resistance genes prior to positive transformant selection on LB agar plates containing the appropriate antibiotics. Antibiotics used: 100 μg/ml Ampicilin; 30 μg/ml Kanamycin; 34 μg/ml Chloramphenicol (*E. coli Rosetta DE3* is chloramphenicol-resistant). Plates were incubated overnight at 37 °C. Positive transformants were verified to carry the plasmids of interest through plasmid extraction and agarose gel electrophoresis with ethidium bromide staining (1% (w/v) Agarose in Tris-Acetate-EDTA buffer (40 mM Tris pH8, 20 mM Acetate, 1 mM EDTA)). DNA was visualized in a UV light box with a CCD camera attached (Syngene). Once verified, positive transformants were made into

stocks by resuspending the bacteria in LB broth containing 15% (v/v) glycerol, and snap freezing 100 μl aliquots with liquid nitrogen for storage at -80 °C.

1.2.4 Recombinant protein expression

All plasmids used have a *Lac* promoter that drives expression of genes of interest upon induction by lactose or non-hydrolysable lactose homologue Isopropyl β-D-1-thiogalactopyranoside (IPTG). The antibiotic resistances, hosts for expressions, the respective induction temperatures, IPTG concentrations and durations are summarized in Table 4. Overnight cultures were made from frozen bacterial stocks using LB broth containing the respective antibiotics, resistance to which is conferred by the plasmids. 10 ml of overnight culture was used to inoculate 800 ml of fresh LB broth for protein expression. Culture was grown to the respective OD_{600} before induction with IPTG and at respective temperatures and durations. Subsequently, bacteria were pelleted by centrifugation (Beckman JA-10 rotor 13,600 x g, 4°C) and frozen at -80 °C. Pellets were used within a week from expression to minimize undesirable protein modifications.

1.2.5 Protein purification

Frozen bacterial pellets with the respective proteins expressed were thawed on ice and re-suspended in lysis buffer consisting of 50 mM sodium phosphate, 300 mM NaCl, 5 mM β-mercaptoethanol. Complete EDTA-free protease inhibitor from Roche was included at the manufacturer's recommendation (1 tablet for 50 ml of lysis buffer).

Plasmid	Tag	Antibiotic Resistance	Protein	Host	Induction Temperature	Induction OD_{600}	[IPTG]	Induction Duration
pET-26B-p97	C-terminus 6xHis	Kanamycin	**p97**	***E.coli Rosetta DE3 (P.lyss)***	25 °C	1.0	0.5 mM	**3 Hours**
pET-26B-Ufd1	N-terminus 6xHis		**Ufd1**		37 °C	0.6 - 0.8	1 mM	**4 Hours**
pET-30-Npl4	Untagged, copurified through Ufd1		**Npl4**		16 °C			
pTrcHis-p47	N-terminus 6xHis	Ampicilin	**p47**		37 °C			
pQE-p97-N-D1	N-terminus 6xHis		**p97-N-D1**		25 °C	1.0	0.5 mM	**3 Hours**

Table 1.2.2 – Culture conditions for expression of recombinant proteins.
A summary of respective plasmids used and their antibiotic resistances, hosts, induction temperature, durations and IPTG concentrations.

Chilled lysis buffer was added to bacterial pellet at a weight to volume ratio of 10:1 and the re-suspension was sonicated on ice with 1 second pulse on/pulse off cycles for a total of 10 minutes in a beaker, using Sonics Ultrasonicator ultrasonic probe. Lysate was visually inspected for lysis (i.e. color/transparency/viscosity change), and when it was not satisfactory, sonication was carried out for additional 10 minutes. Lysate was clarified by centrifugation (Beckman JA 25.50 rotor, 50,000 x g, 20 minutes, 4°C). Clarified lysate was filtered through a 0.2 µm polyethylsulphone filter and His-tag affinity pull down with nickel immobilized metal-ion affinity chromatography (IMAC) resin was carried out at a ratio of 1 ml resin for lysate obtained from 1 litre of bacterial culture. Lysate was incubated with nickel IMAC resin for 2 hours before resin was packed into a Bio-Rad econo column, washed with lysis buffer, and bound proteins were eluted with five column volumes of 250 mM Imidazole in lysis buffer with 5% (v/v) glycerol, and collected into five fractions. Ufd1 and Npl4 were co-purified as a heterodimer through the His_6-taged Ufd1. To that end, a culture of bacteria expressing Npl4 mixed with Ufd1 culture at a ratio of 2:1 was co-pelleted by centrifugation and lysed by sonication. Excess Npl4 ensures that all His-tagged Ufd1 pulled down is bound to Npl4. Fractions eluted from nickel IMAC resin were subjected to 10% Sodium-dodecyl sulphate – Polyacrylamide gel electrophoresis (SDS-PAGE) and Coomassie brilliant blue staining to identify the fractions containing the proteins of interest and their purity. A 10-250 kDa protein ladder from Bio-Rad was used as molecular weight markers. Eluted proteins were generally pure enough to be further purified by a single gel filtration step from which eluants were re-checked for purity on 10% SDS-PAGE. The exception is p97/VCP-N-D1,

which had to be subjected to anion exchange chromatography to remove contaminants.

1.2.6 Anion exchange chromatography

Anion exchange chromatography was carried out for p97/VCP-N-D1 on the AKTA FPLC (GE Healthcare). IMAC elutions from nickel resin containing p97/VCP-N-D1 protein were de-salted into 50 mM sodium phosphate buffer pH 8 (Buffer A) with no salt, using a PD-10 desalting column, and then injected into a 1 ml HiTrap Q FF column at a flow rate of 0.1 ml/min to facilitate binding. The column was washed with 5 column volumes of Buffer A and then eluted with 20 column volumes of NaCl in a concentration gradient from 0 to 1 M. 0.5ml fractions were collected and analysed with 10% SDS-PAGE and Coomassie brilliant blue staining to identify fractions containing the protein of interest.

1.2.7 Size exclusion chromatography

Size exclusion chromatography was carried out on a calibrated Superose 6 300/10GL on an AKTA FPLC. Calibration was carried out with protein standards in the size range of our proteins of interest, including Thyroglobulin (667 kDa), Ferritin (440 kDa), Lactate Dehydrogenase (132 kDa) and Bovine Serum Albumin (66 kDa). Phosphate-buffered saline (PBS) containing 5 mM β-mercaptoethanol and 0.005% (v/v) p20 was used for column equilibration (2 column volumes) and sample purification. The buffer used for size exclusion chromatography was also used as a running buffer in SPR binding

experiments. Briefly, 0.5 ml of protein sample was loaded onto the column and gel filtration was carried out at a flow rate of 0.4 ml/min. Elution was monitored by 280 nm absorbance and fractionation was set to collect eluants with an absorbance of above 5 milli-absorbance units. Peaks eluting at volumes corresponding to their molecular weights were collected and used for SPR binding assays. 10% SDS-PAGE using Coomassie brilliant blue staining was used for final assessment of protein purity.

1.2.8 Protein concentration measurements

Protein concentration was measured by Bradford assay (Pierce Coomassie Plus Assay kit 23236) and typical regressions of r^2 = 0.97 to 0.99 for Bovine Serum Albumin (BSA) standards curves were used for estimation of protein concentration in samples.

1.2.9 SPR binding assays

1.2.9.1 Buffer

All SPR binding experiments were carried out at 25 °C, using PBS containing 5 mM β-mercaptoethanol and 0.005% (v/v) p20, the exact same buffer into which proteins of interests were gel-filtered.

1.2.9.2 Immobilization of ligands

Ligands were amine coupled to the CMD surface of a Biacore CM5 sensorchip. Optimal immobilization pH was determined for the respective ligands in a pH scouting experiment before surface activation for amine coupling. A 1:1

mixture of 0.2 M 1-ethyl-3-(3-dimethylpropyl)-carbodiimide and 0.1 M N-hydroxysuccinimide was injected across the flow cell to derivatize the carboxyl groups present on the dextran into amine-reactive esters. Dilute acidified ligands was then injected until the desired immobilization levels were achieved, then the surface was blocked with 50 mM ethanolamine in 1 M NaCl. The control surface was treated in an identical way, omitting the injection of the protein.

1.2.9.3 Binding experiments

Experiments for determining binding kinetics were carried out at a flow rate of 30 µl/min. Serial dilutions of analytes were injected across the reference flow cell followed by the ligand flow cell for 1 to 2 minutes, with a dissociation phase of 2 minutes. All nucleotides used in SPR experiments were purchased from Sigma Aldrich (Sigma A26209, A1388, A2647 and A2754) and prepared as a 1:1 magnesium-nucleotide complex. Sensorgrams from binding experiments were double referenced to both the inline reference flow cell and also with corresponding buffer injections to subtract refractive index bulk effects and non-specific bindings. All proteins used as analytes in our experiments have negligible non-specific bindings or do not bind at all to reference surfaces, demonstrating specificity of interaction with the ligand. All collected binding experiment data were analysed in Biaevaluation 4.1 software (GE Healthcare) and TraceDrawer 1.4 (Ridgeview Instruments AB, Uppsala, Sweden). Sensorgrams of the interactions were submitted for Interaction Map analysis using the Trace Drawer 1.4 software, which provided advanced

mathematical fittings and presentation of interaction components as a visual map.

1.2.9.4 Competition experiments

Competition experiments were carried out at a flow rate of 20 µl/min. In competition experiments, comparing adaptor protein preference, p47 was the preferred ligand for immobilization on the sensorchip surface, as it was the only adaptor protein that was resistant to multiple cycles of regeneration with 50 mM NaOH with minimal deterioriation of its activity, allowing high levels of reproducibility. p97/VCP was injected across immobilized p47, and captured to a level of approximately 500 RUs. At the end of injection, or start of the dissociation phase, the competing protein was co-injected, either in the presence or absence of ATP (Figure 1.2.1). Both the automixing and co-injection functions on the Biacore 3000 system were utilized to provide consistency and eliminate possibility of bias in the experiment. The system was programmed to mix the mixture for co-injection in a 1:1 ratio, in the permutations of Ufd1/Npl4 or buffer, with either buffer or buffer containing ATP using the method written on the Biacore Control Software (Figure 1.2.2).

1.2.10 Dynamic light scattering (DLS) measurements

Dynamic light scattering (DLS) was performed on a Malvern Zetasizer Nano ZS using non-invasive back scatter (173°C). 1ml of 1µM protein freshly eluted from size exclusion chromatography was pipetted into a 1ml poly-methyl-methyl-acrylate (PMMA) cuvette and subjected to reading on the DLS machine.

Each sample was subjected to multiple reads for averaging, allowing accuracy and statistical significance. For monitoring thermal denaturation via DLS, heating was carried out by the built-in heating system in the Malvern Zetasizer NanoZS. Poly methyl-methyl-acrylate (PMMA) cuvettes were used in all measurements due to thermal stability.

Figure 1.2.1 – The design of the competition experiments using a Biacore 3000 instrument.
The diagram depicts the different steps in each binding cycle designed to observe competition between Ufd1/Npl4 (UN) and p47 for binding to p97/VCP in real time. p97/VCP (500 RUs) was captured by immobilized p47 (2000 RUs) on the surface in the sample injection phase. At the end of sample injection, either running buffer takes over or a co-injection is performed serially with the dissociation of p97/VCP from the surface being monitored. The co-injection is a 1:1 mixture of either buffer alone, ATP with buffer, protein with buffer, or protein with ATP. Mixing was carried out in fresh tubes (green in diagram), with each tube being used only once.

Cycle Settings
Temperature: 25 (°C)
Detection Mode: 4-3
Flow
Flow: 20 (µl/min)
Transfer
From Solution: Coinject_2 - *Vary by Cycle*
To Variable: Mix_ID2 (New vial for each cycle)
Transfer Volume: 50 (µl)
Transfer
From Solution: Coinject2_Buffer - *Vary by Cycle*
To Variable: Mix_ID2 (New vial for each cycle)
Transfer Volume: 50 (µl)
Mix
Mix Position: Mix_ID2 - *Vary by Cycle*
Auto Mix
Inject
Injection Mode: Dual injection (COINJECT)
Solution: Sample_ID - *Vary by Cycle*
Volume: 20 (µl)
Solution 2: Mix_ID2 - *Vary by Cycle*
Volume 2: 40 (µl)
Extra Cleanup
Flow
Flow: 100 (µl/min)
Inject
Injection Mode: Normal injection (INJECT)
Solution: "Regen"
Volume: 10 (µl)

Figure 1.2.2 – The automix method programmed in the Biacore 3000 Control Software .
The programmed method allows for the 1:1 mixture of co-injection buffers, in all specificed permutations that facilitate competion during dissociation, including buffer with ATP or protein with ATP or protein with buffer. A six second pulse of 50 mM NaOH is used to dissociate residual analyte bound to the immobilized ligands. The 1:1 automated mixing mechanism eliminates possible sources of bias in dilution errors by using the same solutions to dilute either protein or buffer.

1.2.11 Differential scanning fluorimetry (DSF)

Different scanning fluorimetry (DSF) based on the method of Nielsen *et al.* 2007(was used to observe conformational changes in p97/VCP and p97/VCP-N-D1 upon ATP binding. In DSF, the protein of interest is pre-coated with Sypro Orange by incubating 2 µM of protein with a 1:1 mixture of 10x Sypro

Orange (Sigma Aldrich S5692) dissolved in PBS. Incubation was performed on ice and 40 µl triplicates were transferred into 0.2 ml PCR tubes (Applied Biosystems MicroAmp Optical 8 Tube strip and caps). Thermal unfolding was carried out in the presence or absence of ATP using a Biorad IQ5 real-time PCR thermocycler. Upon thermal unfolding of the protein, Sypro Orange binds to newly exposed hydrophobic residues, resulting in a fluorescence readout (excitation at 492nm, emission at 610 nm). Results from DSF were analyzed in the Biorad IQ2 Software, with the melting curves of the proteins generally sigmoidal, and the melting temperature represented by the inflection point on the differential fluorescence plots. As binding of ligand brings about additional bonds formed and conformational changes, more energy is required to release these bonds and unfold the protein during the thermal shift assay, and thus the melting temperature increases in response to ligand presence, with larger increments when binding to ligands is strong.

1.3 Results

1.3.1 Protein Purification

The recombinant p97/VCP, p97-N-D1, p47 and Ufd1/Npl4 used in our SPR, DSF and DLS assays were expressed in bacteria and purified to homogeneity (Figure 1.3.1), as described in Experimental Procedures. The calibration of the Superose 6 column used for purification is shown in Figure 1.3.1A and a table presenting the elution volumes and the oligomeric states of the purified proteins are shown in Figure 1.3.1C. Ufd1/Npl4 heterodimer was eluted in gel filtration at an apparent molecular mass of 200 kDa due to its shape, despite its molecular weight of 105 kDa, similar to previous observations (Bruderer *et al*., 2004). p47 was eluted as a homotrimer at 16.25 ml, identical to previously reported purifications (Kondo *et al*., 1997). p97/VCP was eluted as a very stable homohexamer and p97/VCP-N-D1 fragment was eluted as two different fractions, a minor monomeric fraction at 17.7 ml and a homohexameric fraction at 14.5 ml. The homohexameric fraction was used for all our assays. To verify that the proteins we used were hexameric, dynamic light scattering (DLS) was performed on both full length p97/VCP and p97/VCP-N-D1 fragment.

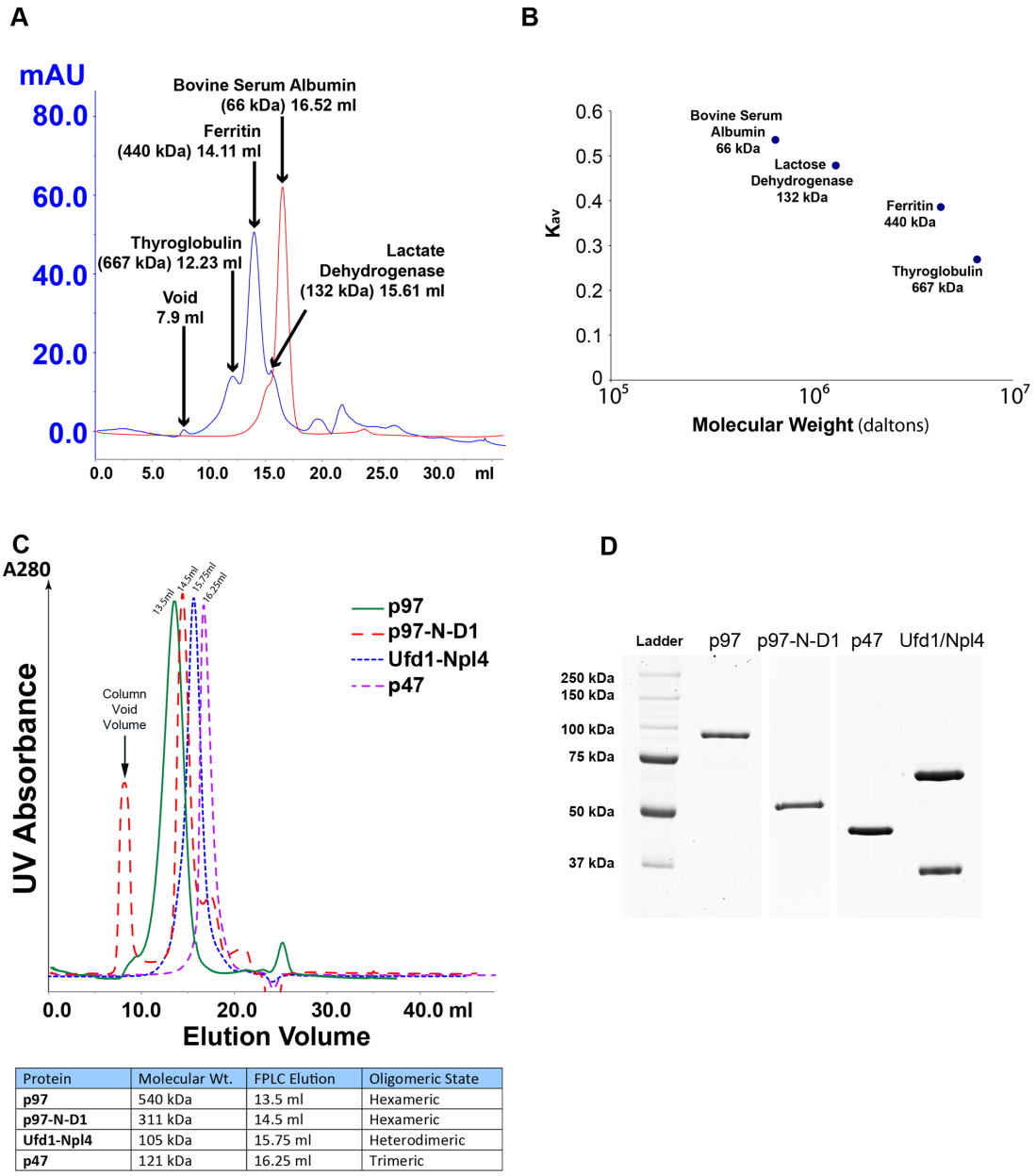

Protein	Molecular Wt.	FPLC Elution	Oligomeric State
p97	540 kDa	13.5 ml	Hexameric
p97-N-D1	311 kDa	14.5 ml	Hexameric
Ufd1-Npl4	105 kDa	15.75 ml	Heterodimeric
p47	121 kDa	16.25 ml	Trimeric

Figure 1.3.1 – Proteins purified to homogeneity
(A) Gel Filtration profile of several commercial reference protein markers for column calibration, namely Thyroglobulin (667 kDa), Ferritin (440 kDa), Lactate Dehydrogenase (15.61 kDa), Bovine Serum Albumin (66 kDa) **(B)** The calibration plot of the Superose 6 300/10 GL column used. Gel filtration elution profiles **(C)** and 10% SDS-PAGE gels **(D)** of the respective proteins purified for use in our SPR binding experiments and other assays.

1.3.2 The affinity of the interactions of p97/VCP with either p47 or UN

Using a Biacore 3000 instrument, an attempt was made to determine the affinity of the interactions of p97/VCP with either p47 or UN. For that purpose, p97/VCP was immobilized on the CM5 sensorchip surface and concentration series of p47 or UN were injected over the immobilized surface at two-fold dilutions, as shown in Figure 1.3.2. For the interaction between p97/VCP and UN shown in Figure 1.3.2A, the sensorgrams could not be fitted with a Langmuir 1:1 model, showing a multiphasic behavior. It implies that the interaction is complex even at a low immobilization of p97/VCP, which did not show mass transfer limitation (Figure 1.3.2).

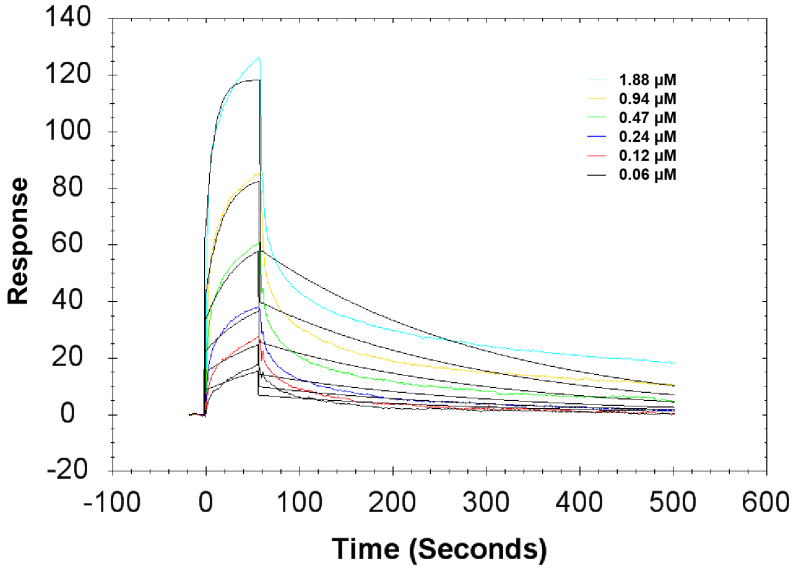

Figure 1.3.2 - Trial of a 1:1 Langmuir model fit.
Sensorgrams from the interaction between Ufd1/Npl4 and p97/VCP were poorly fitted to the 1:1 Langmuir model, suggesting that the interaction may be complex.

To determine the components of the p97/VCP-UN interaction, we have submitted the data of the binding curves for the interaction between UN and p97/VCP to an Interaction Map Analysis service, where advanced mathematical fittings are performed computationally on the curves. From the

results obtained from this analysis, illustrated in Figure 1.3.2A, it is evident that the interaction is complex and can be represented by two independent processes, a dominant weak-affinity component (K_D of approximately 5 μM), represented by peak A, which is the major interaction of p97/VCP and UN, and an additional smaller but stronger interaction component of approximately 400 nM affinity (peak B). Given the complex nature of this interaction, it is impossible to provide one single affinity value but merely to display the Interaction Map Analysis.

For the p97/VCP-p47 interaction, the sensorgrams obtained from the binding of p47 to immobilized p97/VCP or *vice versa* were fitted with a Langmuir model and using Interaction Map Analysis they showed a single kinetic component (Figure 1.3.2C, D). However there are kinetic and affinity differences depending on the immobilized interactant. When p47 was immobilized and p97/VCP passed across, a strong interaction was observed (31.3 nM). A strong interaction between p97/VCP and p47 had been reported by Kondo *et al.* (Kondo *et al*., 1997), who showed that p47 could not be removed from p97/VCP in their gels, and Dreveny *et al.* (Dreveny *et al*., 2004a) stated that the interaction between p97/VCP and p47 was stable up to 0.5M KCl. This could be due to one p97/VCP homohexamer interacting with more than one immobilized p47, having a higher interaction stoichiometry contributing to avidity. When p97/VCP was immobilized and p47 was passed across as an analyte, the kinetics of the interaction presented fast association and dissociation, with a K_D of around 5 μM. In this case, one could envision p47 interacting with individual sites on p97/VCP and falling off, instead of locking in as a stable complex.

Given the complexity of the interactions between p97/VCP and UN, which renders quantitative measurements and comparisons difficult, we have adopted a qualitative approach. In our attempts to study adaptor preference, we perform competition assays between p47 and UN in their binding to p97/VCP.

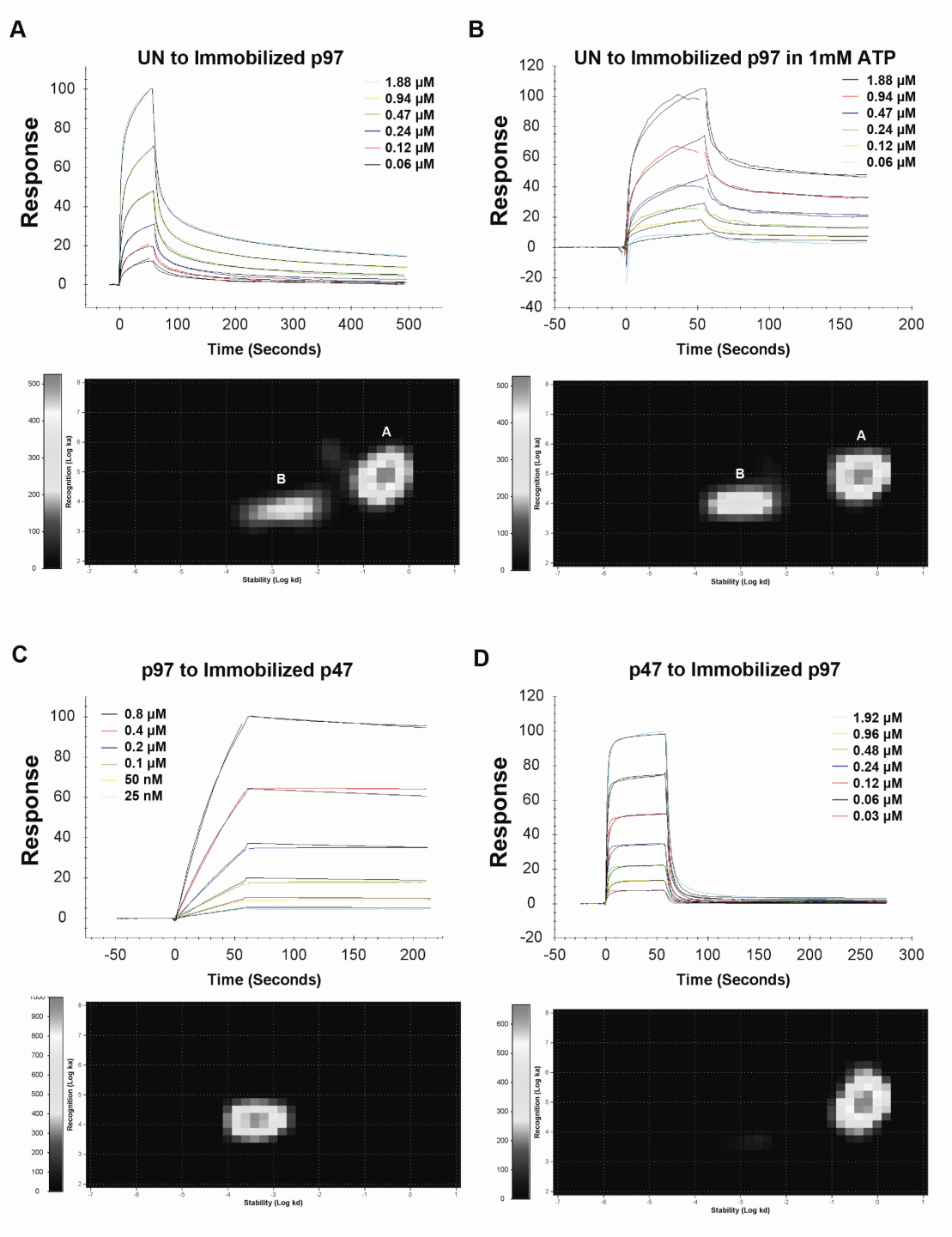

Figure 1.3.3 - Binding affinities of the interactions between p97/VCP and its adaptor proteins

p97/VCP was immobilized on a CM5 sensorchip surface, using amine coupling procedure, and a concentration series of p47 (two fold dilutions from 1.92 µM) or UN (two fold dilutions from 1.88 µM) were injected over the immobilized surface at a flow rate of 30 µl/min, at 25 ºC, using PBS as the sample and running buffer. Sensorgrams and the corresponding interaction maps for the p97/VCP-UN interaction without ATP (A), with ATP during UN association and dissociation (B) and for p97/VCP-p47 interactions when p47 is immobilized (C) and when p97/VCP is immobilized (D) are shown.).

1.3.3 UN competes more effectively with p47 for binding to p97/VCP in the presence of ATP

To gain insights into the regulation of recruitment of the various adaptor proteins of p97/VCP, an SPR-based competition assay was designed and carried out using a Biacore 3000 Instrument (Figure 1.1.15). In this assay, we were able to investigate the competition between p47 and UN for binding to p97/VCP, using a customized protocol (Figure 1.1.16) that allowed high reproducibility and accuracy in real time observations.

To follow the competition between UN and p47 for p97/VCP, we selected p47 for immobilization on the sensorchip surface. This was based on the high stability of p47 and its resistance to surface regeneration conditions, which allowed tens of analyte injections and regeneration cycles with minimal surface deterioration. Approximately 500 response units (RU) of p97/VCP were initially captured on the p47-immobilized surface (Figure 1.3.3). During the dissociation phase, various concentrations of UN were injected in the absence (Figure 1.3.3A) or presence (Figure 1.3.3B) of ATP. Clearly, in the presence of ATP, UN competed with p47 for p97/VCP binding more effectively. When 2 mM ATP was co-injected, 0.5 μM of UN was as effective as 5 μM UN in the absence of the nucleotide (compare Figure 1.3.3A and B). It indicates a ten-fold increase in the capability of UN to compete with p47. Note that without UN, ATP had no effect on the dissociation of p97/VCP from p47 (Figure 1.3.3C). The specificity of this competition was confirmed by substitution of UN with bovine serum albumin (BSA), where BSA failed to remove p97/VCP from the p47 surface (Figure 1.3.3D).

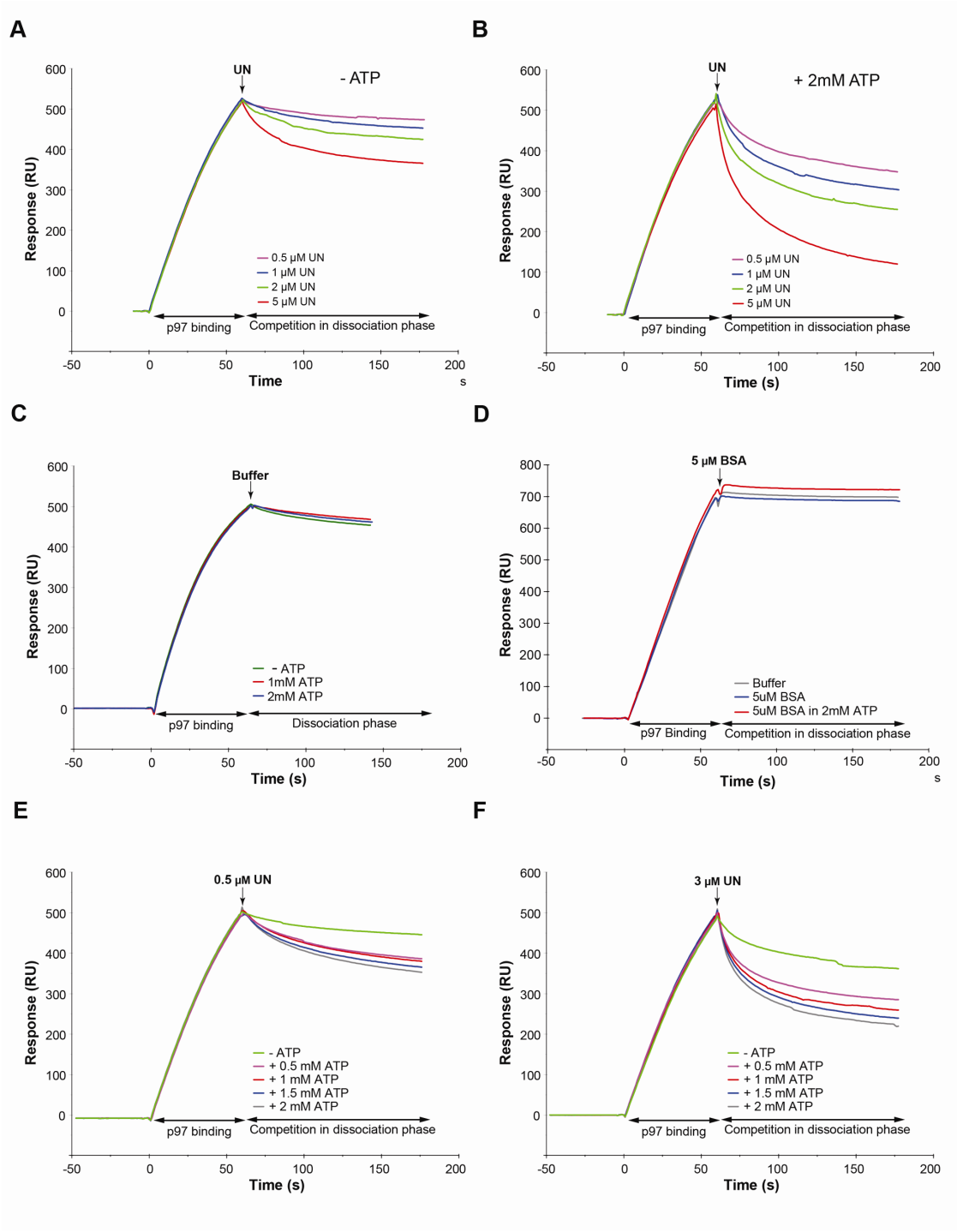

Figure 1.3.4 - Ufd1/Npl4 competes with p47 for binding to p97/VCP more effectively in the presence of ATP

p47 (2000 RU) was amine-coupled onto a flowcell of a CM5 sensorchip and p97/VCP (500 RU) was repeatedly captured by the immobilized p47 as depicted in Figure 1.3.2 and described in Experimental Procedures. UN at the indicated concentrations was coinjected across the surface, in the absence (A) or presence (B) of 2 mM ATP. In control experiments, 2 mM ATP with no UN (C) or 5 µM BSA instead of UN (D) were coinjected. UN was coinjected at fixed concentrations of either 0.5 µM (E) or 3 µM (F) in the presence of the indicated ATP concentrations.

Finally, by varying both UN and ATP concentrations, we demonstrated that ATP influenced the competitive binding in a concentration-dependent manner, as the enhanced competition by elevated amounts of UN was further improved in correlation with increasing ATP concentration (Figure 1.3.3E, F).

1.3.4 ATP binding, not hydrolysis, to the D1 domain of p97/VCP regulates adaptors' competition

To discern whether ATP binding or its hydrolysis is responsible for regulating the observed competition between the adaptor proteins, we utilized the non-hydrolysable ATP analogue ATPγS. Clearly, competition was as effective with the non-hydrolysable analogue as with ATP (Figure 1.3.4A). It indicates that ATP binding rather than its hydrolysis is responsible for the regulatory effect on the adaptors' recruitment.

Among the two ATPase domains present in p97/VCP, the D2 domain is implicated in most of the activities of p97/VCP that depend on ATP hydrolysis. We focused on the D1 domain, whose hydrolytic activity is much weaker, but it is in close proximity to the N-domain, the main p97/VCP adaptor recruiting region. Encouraged by recent publications on N-domain conformational changes upon ATP binding to p97-D1 (Tang *et al*., 2010), we hypothesized that the D1 domain is key to this regulation of the adaptor proteins competition. To rule out any contribution of the D2 domain, we carried out experiments with the p97-N-D1 fragment lacking the D2 domain. We found that ATP binding to the D1 domain itself was sufficient for regulating the adaptors' interactions with p97/VCP. Clearly, the p97-N-D1 fragment (Figure 1.3.4B) faithfully mimicked the behavior of the full length p97/VCP (Figure 1.3.4A) vis-à-vis the enhancing

effects of ATP or ATPγS on the ability of UN to compete with p47 for association with the N-domain of either the full length p97/VCP or its p97-N-D1 fragment.

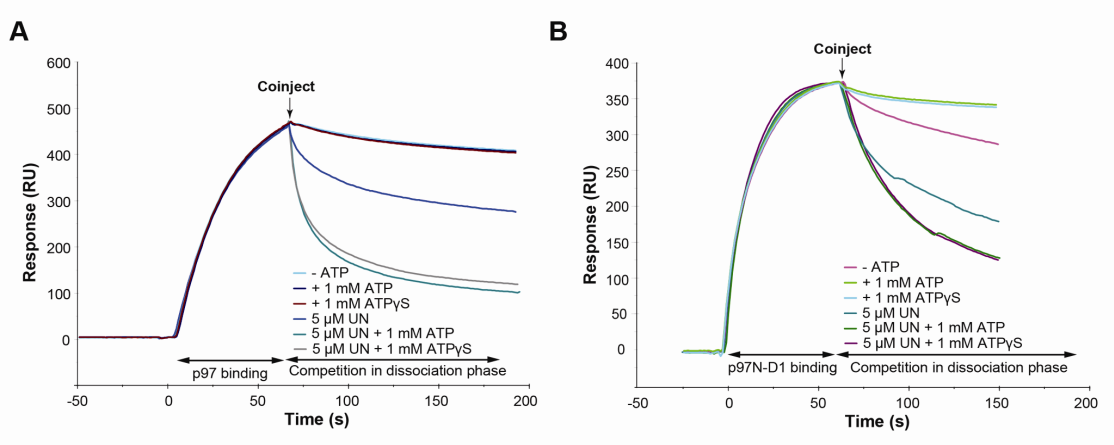

Figure 1.3.5 - ATP binding to the p97/VCP D1 domain regulates the adaptor protein competition
Full length p97/VCP (A) or p97-N-D1 fragment (B) were captured on the p47 surface to a level of 500 RU. 5 μM of UN was coinjected across the surface in the presence of 1 mM of either ATP or ATPγS, using the same experimental setup described in Figure 1.3.3.

1.3.5 ATP enhances the binding of UN to p97/VCP but does not affect the binding of p47

The results obtained from the competition experiments suggest that either ATP strengthens the binding of UN and/or weakens the binding of p47 to p97/VCP. To discern between these two mechanistic options, we tested the effects of ATP on the binding of either p47 or UN to p97/VCP. Our results showed unequivocally that ATP enhanced the binding of UN to p97/VCP (Figure 1.3.5A), while no effect of ATP could be detected on the binding of p47 (Figure 1.3.5B). Interaction Map Analysis of the sensorgrams of the p97/VCP-UN interaction showed that the second component of this interaction was

strengthened from ~400 nM in the absence of ATP to ~100 nM affinity in the presence of 1mM ATP (Figure 1.3.2B).

This finding provides a mechanistic explanation for the results obtained in the experiments showing the effect of ATP on the competition between UN and p47 for the binding to p97/VCP shown above. Again, when comparing the effects of ATP, ADP, and the poorly hydrolysable ATP analogue AMP-PNP, we noticed that both ATP and AMP-PNP exerted very similar effects, as both nucleotides strengthened the binding of UN to p97/VCP irrespective of hydrolysis (Figure 1.3.5C).

This experiment confirms that ATP binding rather than its hydrolysis is responsible for the improved binding of UN that, in turn, enhances its ability to compete more effectively with p47 for binding to p97/VCP.

1.3.6 ATP binding exerts conformational changes on homohexamers of p97/VCP or its p97-N-D1 fragment

Dynamic light scattering was performed on purified hexamers of either full length p97/VCP (A) or p97-N-D1 fragment (B) in the absence or presence of ATP. Upon addition of 1 mM ATP the hydrodynamic diameter of full length p97/VCP shifted from 19.41 nm to 19.74 nm and that of p97-N-D1 fragment shifted from 16.14 nm to 18.18 nm. The observed single peak homogeneities reflect no aggregation and stable hexamers. Both full length p97/VCP (C) and p97-N-D1 fragment (D) were subjected to thermal denaturation monitored by dynamic light scattering, showing no signs of hexamer dissociation when heated from 25 °C to 70 °C.

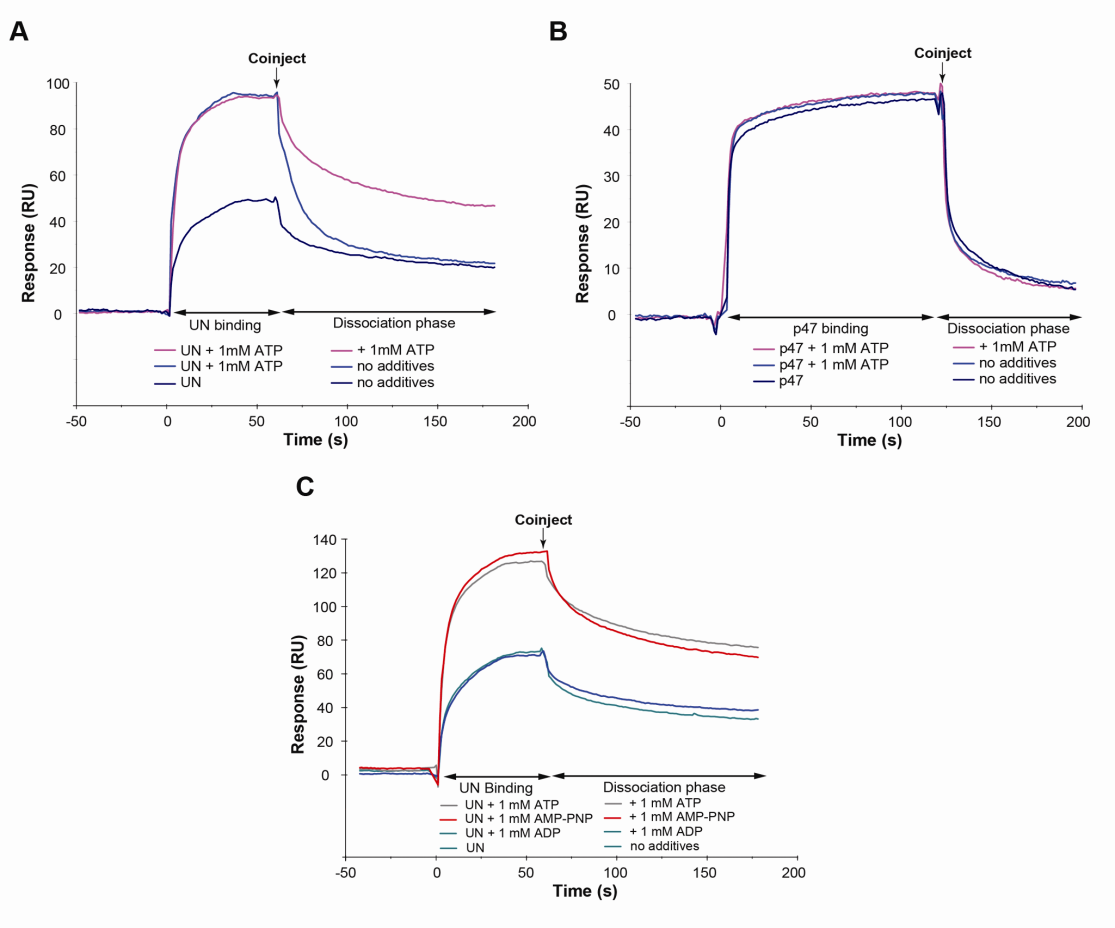

Figure 1.3.6 - ATP binding to p97/VCP affects Ufd1/Npl4 association with p97/VCP
p97/VCP (1000 RU) was immobilized on a CM5 sensorchip and either UN (A)or p47 (B) were injected over the p97/VCP surface at a concentration of 0.15 μM in the absence or presence of 1 mM ATP during the binding and/or dissociation phases, as indicated. (C) 0.16 μM UN was injected across 1000 RU of immobilized p97/VCP in the absence or presence of 1 mM of ATP, AMP-PNP or ADP.

The effects of ATP on strengthening the binding of UN to p97/VCP and potentiating its ability to compete with p47 may reflect conformational changes in p97/VCP. To probe for such changes, we utilized differential scanning fluorimetry (DSF) that correlates fluorescence with protein unfolding at elevated temperatures. Prior to carrying out DSF experiments, both p97/VCP and p97-N-D1 were assessed by DLS experiments, which confirmed their homohexameric structures (Figure 1.3.6).

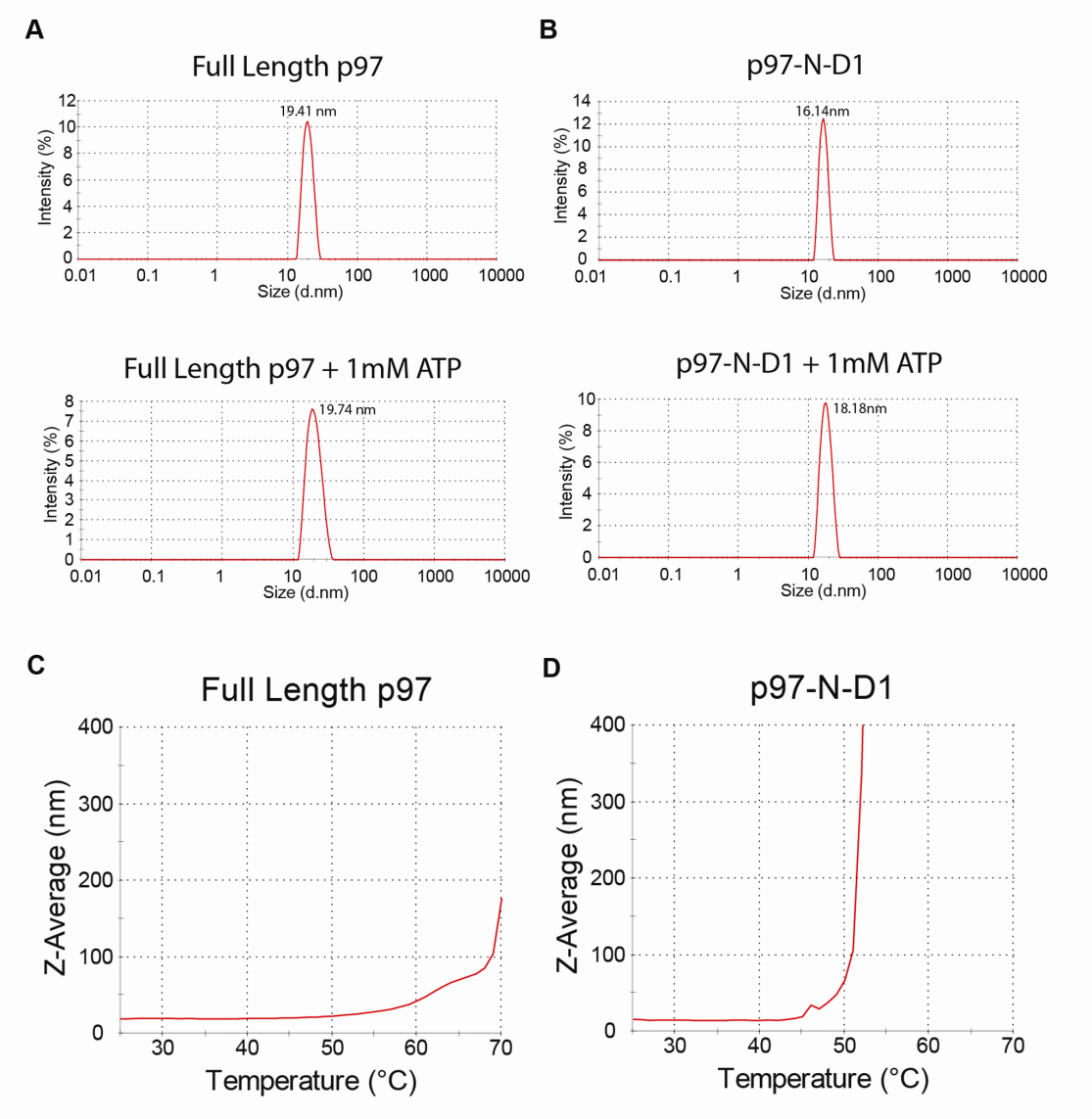

Figure 1.3.7 - Dynamic light scattering demonstates the stability of p97/VCP and p97-N-D1 hexamers

Hydrodynamic diameters of 19.4 nm for the full length p97/VCP (Figure 1.3.6A) and of 16.14 nm for the p97-N-D1 (Figure 1.3.6B) indicate that the proteins we worked with were homohexamers. These parameters are within the range of the molecular diameters estimated from published crystal structures of homohexameric p97/VCP (DeLaBarre and Brunger, 2003; Huyton *et al*., 2003; Zhang *et al*., 2000b). In the presence of ATP, there was a

slight shift in diameter (Figure 1.3.6A, B), suggesting an extended/expanded conformation. Both p97/VCP (Figure 1.3.6C) and p97-N-D1 (Figure 1.3.6D) were subjected to thermal denaturation with their diameters being monitored by DLS. During the process, the homohexameric structures were stable without falling into their monomers, suggesting high thermodynamic stability of the homohexamers. To further ensure that we were observing the homohexameric structures, we attempted to denature p97/VCP with urea. Disassembly of the hexamers was induced by urea in a concentration-dependent manner, resulting in a hydrodynamic diameter of below 1 nm for the p97/VCP monomer (Figure 1.3.7)

More importantly, the DSF results revealed that while for the full length p97/VCP there was a minor but reproducible change in the temperature at which the protein unfolded in the presence of 1 mM ATP, (Figure 1.3.8A), the p97-N-D1 fragment showed a more dramatic thermostabilization upon ATP binding, with the melting temperature shifting by 14 °C, from 50 °C in the absence of ATP, to 64 °C in the presence of 1mM ATP (Figure 1.3.8B).

By titrating hexamers of both full length p97/VCP (Figure 1.3.7C) and the p97-N-D1 fragment (Figure 1.3.8D) with a series of ATP concentrations, we observed concentration-dependent stabilization. It suggests that ATP binding results in conformational changes that bring about stability against thermal unfolding.

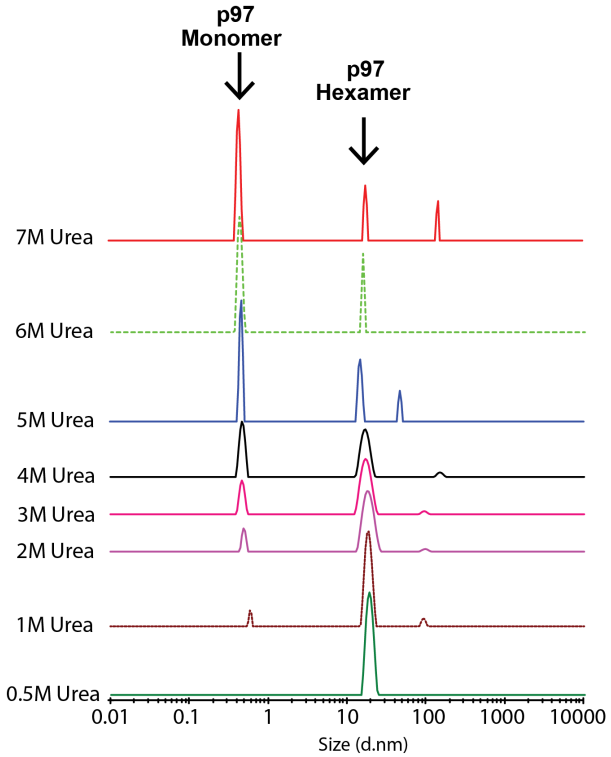

Figure 1.3.8 – Dissociation of p97/VCP with urea under DLS.
1 µM of p97/VCP was subjected to denaturation by varying concentrations of urea from 0.5 M to 7M with the dissociation of p97/VCP into its monomoers observed under DLS.

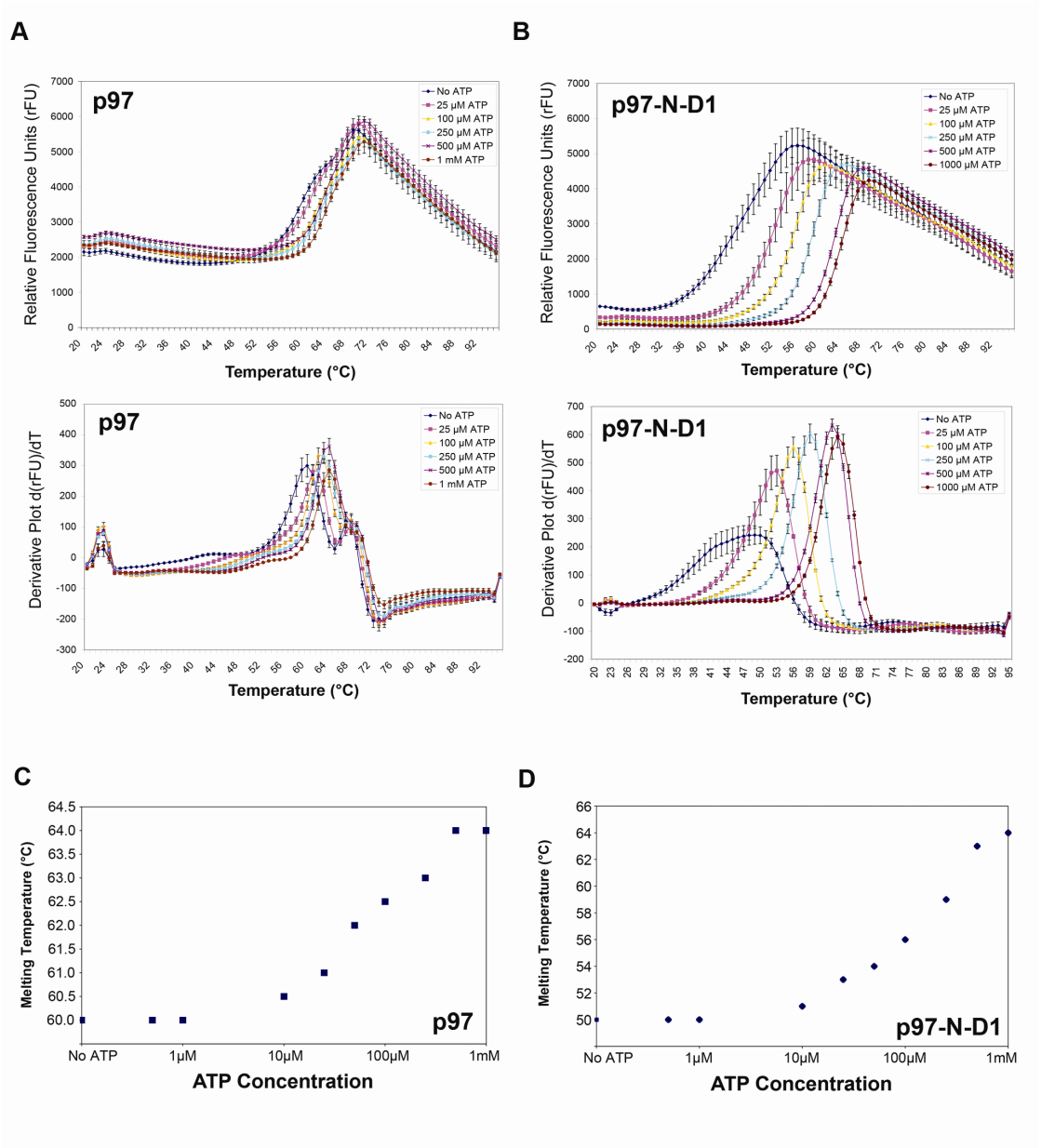

Figure 1.3.9 - Conformational changes upon ATP binding to p97/VCP and p97/VCP-N-D1 observed by differential scanning fluorimetry
Hexamers of either full length p97/VCP (A) or p97-N-D1 fragment (B) were subjected to differential scanning fluorimetry in the absence or presence of 1 mM ATP. Concentration-dependent thermostabilizations were observed by measurements of melting temperatures of full length p97/VCP (C) or p97-N-D1 fragment (D) at the indicated concentrations of ATP.

1.4 Discussion

p97/VCP functions in a myriad of cellular processes to which this AAA-ATPase is targeted by the recruitment of various adaptor proteins. Most of these adaptors bind to the same N-domain, either in a mutually exclusive way, as previously reported and shown here, or in hierarchical manner. Thus, the binding of the various adaptor proteins should be finely regulated. Several studies have provided the structural basis for the interaction between p97/VCP and its adaptor proteins (Dreveny *et al*., 2004a). p97-UN has been postulated to be a core complex platform for subsequent recruitment of other proteins into a functional mega protein complex, while p97-p47 forms another distinct core complex (Kloppsteck *et al*., 2011). The competition between UN and p47 addressed in this study becomes important as it determines the population of core complexes and the consequent directing of p97/VCP to its various functions.

Our qualitative competition and binding assays show, for the first time, that the concentration of ATP and its binding to the D1 domain affect the affinity of the interactions between p97/VCP and either p47 or UN. Indeed, our attempts to determine the actual affinity values of p97/VCP to UN yielded multi-phasic curves that could not be fitted to a standard Langmuir interaction model. These multi-phasic binding SPR curves may be explained by a very recent paper by Bebeacua *et al*., demonstrating through cryo-electron microscopy that p97/VCP harbors several distinct binding sites for UN, with UN interacting via single or double binding site models (Bebeacua *et al*., 2012). Also, applying Interaction Map Analysis we were able to deconvolute the interaction between UN and p97/VCP into two main components, which make

the comparison of the respective affinities to that of p97-p47 difficult. Irrespective of this shortcoming, we demonstrate that ATP exerts differential effects by strengthening the binding of UN, while not affecting the binding of p47, and therefore significantly enhancing the capacity of UN to compete with p47 for p97/VCP binding. The experiments performed with varying concentrations of ATP and UN, showing their co-dependence in competition with p47, suggest that in addition to the relative levels of these adaptor proteins, the cellular metabolic state referred to as ATP level affects the exclusive recruitment of either UN or p47 and the consequent function of p97/VCP in either ERAD or homotypic fusion. Moreover, with the use of the non-hydrolysable ATP analogues we attribute the effect of ATP to its binding rather than its hydrolysis.

While most ATPases have a single ATPase domain, it is not clear why each p97/VCP subunit contains two ATPases, the N-terminal D1 and the C-terminal D2. Especially intriguing is the role of the D1 domain, which has a low ATPase activity and is often ADP-bound, while the dominant ATPase activity is attributed to D2 that is observed in several nucleotide states (Pye *et al*., 2006). ATP binding to D1, and not ATP hydrolysis, is implicated in accelerating hexamerization. Systematic analyses of mutations in p97/VCP revealed that the loss of ATPase activity of D2 led to the loss of function of the protein *in vivo*, while ATPase activity of D1 *per se* was not essential. Nevertheless, a mutation locking D1 in an ATP-bound form was exceptionally lethal, probably because this form of D1 changed an inter-domain interaction (Esaki and Ogura, 2010). Here we attribute a novel role to the D1 domain as an ATP-sensing domain that regulates the binding of p97/VCP to its different adaptor proteins. To directly demonstrate the exclusive contribution of the D1 domain to adaptor

recruitment, we have used the p97-N-D1 fragment, which lacks the major ATPase domain D2. Clearly, the D1 domain is responsible for regulating the ATP-enhanced competition between UN and p47 for the proximal N-domain of p97/VCP. Our results indicate that the D1-ATP-bound conformational state of the p97/VCP N-domain favors binding to UN over p47. Indeed, crystal structure and solution X-ray scattering studies by Tang *et al.* confirm conformational changes in the N-domain upon binding of ATPγS (Tang *et al*., 2010).

Our results show that 0.5 μM of UN in the presence of 2 mM ATP competes with p47 for binding to p97/VCP as effectively as 5 μM of UN in the absence of ATP. This may be of high relevance in the cellular context, where ATP fluxes and gradients can exist locally or transiently (Ando *et al*., 2012; Ataullakhanov and Vitvitsky, 2002; Imamura *et al*., 2009; Liemburg-Apers *et al*., 2011). Namely, under ATP-limiting conditions, p97/VCP favors binding to p47 over UN, whereas under ATP-abundance, p97/VCP binds preferably to UN. Recalling that p47 is an inhibitor of the ATPase activity of p97/VCP, the latter is more likely to remain bound to p47 when ATP is limiting and thus inhibiting hydrolysis (Meyer *et al*., 1998). Conversely, binding of p97/VCP to UN promotes retrotranslocation of ER proteins and their ubiquitylation and chaperoning to the 26S proteasome in the ERAD pathway (Bays and Hampton, 2002; Kondo *et al*., 1997; Lass *et al*., 2008; Meyer *et al*., 2000). This suggests that in an ATP-abundant environment, p97/VCP readily binds to UN over p47, to carry out removal of misfolded proteins or participate in its different roles in the nucleus such as mitotic progression or transcription factor activation. Taken together, competition between p47 and UN for p97/VCP can become heavily biased in certain cells or tissues where the ratio between p97/VCP and

these adaptors is altered and ATP is limiting. The physiological relevance of this novel role of ATP in regulating adaptors recruitment and consequent engagement of p97/VCP in either ERAD or homotypic fusion implicates altered metabolic fluxes of ATP as key players. ATP levels may fluctuate within the same cell in different organelles, within different cell types and tissues and may even be affected by age or disease (Parihar and Brewer, 2007; Wallace, 2005). In this respect, it is interesting that the ability of p97/VCP to bind the Werner syndrome protein is ATP-dependent, suggesting a role for p97/VCP in releasing the Werner syndrome protein from the nucleus (Indig *et al*., 2004). Also in the p97/VCP R155H mutant, a seven-fold reduction in affinity to SVIP was observed when ATPγS was bound. Finally, the importance of the adaptors' recruitment to the functions of p97/VCP is underscored by the observation that the IBMPFD mutations are located at the hinge region between the N and D1 domains, that the majority of these mutants show higher affinity towards ATP and by the imbalanced binding of adaptor proteins to the IBMPFD mutant of p97/VCP (Tang *et al*., 2010). The importance of ATP levels has been shown in a *Drosophila melanogaster* IBMPFD model, where a high energy metabolic diet alleviates neurodegeneration (Chang *et al*., 2011). Since p97/VCP is implicated in several diseases including cancer, modulators of p97/VCP can be therapeutic. Our competition assay provides a possible drug screening method, which will allow a high throughput screen for molecules that specifically increase or decrease p97/VCP's interaction with a particular adaptor protein, and thus achieving a specific and refined form of inhibition than the general pleiotrophic modulation of overall p97/VCP functions.

1.5 References to Chapter 1

Acs, K., Luijsterburg, M.S., Ackermann, L., Salomons, F.A., Hoppe, T., Dantuma, N.P., 2011. The AAA-ATPase VCP/p97 promotes 53BP1 recruitment by removing L3MBTL1 from DNA double-strand breaks. Nat Struct Mol Biol 18, 1345-1350.

Alexandru, G., Graumann, J., Smith, G.T., Kolawa, N.J., Fang, R., Deshaies, R.J., 2008. UBXD7 binds multiple ubiquitin ligases and implicates p97 in HIF1alpha turnover. Cell 134, 804-816.

Ando, T., Imamura, H., Suzuki, R., Aizaki, H., Watanabe, T., Wakita, T., Suzuki, T., 2012. Visualization and measurement of ATP levels in living cells replicating hepatitis C virus genome RNA. PLoS Pathog 8, e1002561.

Araki, K., Nagata, K., 2011. Protein folding and quality control in the ER. Cold Spring Harb Perspect Biol 3, a007526.

Ataullakhanov, F.I., Vitvitsky, V.M., 2002. What determines the intracellular ATP concentration. Biosci Rep 22, 501-511.

Bays, N.W., Hampton, R.Y., 2002. Cdc48-Ufd1-Npl4: stuck in the middle with Ub. Curr Biol 12, R366-371.

Bebeacua, C., Forster, A., McKeown, C., Meyer, H.H., Zhang, X., Freemont, P.S., 2012. Distinct conformations of the protein complex p97-Ufd1-Npl4 revealed by electron cryomicroscopy. Proc Natl Acad Sci U S A 109, 1098-1103.

Bernasconi, R., Molinari, M., 2011. ERAD and ERAD tuning: disposal of cargo and of ERAD regulators from the mammalian ER. Curr Opin Cell Biol 23, 176-183.

Beuron, F., Dreveny, I., Yuan, X., Pye, V.E., McKeown, C., Briggs, L.C., Cliff, M.J., Kaneko, Y., Wallis, R., Isaacson, R.L., Ladbury, J.E., Matthews, S.J., Kondo, H., Zhang, X., Freemont, P.S., 2006. Conformational changes in the AAA ATPase p97-p47 adaptor complex. EMBO J 25, 1967-1976.

Boyault, C., Gilquin, B., Zhang, Y., Rybin, V., Garman, E., Meyer-Klaucke, W., Matthias, P., Muller, C.W., Khochbin, S., 2006. HDAC6-p97/VCP controlled polyubiquitin chain turnover. EMBO J 25, 3357-3366.

Braun, S., Matuschewski, K., Rape, M., Thoms, S., Jentsch, S., 2002. Role of the ubiquitin-selective CDC48(UFD1/NPL4)chaperone (segregase) in ERAD of OLE1 and other substrates. EMBO J 21, 615-621.

Briggs, L.C., Baldwin, G.S., Miyata, N., Kondo, H., Zhang, X., Freemont, P.S., 2008. Analysis of nucleotide binding to P97 reveals the properties of a tandem AAA hexameric ATPase. J Biol Chem 283, 13745-13752.

Bruderer, R.M., Brasseur, C., Meyer, H.H., 2004. The AAA ATPase p97/VCP interacts with its alternative co-factors, Ufd1-Npl4 and p47, through a common bipartite binding mechanism. J Biol Chem 279, 49609-49616.

Cao, K., Nakajima, R., Meyer, H.H., Zheng, Y., 2003. The AAA-ATPase Cdc48/p97 regulates spindle disassembly at the end of mitosis. Cell 115, 355-367.

Chang, Y.C., Hung, W.T., Chang, H.C., Wu, C.L., Chiang, A.S., Jackson, G.R., Sang, T.K., 2011. Pathogenic VCP/TER94 alleles are dominant actives and contribute to neurodegeneration by altering cellular ATP level in a Drosophila IBMPFD model. PLoS Genet 7, e1001288.

Consortium, C.e.S., 1998. Genome sequence of the nematode C. elegans: a platform for investigating biology. Science 282, 2012-2018.

DeLaBarre, B., Brunger, A.T., 2003. Complete structure of p97/valosin-containing protein reveals communication between nucleotide domains. Nat Struct Biol 10, 856-863.

Dobrynin, G., Popp, O., Romer, T., Bremer, S., Schmitz, M.H., Gerlich, D.W., Meyer, H., 2011. Cdc48/p97-Ufd1-Npl4 antagonizes Aurora B during chromosome segregation in HeLa cells. J Cell Sci 124, 1571-1580.

Dreveny, I., Kondo, H., Uchiyama, K., Shaw, A., Zhang, X., Freemont, P.S., 2004a. Structural basis of the interaction between the AAA ATPase p97/VCP and its adaptor protein p47. EMBO J 23, 1030-1039.

Dreveny, I., Pye, V.E., Beuron, F., Briggs, L.C., Isaacson, R.L., Matthews, S.J., McKeown, C., Yuan, X., Zhang, X., Freemont, P.S., 2004b. p97 and close encounters of every kind: a brief review. Biochem Soc Trans 32, 715-720.

Egerton, M., Samelson, L.E., 1994. Biochemical characterization of valosin-containing protein, a protein tyrosine kinase substrate in hematopoietic cells. J Biol Chem 269, 11435-11441.
Ernst, R., Mueller, B., Ploegh, H.L., Schlieker, C., 2009. The otubain YOD1 is a deubiquitinating enzyme that associates with p97 to facilitate protein dislocation from the ER. Mol Cell 36, 28-38.

Esaki, M., Ogura, T., 2010. ATP-bound form of the D1 AAA domain inhibits an essential function of Cdc48p/p97. Biochem Cell Biol 88, 109-117.

Guerriero, C.J., Brodsky, J.L., 2012. The delicate balance between secreted protein folding and endoplasmic reticulum-associated degradation in human physiology. Physiol Rev 92, 537-576.

Hakkinen, H., 2012. The gold-sulfur interface at the nanoscale. Nat Chem 4, 443-455.

Hetzer, M., Meyer, H.H., Walther, T.C., Bilbao-Cortes, D., Warren, G., Mattaj, I.W., 2001. Distinct AAA-ATPase p97 complexes function in discrete steps of nuclear assembly. Nat Cell Biol 3, 1086-1091.

Huyton, T., Pye, V.E., Briggs, L.C., Flynn, T.C., Beuron, F., Kondo, H., Ma, J., Zhang, X.,

Freemont, P.S., 2003. The crystal structure of murine p97/VCP at 3.6A. J Struct Biol 144, 337-348.

Ikai, N., Yanagida, M., 2006. Cdc48 is required for the stability of Cut1/separase in mitotic anaphase. J Struct Biol 156, 50-61.

Imamura, H., Nhat, K.P., Togawa, H., Saito, K., Iino, R., Kato-Yamada, Y., Nagai, T., Noji, H., 2009. Visualization of ATP levels inside single living cells with fluorescence

resonance energy transfer-based genetically encoded indicators. Proc Natl Acad Sci U S A 106, 15651-15656.

Indig, F.E., Partridge, J.J., von Kobbe, C., Aladjem, M.I., Latterich, M., Bohr, V.A., 2004. Werner syndrome protein directly binds to the AAA ATPase p97/VCP in an ATP-dependent fashion. J Struct Biol 146, 251-259.

Johnson, J.O., Mandrioli, J., Benatar, M., Abramzon, Y., Van Deerlin, V.M., Trojanowski, J.Q., Gibbs, J.R., Brunetti, M., Gronka, S., Wuu, J., Ding, J., McCluskey, L., Martinez-Lage, M., Falcone, D., Hernandez, D.G., Arepalli, S., Chong, S., Schymick, J.C., Rothstein, J., Landi, F., Wang, Y.D., Calvo, A., Mora, G., Sabatelli, M., Monsurro, M.R., Battistini, S., Salvi, F., Spataro, R., Sola, P., Borghero, G., Galassi, G., Scholz, S.W., Taylor, J.P., Restagno, G., Chio, A., Traynor, B.J., 2010. Exome sequencing reveals VCP mutations as a cause of familial ALS. Neuron 68, 857-864.

Kimonis, V., Donkervoort, S., Watts, G., 1993. Inclusion Body Myopathy with Paget Disease of Bone and/or Frontotemporal Dementia. In: Pagon, R.A., Bird, T.D., Dolan, C.R., Stephens, K., Adam, M.P. (Eds.), GeneReviews, Seattle (WA).

Kloppsteck, P., Ewens, C.A., Forster, A., Zhang, X., Freemont, P.S., 2011. Regulation of p97 in the ubiquitin-proteasome system by the UBX protein-family. Biochim Biophys Acta 1823, 125-129.

Koller, K.J., Brownstein, M.J., 1987. Use of a cDNA clone to identify a supposed precursor protein containing valosin. Nature 325, 542-545.

Kondo, H., Rabouille, C., Newman, R., Levine, T.P., Pappin, D., Freemont, P., Warren, G., 1997. p47 is a cofactor for p97-mediated membrane fusion. Nature 388, 75-78.

Kretschmann, E., Raether, H., 1968. Radiative decay of nonradiative surface plasmons excited by light. Z. Naturforsch. A 23, 2135.

Krick, R., Bremer, S., Welter, E., Schlotterhose, P., Muehe, Y., Eskelinen, E.L., Thumm, M., 2010. Cdc48/p97 and Shp1/p47 regulate autophagosome biogenesis in concert with ubiquitin-like Atg8. J Cell Biol 190, 965-973.

Lass, A., McConnell, E., Fleck, K., Palamarchuk, A., Wojcik, C., 2008. Analysis of Npl4 deletion mutants in mammalian cells unravels new Ufd1-interacting motifs and suggests a regulatory role of Npl4 in ERAD. Exp Cell Res 314, 2715-2723.

Latterich, M., 2006. p97 adaptor choice regulates organelle biogenesis. Dev Cell 11, 755-757.

Latterich, M., Frohlich, K.U., Schekman, R., 1995. Membrane fusion and the cell cycle: Cdc48p participates in the fusion of ER membranes. Cell 82, 885-893.

Leon, A., McKearin, D., 1999. Identification of TER94, an AAA ATPase protein, as a Bam-dependent component of the Drosophila fusome. Mol Biol Cell 10, 3825-3834.

Liedberg, B., Nylander, C., Lunström, I., 1983. Surface plasmon resonance for gas detection and biosensing. Sensors and Actuators 4, 299-304.

Liemburg-Apers, D.C., Imamura, H., Forkink, M., Nooteboom, M., Swarts, H.G., Brock, R., Smeitink, J.A., Willems, P.H., Koopman, W.J., 2011. Quantitative glucose and ATP sensing in mammalian cells. Pharm Res 28, 2745-2757.

Lofas, S., 1995. Dextran modified self-assembled monolayer surfaces for use in biointeraction analysis with surface plasmon resonance. Pure and Applied Chemistry 629, 829-834.

Madsen, L., Seeger, M., Semple, C.A., Hartmann-Petersen, R., 2009. New ATPase regulators--p97 goes to the PUB. Int J Biochem Cell Biol 41, 2380-2388.

Meerang, M., Ritz, D., Paliwal, S., Garajova, Z., Bosshard, M., Mailand, N., Janscak, P., Hubscher, U., Meyer, H., Ramadan, K., 2011. The ubiquitin-selective segregase VCP/p97 orchestrates the response to DNA double-strand breaks. Nat Cell Biol 13, 1376-1382.

Meyer, H., 2012. p97 complexes as signal integration hubs. BMC Biol 10, 48.

Meyer, H., Bug, M., Bremer, S., 2012. Emerging functions of the VCP/p97 AAA-ATPase in the ubiquitin system. Nat Cell Biol 14, 117-123.

Meyer, H.H., Kondo, H., Warren, G., 1998. The p47 co-factor regulates the ATPase activity of the membrane fusion protein, p97. FEBS Lett 437, 255-257.

Meyer, H.H., Shorter, J.G., Seemann, J., Pappin, D., Warren, G., 2000. A complex of mammalian ufd1 and npl4 links the AAA-ATPase, p97, to ubiquitin and nuclear transport pathways. EMBO J 19, 2181-2192.

Moir, D., Stewart, S.E., Osmond, B.C., Botstein, D., 1982. Cold-sensitive cell-division-cycle mutants of yeast: isolation, properties, and pseudoreversion studies. Genetics 100, 547-563.

Nagahama, M., Suzuki, M., Hamada, Y., Hatsuzawa, K., Tani, K., Yamamoto, A., Tagaya, M., 2003. SVIP is a novel VCP/p97-interacting protein whose expression causes cell vacuolation. Mol Biol Cell 14, 262-273.

Niesen, F.H., Berglund, H., Vedadi, M., 2007. The use of differential scanning fluorimetry to detect ligand interactions that promote protein stability. Nat. Protocols 2, 2212-2221.

Otto, A., 1968. Excitation of nonradiative surface plasma waves in silver by the method of frustrated total reflection. Z. Physik 216, 398-410.

Pamnani, V., Tamura, T., Lupas, A., Peters, J., Cejka, Z., Ashraf, W., Baumeister, W., 1997. Cloning, sequencing and expression of VAT, a CDC48/p97 ATPase homologue from the archaeon Thermoplasma acidophilum. FEBS Lett 404, 263-268.

Parihar, M.S., Brewer, G.J., 2007. Mitoenergetic failure in Alzheimer disease. Am J Physiol Cell Physiol 292, C8-23.

Park, M.Y., Moon, J.H., Lee, K.S., Choi, H.I., Chung, J., Hong, H.J., Kim, E., 2007. FAF1 suppresses IkappaB kinase (IKK) activation by disrupting the IKK complex assembly. J Biol Chem 282, 27572-27577.

Partridge, J.J., Lopreiato, J.O., Jr., Latterich, M., Indig, F.E., 2003. DNA damage modulates nucleolar interaction of the Werner protein with the AAA ATPase p97/VCP. Mol Biol Cell 14, 4221-4229.

Pleasure, I.T., Black, M.M., Keen, J.H., 1993. Valosin-containing protein, VCP, is a ubiquitous clathrin-binding protein. Nature 365, 459-462.

Pye, V.E., Dreveny, I., Briggs, L.C., Sands, C., Beuron, F., Zhang, X., Freemont, P.S., 2006. Going through the motions: the ATPase cycle of p97. J Struct Biol 156, 12-28.

Pye, V.E., Beuron, F., Keetch, C.A., McKeown, C., Robinson, C.V., Meyer, H.H., Zhang, X., Freemont, P.S., 2007. Structural insights into the p97-Ufd1-Npl4 complex. Proc Natl Acad Sci U S A 104, 467-472.

Rabinovich, E., Kerem, A., Frohlich, K.U., Diamant, N., Bar-Nun, S., 2002. AAA-ATPase p97/Cdc48p, a cytosolic chaperone required for endoplasmic reticulum-associated protein degradation. Mol Cell Biol 22, 626-634.

Ramadan, K., 2012. p97/VCP- and Lys48-linked polyubiquitination form a new signaling pathway in DNA damage response. Cell Cycle 11, 1062-1069.

Ramadan, K., Bruderer, R., Spiga, F.M., Popp, O., Baur, T., Gotta, M., Meyer, H.H., 2007. Cdc48/p97 promotes reformation of the nucleus by extracting the kinase Aurora B from chromatin. Nature 450, 1258-1262.

Renzette, N., 2005. Generation of Transformation Competent E. coli, Current Protocols in Microbiology. John Wiley & Sons, Inc.

Schmidt, W.E., Mutt, V., Carlquist, M., Kratzin, H., Conlon, J.M., Creutzfeldt, W., 1985. Valosin: isolation and characterization of a novel peptide from porcine intestine. FEBS Lett 191, 264-268.

Schwieger, I., Lautz, K., Krause, E., Rosenthal, W., Wiesner, B., Hermosilla, R., 2008. Derlin-1 and p97/valosin-containing protein mediate the endoplasmic reticulum-associated degradation of human V2 vasopressin receptors. Mol Pharmacol 73, 697-708.

Smith, M.H., Ploegh, H.L., Weissman, J.S., 2011. Road to ruin: targeting proteins for degradation in the endoplasmic reticulum. Science 334, 1086-1090.

Tang, W.K., Li, D., Li, C.C., Esser, L., Dai, R., Guo, L., Xia, D., 2010. A novel ATP-dependent conformation in p97 N-D1 fragment revealed by crystal structures of disease-related mutants. EMBO J 29, 2217-2229.

Uchiyama, K., Jokitalo, E., Kano, F., Murata, M., Zhang, X., Canas, B., Newman, R., Rabouille, C., Pappin, D., Freemont, P., Kondo, H., 2002. VCIP135, a novel essential factor for p97/p47-mediated membrane fusion, is required for Golgi and ER assembly in vivo. J Cell Biol 159, 855-866.

Wallace, D.C., 2005. A mitochondrial paradigm of metabolic and degenerative diseases, aging, and cancer: a dawn for evolutionary medicine. Annu Rev Genet 39, 359-407.

Wang, B., Alam, S.L., Meyer, H.H., Payne, M., Stemmler, T.L., Davis, D.R., Sundquist, W.I., 2003a. Structure and ubiquitin interactions of the conserved zinc finger domain of Npl4. J Biol Chem 278, 20225-20234.

Wang, Q., Song, C., Li, C.C., 2003b. Hexamerization of p97-VCP is promoted by ATP binding to the D1 domain and required for ATPase and biological activities. Biochem Biophys Res Commun 300, 253-260.

Ye, Y., Meyer, H.H., Rapoport, T.A., 2001. The AAA ATPase Cdc48/p97 and its partners transport proteins from the ER into the cytosol. Nature 414, 652-656.

Ye, Y., Shibata, Y., Kikkert, M., van Voorden, S., Wiertz, E., Rapoport, T.A., 2005. Recruitment of the p97 ATPase and ubiquitin ligases to the site of retrotranslocation at the endoplasmic reticulum membrane. Proc Natl Acad Sci U S A 102, 14132-14138.

Yeung, H.O., Kloppsteck, P., Niwa, H., Isaacson, R.L., Matthews, S., Zhang, X., Freemont, P.S., 2008. Insights into adaptor binding to the AAA protein p97. Biochem Soc Trans 36, 62-67.

Yuan, X., Simpson, P., McKeown, C., Kondo, H., Uchiyama, K., Wallis, R., Dreveny, I., Keetch, C., Zhang, X., Robinson, C., Freemont, P., Matthews, S., 2004. Structure, dynamics and interactions of p47, a major adaptor of the AAA ATPase, p97. EMBO J 23, 1463-1473.

Zhang, H., Wang, Q., Kajino, K., Greene, M.I., 2000a. VCP, a weak ATPase involved in multiple cellular events, interacts physically with BRCA1 in the nucleus of living cells. DNA Cell Biol 19, 253-263.

Zhang, X., Shaw, A., Bates, P.A., Newman, R.H., Gowen, B., Orlova, E., Gorman, M.A., Kondo, H., Dokurno, P., Lally, J., Leonard, G., Meyer, H., van Heel, M., Freemont, P.S., 2000b. Structure of the AAA ATPase p97. Mol Cell 6, 1473-1484.

Zhong, X., Pittman, R.N., 2006. Ataxin-3 binds VCP/p97 and regulates retrotranslocation of ERAD substrates. Hum Mol Genet 15, 2409-2420.

Zhong, X., Shen, Y., Ballar, P., Apostolou, A., Agami, R., Fang, S., 2004. AAA ATPase p97/valosin-containing protein interacts with gp78, a ubiquitin ligase for endoplasmic reticulum-associated degradation. J Biol Chem 279, 45676-45684.

Chapter 2

Characterization of AIRAPL – A novel p97/VCP adaptor protein

2.1.1 Introduction

Arsenic-inducible proteasomal 19S regulatory particle associated protein-like protein (AIRAPL) is a novel, constitutively expressed protein that is predominantly localized on the outer surface of the endoplasmic reticulum (ER). Coded by ZNF2B gene on chromosome 2, AIRAPL is 257 amino acids long, with 17 cysteines making up 6.6% of the amino acid composition, way above the human protein average of 2.3% (NCBI-GENE), Table 2.1.1). Localized in the cytoplasm, where conditions are reducing, most of the cysteines of AIRAPL are reduced and can perform metal ion scavenging or binding functions.

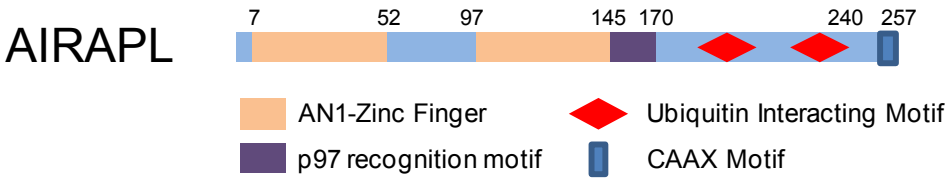

AIRAPL Amino Acid Sequence

```
       10         20         30         40         50         60         70         80         90
MEFPDLGAHC SEPSCQRLDF LPLKCDACSG IFCADHVAYA QHHCGSAYQK DIQVPVCPLC NVPVPVARGE PPDRAVGEHI DRDCRSDPAQ

       100        110        120        130        140        150        160        170        180
QKRKIFTNKC ERSGCRQREM MKLTCDRCGR NFCIKHRHPL DHECSGEGHQ TSRAGLAAIS RAQGLASTST APSPSRTLPS SSSPSRATPQ

       190        200        210        220        230        240        250
LPTRTASPVI ALQNGLSEDE ALQRALELSL AEAKPQVLSS QEEDDLALAQ ALSASEAEYQ QQQAQSRSLK PSNCSLC
```

Figure 2.1.1 – Arrangement of the various domains in AIRAPL
In its primary structure, AIRAPL contains two AN1-Zinc Finger domains and a p97/VCP recognition motif (VIM) followed by two tandem ubiquitin interacting motifs (UIMs) and a C-terminal CAAX motif. Three C-X-2-C sequences (in bold) exist in the amino acid sequence of AIRAPL.

In AIRAPL, there are at least 3 C-X2-C motifs which are common in metal binding proteins or in oxido-reductases (Quan *et al*., 2007) as depicted in Figure 2.1.1.

	Average Cysteine Content in Proteins
AIRAPL Protein	**6.6 %**
Human	2.3 %
Drosophila Melanogaster	1.9 %
Yeast (*Saccharomyces cerevisiae*)	1.3 %
Escherichia Coli	1.1 %
Haloarculamaresmortui	0.5 %
Thermusaquaticus	0.4 %

Table 2.1.1 - A summary of the average cysteine content across different organisms. A correlation is observed between the increase in cysteine content with higher organisms, but AIRAPL stands out amongst the rest, with 6.6% cysteine content, above the human average.

Although the molecular structure of AIRAPL has yet to be solved, based on sequence analyses and homologies, AIRAPL appears to have two AN1-type zinc fingers between amino acids 7-52 and 97-145, respectively, followed by an interesting tandem double-sided ubiquitin interacting motif (UIM) between amino acids 160-240. On the C-terminus of AIRAPL, there is a CAAX motif that can be prenylated, facilitating its anchoring to the ER membrane as a membrane associated protein (UNI-Prot) (Figure 2.1.1).

While the exact function of AIRAPL has yet to be identified, results from the only two publications addressing AIRAPL appear to implicate AIRAPL in protein quality control and degradation. In the presence of arsenic, AIRAPL binds to the 26S proteasome via its N-terminus regions, and this association has been observed to enhance proteasomal proteolysis activities, improving protein degradation rates (Yun *et al*., 2008). Overexpression of AIP-1, the *C.*

elegans homologue of mammalian AIRAPL, increases worm lifespan, confers resistance to protein misfolding and reduces polyglutamine/amyloidogenic-induced toxicity (Hassan *et al*., 2009).

AIRAPL, in recent unpublished data, has been shown to be an adaptor protein of p97/VCP, the major AAA-ATPase involved in ERAD (A. Stanhill, personal communication, Supplementary Figure 2). Pull-down data suggest that p97/VCP binding domain spans AIRAPL amino acids 140-170, a unique sequence with previously unknown homologous motifs. In a recent publication, a new p97/VCP interacting motif known as the VCP interacting motif (VIM), with consensus sequence R-xxxxx-AA-xx-R, was described. Hence, AIRAPL now falls under this new category of p97/VCP interactants (Stapf *et al*., 2011). The p97/VCP binding region in AIRAPL and the different proteins that have been found to contain VIM are shown in Figure 2.1.2.

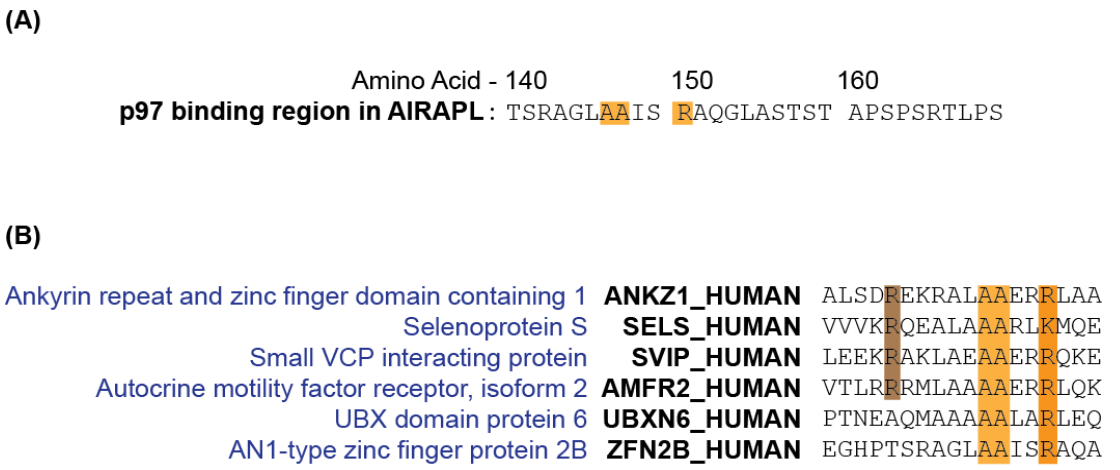

Figure 2.1.2 – p97/VCP binding domain in AIRAPL
AIRAPL has been shown to bind p97/VCP through amino acids 140-170. Based on the recent postulated VIM sequence (R-X5-AA-X2-R), AIRAPL appears to have some degree of homology, which may classify AIRAPL as a VIM-based interactant of p97/VCP.

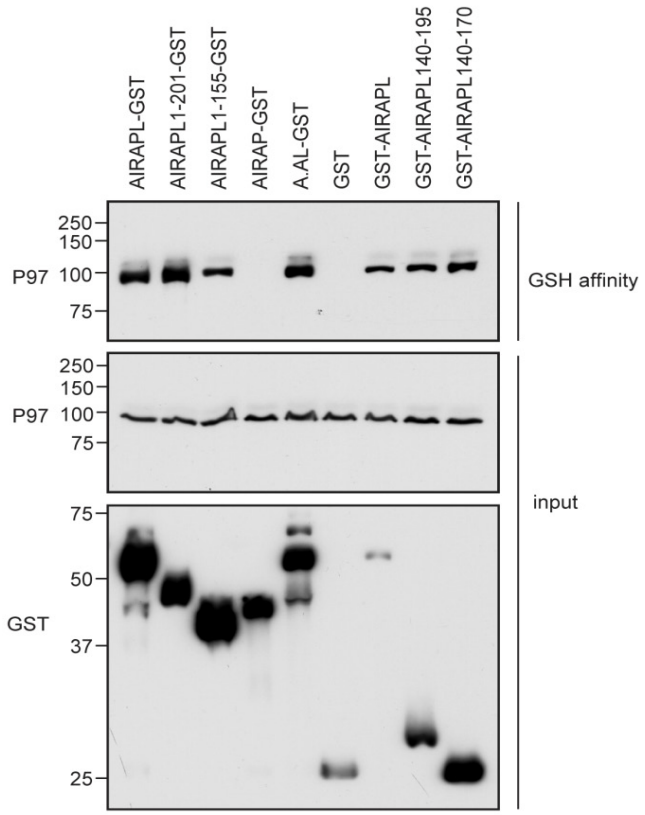

Figure 2.1.3 Pull-down data from Dr Ariel Stanhill (Personal communication). AIRAPL-140-170 was shown to be bind and allow the pull down of p97/VCP.

2.1.2 Aim

With still many open questions concerning AIRAPL, we aimed to use SPR biosensor technology and relevant assays to further characterize AIRAPL and its interactions with other proteins and to contribute to a better understanding of AIRAPL functions.

2.2. Materials & Methods

2.2.1. Plasmids for recombinant protein expression in bacteria

Plasmids for expressing the respective proteins of interests, pET30a-AIRAPL-6xHis, pGEX4T-AIRAPL 140-170-GST and pGEX4T-AIRAPL-160-240-GST were kind gifts from our collaborator Dr. Ariel Stanhill (Technion). pET30-Npl4 and pET26-Ufd1-6xHis (kind gifts from Professor Hemmo Meyer through the addgene plasmid depository (Addgene #21267 & #21266) and the gene p97/VCP with a C-terminal 6x His- tag were described in Chapter 1.2.5. All plasmids have the gene of interest controlled by the *lac* operon, where expression can be induced by lactose or its non-hydrolysable analogue Isopropyl β-D-1-thiogalactopyranoside (IPTG) (Table 2.2.1).

2.2.2. Protein Expression

Proteins were produced recombinantly by *E.coli Rosetta DE3* transformed with the various plasmids for expression of the proteins of interest as described in Chapter 1.2.4. Transformation, bacteria culture and harvesting were performed as described in Chapter 1.2.3. Culture conditions for the different proteins of interest are summarized in Table 2.2.1.

<table>
<tr><th rowspan="2">Plasmid</th><th rowspan="2">Host</th><th rowspan="2">Induction Duration</th><th rowspan="2">IPTG concentration</th><th colspan="2">Temperature</th></tr>
<tr><th>Culture</th><th>Induction</th></tr>
<tr><td>pET26b-p97</td><td rowspan="4">Rosetta DE3</td><td rowspan="6">4 hours</td><td rowspan="2">0.5 mM</td><td>37 °C</td><td>24 °C</td></tr>
<tr><td>pET30a-AIRAPL-6xHis</td><td>16 °C</td><td>16 °C</td></tr>
<tr><td>pET26-Ufd1-6xHis</td><td rowspan="4">1 mM</td><td>37 °C</td><td>37 °C</td></tr>
<tr><td>pET30-Npl4</td><td>37 °C</td><td>16 °C</td></tr>
<tr><td>pGEX4T-AIRAPL 140-170-GST</td><td rowspan="2">BL21-DE3 PLYSS</td><td>37 °C</td><td>37 °C</td></tr>
<tr><td>pGEX4T-AIRAPL-160-240-GST</td><td>37 °C</td><td>37 °C</td></tr>
</table>

Table 2.2.1 – Plasmids, bacterial hosts, culture and induction conditions used in this study

2.2.3. Protein purification

Purification of recombinantly expressed proteins from bacteria was carried out as described in Chapter 1.2.5, with lysis buffer supplemented with 10 mM β-mercaptoethanol (βME) for the purification of AIRAPL. For the purification of AIRAPL-140-170-GST and AIRAPL-160-240-GST the lysis buffer was 50 mM sodium phosphate pH 7.4, 150 mM NaCl, 2 mM β –mercaptoethanol. His-tagged proteins were purified using nickel-affinity chromatography resin as described in Chapter 1.2.5. For the GST tagged proteins, clarified lysate was incubated with GST-Sepharose resin (GE Healthcare) overnight, at a ratio of 1ml resin per lysate equivalent from 1 litre of bacterial culture, with gentle rolling agitation at 4 °C

His-tagged proteins were eluted as described in Chapter 1.2.5., while GST-tagged proteins were eluted with 5mM glutathione in lysis buffer. Eluates from the column were collected in fraction volumes equivalent to the resin volume and with a total elution volume of five times the resin volume. Before snap freezing with liquid nitrogen and storage at -80 ºC, 25 µl from each fraction were used for analysis with SDS-PAGE and Coomassie brilliant blue staining to locate fractions containing the protein of interest. All proteins were stable upon storage except for AIRAPL which precipitates within a single freeze thaw cycle, and thus was produced fresh and used immediately for all AIRAPL related experiments.

2.2.4. Size Exclusion Chromatography

Gel filtration was carried out on a 24 ml Superose 6 10/300GL column as described in Chapter 1.2.5. Similarly, UV Peak fractions eluting at elution

volumes corresponding to the appropriate size of the respective proteins of interests were subjected to SDS-PAGE for verification and purity check before use.

2.2.5. SPR binding assays

Interaction studies were performed on a Biacore 3000 instrument (GE Healthcare) in the same PBS buffer into which the proteins were gel-filtered. The ligands, analytes and immobilization pHs used for the characterization of the following interactions are summarized in Table 2.2.2.

Interaction	Ligand	Analyte	Immobilization pH for ligand	Buffer condition
P97/VCP to AIRAPL	AIRAPL	P97	pH 4	PBS with 0.05% p20 10 mM βME
P97/VCP to AIRAPL-140-170-GST	AIRAPL-140-170-GST	P97	pH 4.5	PBS with 0.05% p20 2 mM βME
AIRAPL-160-240-GST to	Tetraubiquitin	AIRAPL-160-240-GST	pH 4.5	PBS with 0.05% p20 2 mM βME

Table 2.2.2 – Immobilization buffers and pHs for the respective ligands in SPR binding assays
AIRAPL was immobilized at pH 4 whilst both AIRAPL-140-170-GST and K48-tetraubiquitin were immobilized at pH 4.5.

Immobilization of ligands was carried out as described in Chapter 1.2.9.2, and immobilized surfaces were allowed to stabilize overnight before binding experiments were carried out. All binding assays were carried out at a flow rate of 100 µl/min, with the analyte injected for one minute followed by 15 minutes of dissociation. The competition assay was carried out at a flow rate of 20 µl/min. All sensorgrams from the SPR binding experiments were referenced to a control flow cell to eliminate contributions of non-specific bindings,

analyzed and if necessary, fitted to the bivalent analyte model, in BiaEvaluation 3.1 software (GE Healthcare).

2.2.5.1. p97/VCP-AIRAPL interaction

AIRAPL (3,800 RUs) was immobilized on a flow cell of a sensorchip. The flow cell used as a reference was left unmodified as there was very low non-specific binding. Seven different concentrations of p97/VCP in duplicates were serially injected through the reference and AIRAPL surfaces.

2.2.5.2. p97/VCP-AIRAPL-140-170 interaction

AIRAPL-140-170 (3,600 RUs) was immobilized on a flow cell of a sensorchip with an unmodified flow cell used as a reference. A concentration series of p97/VCP in duplicates was then injected across the surface.

2.2.5.3. AIRAPL-ubiquitin interaction

Monoubiquitin, K48-diubiquitin and K48-tetraubiquitin, purchased from Boston Biochem (U100H, UC-200, UC-210, Cambridge, MA), were immobilized on flow cells 2, 3 and 4, respectively, with flow cell 1 used as a reference flow cell. Full length AIRAPL was injected across the surface and the resulting sensorgrams were normalized to immobilization levels for comparison.

2.2.5.4. Interaction of AIRAPL-160-240 with tetraubiquitin

K48-tetraubiquitin (UC-210) was immobilized on a CM5 sensorchip flow cell via amine coupling to a level of 6,000 RUs. A concentration series of AIRAPL-160-240 in two-fold dilutions was injected sequentially across the K48-tetraubiquitin surface and an empty flow cell which was used as a reference.

2.2.6. AIRAPL and Ufd1/Npl4 competition experiments: AIRAPL was immobilized on a flow cell as previously described. Freshly purified p97/VCP was injected across immobilized AIRAPL and captured to a level of approximately 500 RUs, before co-injection of either running buffer or freshly purified Ufd1/Npl4 hetero-dimer at different concentrations to observe competition with AIRAPL. At the end of the competition assay, the surface was allowed to return back to baseline, or regenerated with a quick pulse of 750 mM NaCl.

2.2.7 Differential Scanning fluorimetry

DSF was performed on 1 µM of purified AIRAPL using the method described in Chapter 1.2.11. AIRAPL was unfolded in the presence and absence of ligands, such as EDTA, magnesium chloride and zinc chloride at 1 mM concentration. In the presence of zinc chloride AIRAPL precipitated rapidly upon heating resulting in no readout. Curves were exported from the Biorad IQ2 real-time PCR software into Microsoft Excel for plotting and analyses.

2.2.8 De-ubiquitinase protection assay

Eleven de-ubiquitinases (DUBs) were purchased from Boston Biochem (K-E10) together with the K48-tetraubiquitin substrate (UC-210). De-ubiquitination reactions were carried out in 50mM HEPES pH 7.4, 150mM NaCl, 0.5mM EDTA and 1mM DTT at 37 °C . In each reaction tube, K48- tetraubiquitin (2µg in reaction buffer), was mixed with either AIRAPL (5 µM) or buffer and each of the DUBs was added in the concentrations range recommended by BostomBiochem (Table 2.2.3).

Deubiquitinase	Recommended Concentration	Concentration used (Final)
Isopeptidase T	0.05-5 nM	1 nM
UCH-L3	0.05-5 nM	1 nM
UCH-L1	0.05-5 nM	1 nM
Ataxin-3	1-5 µM	6 µM
A20CD	1-5 µM	5.5 µM
BAP1	1-5 µM	3 µM
USP2CD	1-5 µM	6 µM
USP7FL	1-5 µM	2 µM
USP8FL	1-5 µM	2 µM
Otubain1	1-5 µM	5 µM
USP14	1-10 µM	7.5 µM

Table 2.2.3. Deubiquitinases and their respective final concentrations used in our assay

To stop the reaction, 5µl were collected from the DUBs reaction mixtures at time intervals of 5, 30, 60 and 120 minutes and10% SDS, 0.5M Tris-HCl pH 6.8, 0.05% (w/v) Bromophenol blue, 20% (v/v) glycerol, 50 mM β-mercaptoethanol was added. Samples were resolved by 15% SDS-PAGE (250V, 38 minutes) and subjected to immunoblotting. Individual 10-well gels were used for each respective DUB, where samples in the presence or absence of AIRAPL were loaded onto the same gel to eliminate bias. All 11 gels from the reactions of 11 different DUBs were blotted concurrently. For the

immuno-blotting, gels were electro-blotted onto polyvinylidene fluoride (PVDF) membranes (Pall, 0.2 µm pore size) for one hour at 50 volts, membranes were blocked with 10% (v/v) milk in PBS containing 1% (v/v) Tween-20 (PBST), and probed with a rabbit anti-ubiquitin antibody (Santa Cruz, SC-1933, 200 µg/ml) at 1:500 dilution in PBST by overnight shaking at 4 °C. Membranes were washed three times (20ml PBST for 5 minutes with shaking) and incubated with a horse-radish peroxidase (HRP)-conjugated goat-anti-rabbit antibody (Santa ruz SC-2004, 200 µg/ml) at 1:5000 dilution. Membranes were developed and visualized with the use of enhanced chemiluminiscent (ECL) substrates (Amersham ECL Plus) and Kodak X-Ray film (Kodak, L5157 Medical). Multiple exposures were taken, from 5 seconds to 1 minute to ensure that the results would be linear and not over-exposed.

2.3. Results

2.3.1. Protein Purification

The recombinant proteins used in our various assays were expressed in bacteria and purified. Using 10% SDS-PAGE and Coomassie Blue staining to check the proteins eluting at the appropriate respective elution volumes on our calibrated Superose 6 column, we were able to demonstrate that all the proteins prepared were of >95% purity (Figure 2.3.1). p97/VCP and Ufd1/Npl4 were purified as hexamers and heterodimers, respectively, as described in Chapter 1.3.1.

2.3.2. AIRAPL is an unstable protein

We attempted to gain an indication for the AIRAPL stability by determining its melting point using DSF. We observed that AIRAPL started to unfold at 40 °C and melted at 47 °C, which is a rather low temperature (Figure 2.3.2). Neither addition of magnesium ions nor EDTA that could strip bound metal ions from AIRAPL appeared to have any effect on stabilizing AIRAPL. This may explain the short half-life of AIRAPL activity seen in our experiments, with the protein losing its activity just a few hours after purification. Thus AIRAPL had to be freshly purified just before performing any experiment. Based on computational predictions via the ProtParam software of UNI-Prot database, the instability index of AIRAPL was computed to be 62.32, implying that the protein is unstable (Noguchi *et al*., 2005; ProtParam).

Figure 2.3.1. Proteins used in studies were purified to homogeneity
Gel filtration purification of AIRAPL (A), AIRAPL-140-170-GST or AIRAPL-160-240 GST (B), and p97/VCP or Ufd1/Npl4 (C) on a Superose 6 300/10 GL column. All peak fractions containing the proteins of interest were resolved by 10% SDS-PAGE followed by Coomassie Blue staining to assess purity (D).

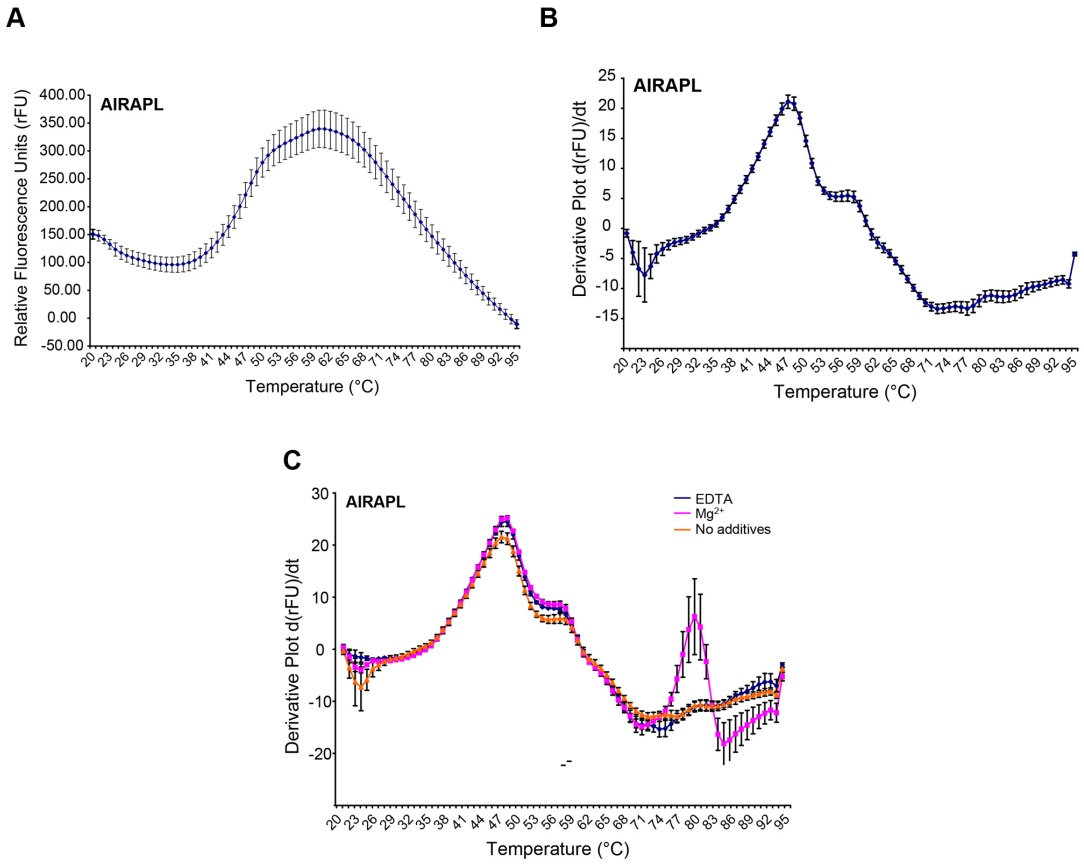

Figure 2.3.2. AIRAPL demonstrates in Differential Scanning Fluorimetry properties of an unstable protein with a low melting point
DSF experiments show that AIRAPL begins to unfold at 40 °C, as seen from the sigmoidal fluorescence readout curve (A), and melts at 47 °C (B), with neither magnesium ions nor EDTA (1mM) having any effect in stabilizing the AIRAPL (C) .

2.3.3. AIRAPL, a novel adaptor protein that binds to p97/VCP

p97/VCP at a concentration of 72 nM was serially diluted two-fold into a series of seven concentrations and sequentially injected across immobilized AIRAPL on a Biacore 3000 instrument. Resulting sensorgrams were referenced using an empty flow cell in order to subtract the bulk refractive index and non-specific binding contributions, to give the specific binding curves that were best fitted to the bivalent analyte model in BiaEvaluation 3.1 (GE Healthcare). Curves (colored) were overlaid with the mathematical fits (black), and the

resulting affinity value of 1.12 μM was calculated from the major association and dissociation constants corresponding to the main component of the interaction (Figure 2.3.3). The affinity of the interaction between p97/VCP and AIRAPL-140-170 (Figure 2.3.3 B,D), which was found to around 3 μM, was of the same order of magnitude as the affinity of the interaction between p97/VCP and the full length AIRAPL (Figure 2.3.3 A,C).

A

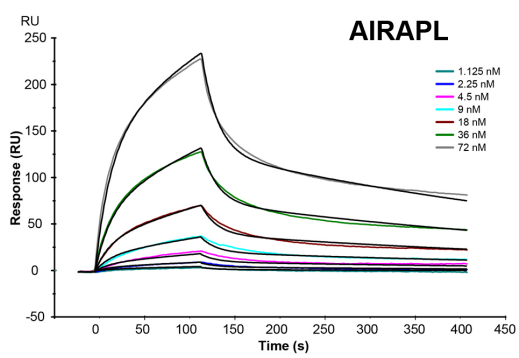

B

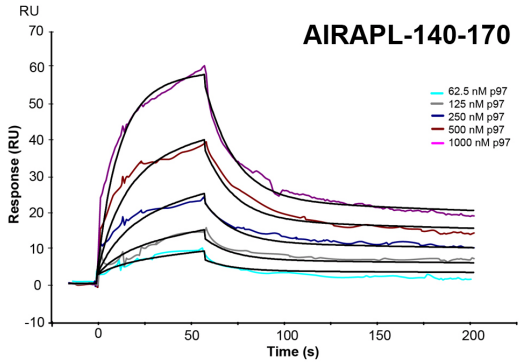

C

Binding of p97/VCP to AIRAPL (full length)	k_{a1} (1/Ms)	k_{d1} (1/s)	k_{a2} (1/RUs)	k_{d2} (1/s)	Affinity
	8.81E+04	0.0991	1.42E-05	2.10E-03	1.12 μM

D

Binding of p97/VCP to AIRAPL-140-170	k_{a1} (1/Ms)	k_{d1} (1/s)	k_{a2} (1/RUs)	k_{d2} (1/s)	Affinity
	1.77E+04	5.29E-02	1.21E-04	5.49E-04	2.99 μM

Figure 2.3.3. Binding sensorgrams of the interactions between p97/VCP and AIRAPL or AIRAPL 140-170
Serial dilutions of p97/VCP were injected serially across immobilized full length AIRAPL (A) or across immobilized AIRAPL-140-170 (B). Referenced curves were best fitted to the bivalent analyte model and the respective binding parameters are summarized in (C) and (D). p97/VCP binds to AIRAPL with an affinity of 1.12 μM for the main component of the interaction.

2.3.4. AIRAPL shows specific binding to K48-tetraubiquitin

Monoubiquitin, K48-diubiquitin and K48-tetraubiquitin were immobilized on separate flow cells on the same sensorchip, with full length AIRAPL serially injected across the surface of all flow cells. Binding responses obtained were normalized to immobilization levels for comparison. AIRAPL exhibited little or no binding to mono- or K48-di-ubiquitin, whereas a large avid binding response was observed to the K48-tetraubiquitin (Figure 2.3.4 A). Given the instability of the full length AIRAPL, which complicated affinity measurements, the AIRAPL-160-240 protein, which contains only the tandem UIM domains of AIRAPL, was used to determine the binding affinities.

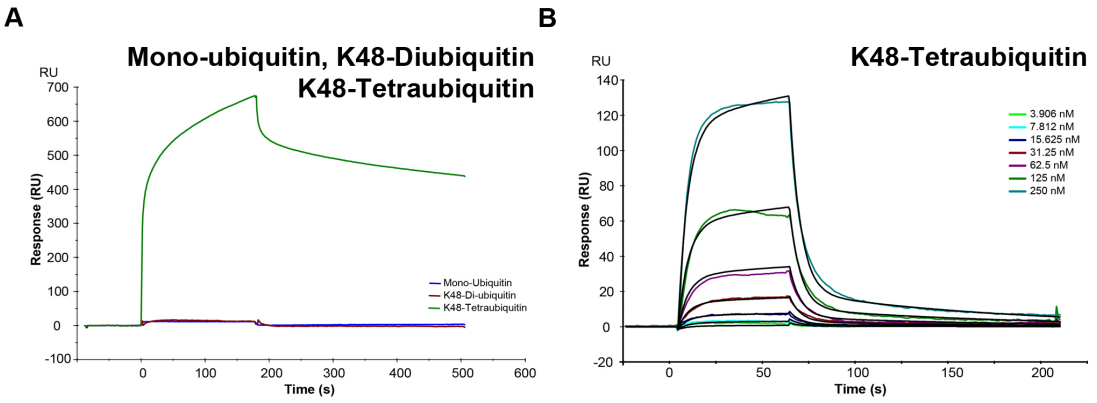

C

Binding of AIRAPL-160-240 to K48-Ub_4	ka1 (1/Ms)	kd1 (1/s)	ka2 (1/RUs)	kd2 (1/s)	K_D[1]
	2.56E+04	0.171	2.05E-06	4.42E-03	**6.68 µM**

Figure 2.3.4 AIRAPL binds K48-tetraubiquitin with an affinity of around 7 µM
Full length AIRAPL shows high affinity to only K48-tetraubiquitin, with minimal binding to either monoubiquitin or K48-diubiquitin (A). AIRAPL-160-240 in two-fold dilutions starting with 250 nM, was injected across immobilized K48-tetraubiquitin (B). The fit (black lines) to the bivalent-analyte model are overlaid with the experimental curves (colored lines), and the calculated affinity for the main component of the interaction was 6.68 µM. The binding parameters of AIRAPL-160-240 are presented (C).

Purified AIRAPL-160-240 in serial 2-fold dilutions were sequentially injected across immobilized K48-tetraubiquitin, using an empty flow cell as a binding reference for correction to obtain specific binding curves. Referenced sensorgrams were analysed in Bia-Evaluation 3.1 and best fitted to the bivalent-analyte model (Figure 2.3.4 B). The use of this model was justified by the presence of more than 1 binding domain, i.e. 2 UIMs in tandem in AIRAPL-160-240. We conclude that AIRAPL binds K48-tetraubiquitin with an affinity of around 7 μM (Figure 2.3.4 C).

2.3.5. Ufd1/Npl4 and AIRAPL are mutually exclusive adaptor proteins of p97/VCP

p97/VCP reproducibly captured by immobilized AIRAPL in every cycle was co-injected with either UN or buffer in the dissociation phase. In the presence of increasing UN concentrations, more p97/VCP was dissociated from AIRAPL (Figure 2.3.5), suggesting that there was mutual exclusivity between these adaptor proteins. If UN and AIRAPL could bind to p97/VCP simultaneously, the dissociation would appear lower in the presence of UN as compared to buffer, since a subsequent binding event of UN to the AIRAPL-bound p97/VCP would be observed.

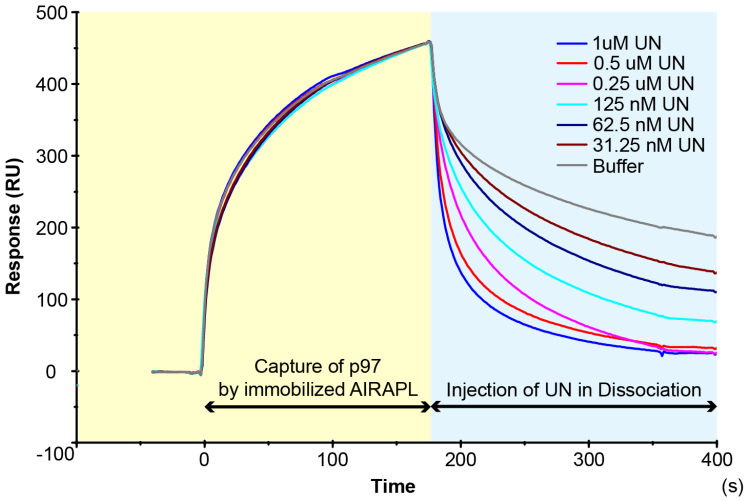

Figure 2.3.5. Ufd1/Npl4 binding to p97/VCP increases the dissociation of the p97/VCP-AIRAPL complex
Approximately 500 RUs of p97/VCP were captured by AIRAPL in sample injection, before either buffer, or UN at the indicated concentrations were injected in the dissociation phase.

2.3.6. AIRAPL modulates the activities of various de-ubiquitinating enzymes

As AIRAPL is a K48-tetraubiquitin binder, which is the typical minimum chain length needed for p97/VCP-UN or proteasomal recognition, we wanted to determine if AIRAPL can serve the role to protect K48-tetraubiquitin chains from de-ubiquitinating enzymes (DUBs) that modulate protein degradation processes. To that end, we tested the effect of AIRAPL on the activities of 11 DUBs with K48-tetraubiquitin as a substrate. The de-ubiquitination process in the absence or presence of AIRAPL was assessed at four time points, 5, 30, 60 and 120 minutes, and the amount of the remaining K48-tetraubiquitin was probed by immuno blotting. Four DUB enzymes, UCH-L3, UCH-L1, Ataxin-3 and BAP1 were unaffected by the presence of AIRAPL during their de-ubuqitination activity assay and USP9 was only slightly inhibited (Figure 2.3.6 A). AIRAPL inhibited and almost blocked the deubiquitination activity of three

DUBs, A20, Otubain-1, USP14 (Figure 2.3.6 B), while enhancing the activity of three other DUBs, Isopeptidase T, USP2 and USP7 (Figure 2.3.6 C). In order to ensure that the acceleration in DUB activity was not an artifact due to poor sample loading or poor immunogenecity during the blot process, experiments with the various DUBs were replicated in an end-point method, where the K48-tetraubiquitin levels were assessed by immuno blot at time 0 and after 15 minutes, with one positive control (Otubain-1 that was inhibited by AIRAPL) and one negative control (UCH-L1 that was not affected by AIRAPL).

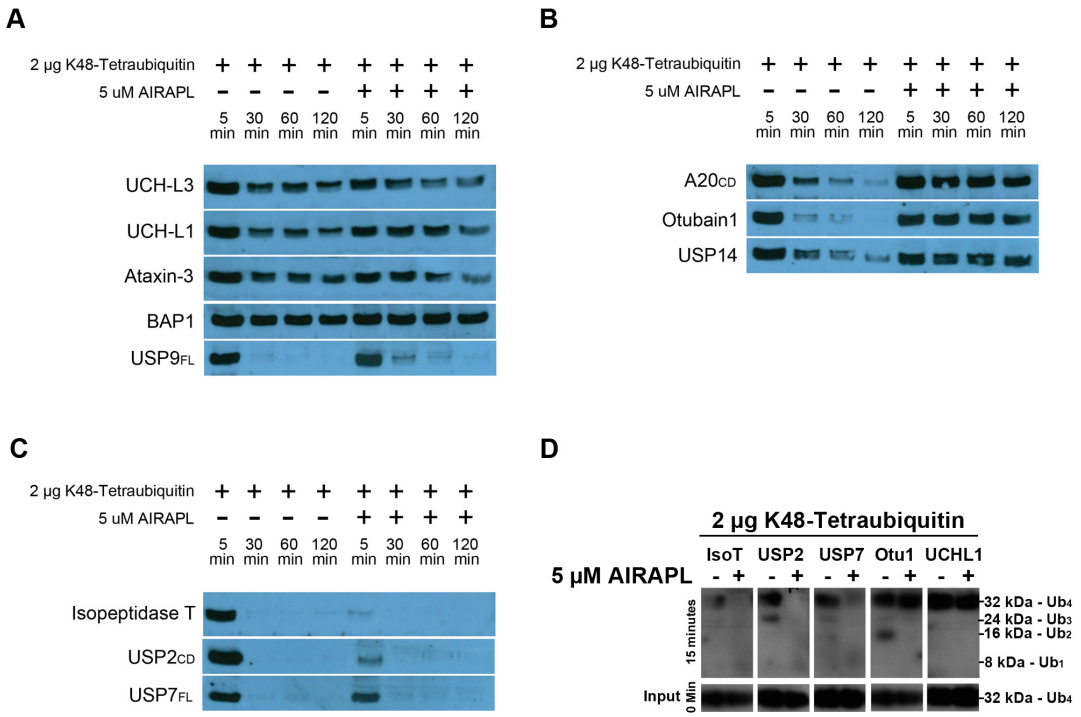

Figure 2.3.6. AIRAPL affects the deubiquitination activity of several DUBs
K48-tetraubiquitin (2 µg) was used as a substrate and the indicated DUBs (for recommended concentrations, see Table 2.2.3, above) were incubated for the indicated times in the absence (-) or presence (+) of AIRAPL (5 µM) The amounts of the remaining K48-tetraubiquitin were detected by SDS-PAGE and immuno blotting, using a rabbit anti-ubiquitin antibody followed by HRP-conjugated goat-anti-rabbit antibody visualized with ECL. DUBs unaffected by AIRAPL (A). DUBs inhibited by AIRAPL (B). DUBs enhanced by AIRAPL (C). An end point assay was carried out on Isopeptidase T, USP2, USP7 with Otu1 and UCHL1 as controls. Similarly, after 15 minutes, in the presence of AIRAPL, the K48-tetraubiqutin band became largely diminished as compared to Otu1 or UCH-L1 (D) .

A chemi-luminiscence substrate (Amersham ECL-Prime) stronger than the Amersham ECL-Plus was used to develop the blot. Again, we observed that for Isopeptidase T, USP2 and USP7 deubiquitination rates were accelerated in the presence of AIRAPL (Figure 2.3.6 D).

2.4. Discussion

Full length AIRAPL is predicted as unstable under the protein instability index (II) value of 62.32. Indeed, when working with AIRAPL, the protein is highly unstable and very prone to aggregation. Using DSF, AIRAPL melts at a low temperature of 47 ºC. EDTA or magnesium ions have no effect on stabilizing the protein (Figure 2.3.2). Given the instability of the protein, it was preferentially immobilized by amine-coupling as a ligand onto the carboxy-methyldextran on the surface of a sensorchip. This immobilization prevented aggregation and precipitation that could render the protein inactive, allowing us to determine the binding kinetics of p97/VCP to AIRAPL. We were unable to use ubiquitin as an analyte due to the high costs of the commercially available ubiquitin chains purchased from Boston Biochem.

In our experiments, the binding of AIRAPL to p97/VCP was validated and that this binding occurs through the unique VIM domain located in the 140-160 region of AIRAPL was confirmed. Both full length AIRAPL and its truncated AIRAPL-140-170 version containing only the VIM domain interact with p97/VCP with similar micromolar affinity for the main component of the interaction, (1.12 μM and 2.99 μM, respectively) Figure 2.3.3. The affinities were calculated from a bivalent analyte fit which fitted best to our experimental data. The use of the bivalent analyte model is justified by p97/VCP's multiple valency, being homo-hexamer with six N-terminus domains each having its own capacity to mediate binding.

For the ubiquitin binding experiments, ubiquitin chains were costly and therefore were immobilized as ligands on a sensorchip in respective flow cells.

AIRAPL shows minimal binding to monoubiquitin and K48-diubiquitin, and instead, AIRAPL recognizes K48-tetraubiqutin avidly, suggesting that ubiquitin chain length plays a role in substrate recognition also by AIRAPL, similar to the recognition by p97/VCP-U/N or the 26S proteasome (Dai and Li, 2001; Verhoef *et al*., 2009). Unpublished data by Dr. Ariel Stanhill suggest a minimum of 3 K48-linked ubiquitins to be the recognition motifs by AIRAPL's tandem UIMs (personal communication). With the use of AIRAPL-160-240 fragment, although it may not be fully representative of the actual full length protein, we were able to determine the affinity of K48-tetraubiquitin binding to the two tandem double-sided UIMs to be around 7 μM. The sensorgram data were similarly best fitted to the bivalent analyte model due to the bivalency of the two tandem UIMs within AIRAPL and its AIRAPL-160-240 fragment (Figure 2.3.4).

Using a competition assay, where p97/VCP is captured by immobilized AIRAPL on an SPR sensorchip, and competed off by Ufd1/Npl4, we were able to observe in real time the competition process, where increasing concentrations of UN appeared to compete more p97/VCP from AIRAPL, suggesting mutual exclusivity (Figure 2.3.5). If UN and AIRAPL could bind to p97/VCP simultaneously, the dissociation would appear lower in the presence of UN as compared to buffer and even further decreases with increasing UN, reflecting subsequent binding of UN to the AIRAPL-bound p97/VCP. With both UN and AIRAPL being adaptor proteins of p97/VCP that recognize K48-ubiquitin chains, we speculate the mutual exclusivity of UN and AIRAPL in binding to p97/VCP to be important for substrate (K48-ubiquitin) hand over before retrotranslocation in ERAD processes.

K48-linked polyubiquitination of substrates is necessary to facilitate proper recognition of ERAD substrates, especially in the retro-translocation step where p97/VCP-UN pulls substrates out of the ER and hands it over to the 26S proteasome for degradation. In the cell, proteasomal degradation is often the outcome of two counteracting processes, balancing between ubiquitin chain removal by DUBs resulting in prolonged existence of a substrate, as opposed to recognition and transfer to the proteasome leading to degradation (Lecker *et al*., 2006; Ravid and Hochstrasser, 2008).

To conclude, AIRAPL is localized to the ER, avidly binding K48-tetraubiquitin characteristic of retro-translocated misfolded ERAD substrates and its binding to p97/VCP is mutually exclusive with Ufd1/Npl4 the p97/VCP complex essential for retro-translocation and ERAD. Therefore, we have speculated that AIRAPL's function on the ER membrane in binding K48-tetraubiquitin may serve to regulate or balance ERAD and its timing. AIRAPL can achieve this regulatory function through delaying or blocking DUBs, thus enhancing the recognition of ubiquitinated ERAD substrates by p97/VCP-UN for retro-translocation and subsequent degradation by the 26S proteasome. In order to test our hypothesis, a de-ubiqutinase protection assay was performed. Indeed, out of the eleven common DUBs tested, three DUBs, A20, Otubain-1 and USP14 could be strongly inhibited and almost entirely blocked by AIRAPL, while three DUBs, IsoT, USP2 and USP7 were activated by AIRAPL (Figure 2.3.6 and Table 2.4)

DUB Enzyme	Biological Activity
Isopeptidase T	Turnover of unanchored ubiquitin chains
Ubiquitin C-terminal Hydrolase L3	Neuro-specific hydrolases targeting amido or c-terminus ubiquitin conjugates
Ubiquitin C-terminal Hydrolase L1	
Ataxin-3	Hydrolysis of complex ubiquitin chains
A20	Regulation of NFKB function by stabilizing IKB which inhibits NFKB.
BAP1	DUB localized to the nucleus, involved in deubiquitination activities pertaining to histones and nuclear proteins, i.e BRCA1
Ubiquitin Specific Peptidase 2 (USP2)	Stabilization of cyclin D1 by deubiquitinations
Ubiquitin Specific Peptidase 7 (USP7)	Herpes-associated Ubiquitin Specific Protease, targets p53 for deubiquitination stabilizing p53 function
Ubiquitin Specific Peptidase 8 (USP8)	Non-specific deubiquitination, involved in endocytic processes
Otubain-1	Specific K48-deubiqutinase, involved in regulating ERAD
Ubiquitin Specific Peptidase 14 (USP14)	Involved in the degradation of chemokine receptor CXCR4

Table 2.4. The biological activities of the 11 DUBs tested for the effects of AIRAPL
The biological activities of the DUBs tested have been previously described.(Berlin *et al*., 2010; Bott *et al*., 2011; Hadari *et al*., 1992; Jensen *et al*., 1998; Larsen *et al*., 1996; Larsen *et al*., 1998; Rumpf and Jentsch, 2006; Shan *et al*., 2009; Shembade and Harhaj, 2012; Sheng *et al*., 2006; Wilkinson *et al*., 1992; Winborn *et al*., 2008; Woo *et al*., 1997). Based on our results, DUBs shaded in blue are inhibited by AIRAPL, while DUBs shaded in orange are activated by AIRAPL, and unshaded DUBs remain unaffected by AIRAPL

To gain insights to the underlying mechanism underlying the effects of AIRAPL on DUBs activities, we looked for the reported biological activities of the various DUBs tested in our assay, as summarized in Table 2.4. Interestingly, YOD1, the yeast homologue of Otubain-1, one of the 3 DUBs that were inhibited by AIRAPL, is another adaptor protein of p97/VCP. This DUB has been shown to be involved in the regulation of the p97/VCP-mediated retro-translocation of ERAD substrates from the ER by removing polyubiqutin chains from substrates (Rumpf and Jentsch, 2006). Also the

expression of non-functional YOD1 results in stabilization and accumulation of ERAD substrates (Ernst *et al.*, 2009). Hence, our finding that AIRAPL inhibits the DUB activity of Otubain-1 adds yet another level of regulation to ERAD. It suggests that AIRAPL may function to down-regulate the retro-translocation processes executed by p97/VCP through blocking Otubain-1 activity, thus attenuating ERAD.

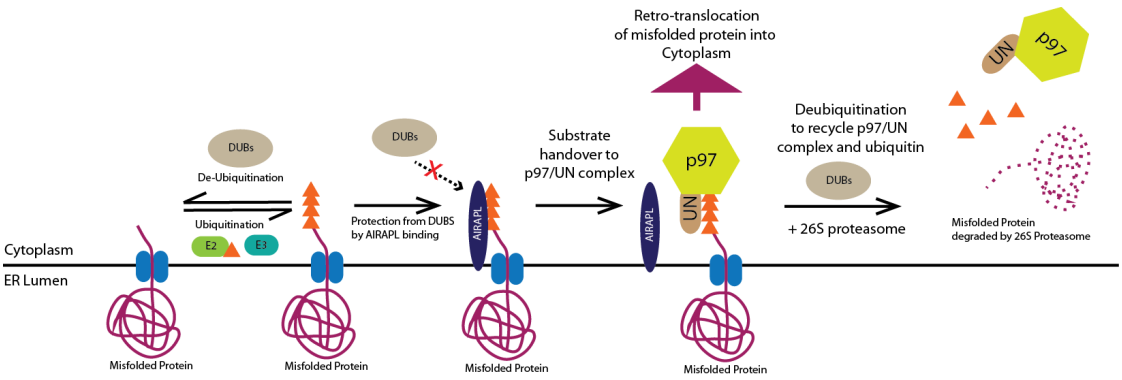

Figure 2.4.1 A model on substrate protection and handover mediated by AIRAPL In ERAD, ubiquitinating and de-ubiquitinating enzymes regulate ubiquitin chain length on the substrate to be retro-translocated. AIRAPL on the ER membrane binds to K_{48}-Tetraubiquitin chains, protecting them from DUB activity, allowing subsequent handover to p97-UN complex for retrotranslocation for degradation by the 26S Proteasome. DUBs act to recycle both p97-UN and ubiquitin moieties.

We propose the following scenario, with the understanding that ubiquitin chains on the ER surface can be easily targeted by cytoplasmic DUBs. During the initiation of retro-translocation, as the misfolded protein in the ER is being ubiquitinated by ubiquitin conjugating E2 and ubiquitin ligase E3 enzymes, it should reach a critical threshold of ubiquitin chain length on the substrate (i.e. above 3 K48-linked ubiquitins). Then AIRAPL could bind to it avidly and protect the ubiquitin chains from DUBs, preventing premature ubiquitin hydrolysis which will impede the ERAD process. p97/VCP can then be recruited to AIRAPL. Joining of Ufd1/Npl4, the main p97/VCP adaptor proteins

involved in retro-translocation, which are mutually exclusive to AIRAPL, competes p97/VCP away from AIRAPL. The leaving AIRAPL dissociates from the polyubiquitin chains and hands over the substrate to p97/VCP-UN. From this step, the p97/VCP-UN-polyubiquitinated protein complex, through ATP hydrolysis, extracts the proteins out of the ER. Otubain-1, in the absence AIRAPL, will then bind to p97/VCP when the protein is totally retro-translocated, to remove the polyubiquitin and release p97/VCP-UN from the substrate, allowing recycling of p97/VCP-UN for re-use. This cycle may reflect the regulation, timing and processivity of ERAD.

2.5 References for Chapter 2

Berlin, I., Higginbotham, K.M., Dise, R.S., Sierra, M.I., Nash, P.D., 2010. The deubiquitinating enzyme USP8 promotes trafficking and degradation of the chemokine receptor 4 at the sorting endosome. J Biol Chem 285, 37895-37908.

Bott, M., Brevet, M., Taylor, B.S., Shimizu, S., Ito, T., Wang, L., Creaney, J., Lake, R.A., Zakowski, M.F., Reva, B., Sander, C., Delsite, R., Powell, S., Zhou, Q., Shen, R., Olshen, A., Rusch, V., Ladanyi, M., 2011. The nuclear deubiquitinase BAP1 is commonly inactivated by somatic mutations and 3p21.1 losses in malignant pleural mesothelioma. Nat Genet 43, 668-672.

Dai, R.M., Li, C.C., 2001. Valosin-containing protein is a multi-ubiquitin chain-targeting factor required in ubiquitin-proteasome degradation. Nat Cell Biol 3, 740-744.

Ernst, R., Mueller, B., Ploegh, H.L., Schlieker, C., 2009. The otubain YOD1 is a deubiquitinating enzyme that associates with p97 to facilitate protein dislocation from the ER. Mol Cell 36, 28-38.

Hadari, T., Warms, J.V., Rose, I.A., Hershko, A., 1992. A ubiquitin C-terminal isopeptidase that acts on polyubiquitin chains. Role in protein degradation. J Biol Chem 267, 719-727.

Hassan, W.M., Merin, D.A., Fonte, V., Link, C.D., 2009. AIP-1 ameliorates beta-amyloid peptide toxicity in a Caenorhabditis elegans Alzheimer's disease model. Hum Mol Genet 18, 2739-2747.

Jensen, D.E., Proctor, M., Marquis, S.T., Gardner, H.P., Ha, S.I., Chodosh, L.A., Ishov, A.M., Tommerup, N., Vissing, H., Sekido, Y., Minna, J., Borodovsky, A., Schultz, D.C., Wilkinson, K.D., Maul, G.G., Barlev, N., Berger, S.L., Prendergast, G.C., Rauscher, F.J., 3rd, 1998. BAP1: a novel ubiquitin hydrolase which binds to the BRCA1 RING finger and enhances BRCA1-mediated cell growth suppression. Oncogene 16, 1097-1112.

Larsen, C.N., Price, J.S., Wilkinson, K.D., 1996. Substrate binding and catalysis by ubiquitin C-terminal hydrolases: identification of two active site residues. Biochemistry 35, 6735-6744.

Larsen, C.N., Krantz, B.A., Wilkinson, K.D., 1998. Substrate specificity of deubiquitinating enzymes: ubiquitin C-terminal hydrolases. Biochemistry 37, 3358-3368.

Lecker, S.H., Goldberg, A.L., Mitch, W.E., 2006. Protein degradation by the ubiquitin-proteasome pathway in normal and disease states. J Am Soc Nephrol 17, 1807-1819.

NCBI-GENE, ZFAND2B zinc finger, AN1-type domain 2B [Homo sapiens]. http://www.ncbi.nlm.nih.gov.

Noguchi, M., Takata, T., Kimura, Y., Manno, A., Murakami, K., Koike, M., Ohizumi, H., Hori, S., Kakizuka, A., 2005. ATPase activity of p97/valosin-containing protein is regulated by oxidative modification of the evolutionally conserved cysteine 522 residue in Walker A motif. J Biol Chem 280, 41332-41341.

ProtParam, ExPASy - ProtParam tool.

Quan, S., Schneider, I., Pan, J., Von Hacht, A., Bardwell, J.C., 2007. The CXXC motif is more than a redox rheostat. J Biol Chem 282, 28823-28833.

Ravid, T., Hochstrasser, M., 2008. Diversity of degradation signals in the ubiquitin-proteasome system. Nat Rev Mol Cell Biol 9, 679-690.

Rumpf, S., Jentsch, S., 2006. Functional division of substrate processing cofactors of the ubiquitin-selective Cdc48 chaperone. Mol Cell 21, 261-269.

Shan, J., Zhao, W., Gu, W., 2009. Suppression of cancer cell growth by promoting cyclin D1 degradation. Molecular cell 36, 469-476.

Shembade, N., Harhaj, E.W., 2012. Regulation of NF-kappaB signaling by the A20 deubiquitinase. Cell Mol Immunol 9, 123-130.

Sheng, Y., Saridakis, V., Sarkari, F., Duan, S., Wu, T., Arrowsmith, C.H., Frappier, L., 2006. Molecular recognition of p53 and MDM2 by USP7/HAUSP. Nat Struct Mol Biol 13, 285-291.
Stapf, C., Cartwright, E., Bycroft, M., Hofmann, K., Buchberger, A., 2011. The general definition of the p97/valosin-containing protein interacting motif (VIM) delineates a new family of p97 co-factors. J Biol Chem.

UNI-Prot, AN1-type zinc finger protein 2B. Q4KLG9.

Verhoef, L.G., Heinen, C., Selivanova, A., Halff, E.F., Salomons, F.A., Dantuma, N.P., 2009. Minimal length requirement for proteasomal degradation of ubiquitin-dependent substrates. Faseb J 23, 123-133.

Wilkinson, K.D., Deshpande, S., Larsen, C.N., 1992. Comparisons of neuronal (PGP 9.5) and non-neuronal ubiquitin C-terminal hydrolases. Biochemical Society transactions 20, 631-637.

Winborn, B.J., Travis, S.M., Todi, S.V., Scaglione, K.M., Xu, P., Williams, A.J., Cohen, R.E., Peng, J., Paulson, H.L., 2008. The deubiquitinating enzyme ataxin-3, a polyglutamine disease protein, edits Lys63 linkages in mixed linkage ubiquitin chains. J Biol Chem 283, 26436-26443.

Woo, S.K., Baek, S.H., Lee, J.I., Yoo, Y.J., Cho, C.M., Kang, M.S., Chung, C.H., 1997. Purification and characterization of a new ubiquitin C-terminal hydrolase (UCH-1) with isopeptidase activity from chick skeletal muscle. Journal of biochemistry 121, 684-689.

Yun, C., Stanhill, A., Yang, Y., Zhang, Y., Haynes, C.M., Xu, C.F., Neubert, T.A., Mor, A., Philips, M.R., Ron, D., 2008. Proteasomal adaptation to environmental stress links resistance to proteotoxicity with longevity in Caenorhabditis elegans. Proc Natl Acad Sci U S A 105, 7094-7099.

Chapter 3

Development and Validation of a novel real-time ATP sensor

3.1 Introduction

Adenosine triphosphate (ATP) is the energy currency of life driving almost all energy requiring processes essential for sustaining life by its constant cyclic turnovers, hydrolysis and reformations. In living organisms, ATP is used for energy provision in a myriad of cellular activities. Examples of activities are DNA/RNA/Protein synthesis, cellular trafficking, protein structure and dynamics i.e. actin polymerizations, maintenance of ionic gradients by ATP driven pumps, proteolysis and proteasomal breakdown of proteins and mechanical force generation by proteins. (Boyer *et al*., 1975; Dean *et al*., 2001; Korn *et al*., 1987; Kuznetsov and Musajev, 1988; Lecker *et al*., 2006; Majumdar and Frankel, 1973; Rolfe and Brown, 1997; Tanaka *et al*., 1983; Zerangue *et al*., 2001). This energy storage and provision by ATP is achieved due to the presence of two high-energy phosphodiester bonds which liberate 30.6 kilojoules of energy per mole upon hydrolysis (Figure 3.1.1). Figure 3.1.2 shows many common processes where ATP is required.

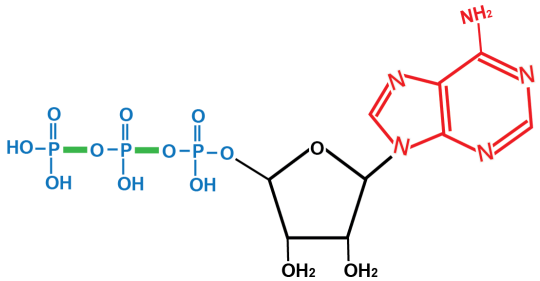

Figure 3.1.1 – Structure of Adenosine Triphosphate (ATP). ATP is made up of 3 moieties: the Ribose sugar (black), the Adenosine moiety (Red) and three phosphate groups (Blue) linked to each other by phosphodiester bonds (Green).

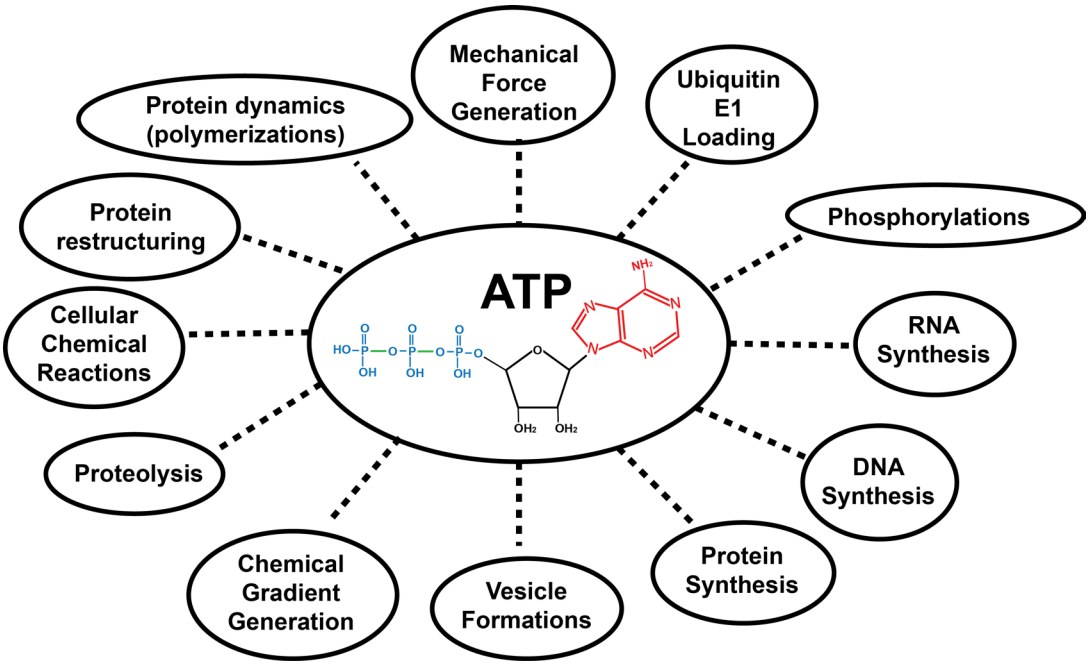

Figure 3.1.2 – Cellular processes that utilize ATP for energy.

Determination of the rate of ATP hydrolysis by ATP hydrolases (ATPases) is important for the understanding of biological processes. This can be achieved in a reconstituted *in-vitro* system with purified proteins and with the use of methods that either detect changes in ATP levels or in the amount of free phosphate generated over time. Current existing methods can be divided into two main categories, end-point assays or real-time assays.

In end-point assays the concentration of a certain molecule within a sample is determined at the end of the reaction. To obtain enzymatic kinetics, sample quenching at different time points to halt the reaction is required, and is achieved typically by denaturation of enzymes with the use of chemicals or heat. As a single reaction is required to be quenched at each time point, to

obtain reaction kinetics, many parallel reactions need to be carried out for data collection for various time points, thus requiring large sample quantities and careful sample preparations to minimize experimental error or bias.

Real-time assays can be followed in real-time, with non-invasive determination of molecular quantities at any point of time during the assay without the need to quench nor stop the assay. Reactions can be followed from start to end by taking multiple readings at different time points on the exact same sample, saving on reagents, and possibly giving more accurate results.

Within these main categories, one can further categorize the methods into direct or coupled methods. Direct methods, which detect the substrate or product, are the most accurate, whereas coupled methods are methods that require reaction intermediates or additional reactions which may complicate the experimental kinetics/readouts. Since ATP is hydrolyzed to give ADP and inorganic phosphate, a typical ATPase assay will either detect the inorganic phosphate being produced, or the depletion of ATP as it is being consumed by the ATPase. Table 3.2 summarizes most of the known ATPase assay methods. In the subsequent pages, the principles of each will be described. Malachite green, radio-labelled ATP, HPLC methods and Luciferase ATPase assays are end-point method. FRET sensors and NADH-coupled ATPase assays are real-time methods. Only MESG phosphorylation for detection of phosphate from ATP hydrolysis can be used as either a real-time or an end-point method.

End-Point Methods	
Direct	**Detection**
Malachite Green-based	Phosphate
P^{32}-Labelled ATP	Phosphate
HPLC	ATP
Coupled	
MESG phosphorylation	Phosphate
Luciferase	ATP
Real-time methods	
Direct	**Detection**
Fret Sensors	ATP
Coupled	
NADH-assay	ADP
MESG phosphorylation	Phosphate

Table 3.1.1 – ATP detection methods – A summary of various ATPase assays either detecting for ATP as a substrate or the products of ATP hydrolysis, i.e. ADP or inorganic phosphate

3.1.1 Malachite Green End-point Assay

The malachite green end-point assay is a common method that has been used since the 1970s to detect phosphate contents, whether in experimental setups or in environmental samples (Hirai *et al*., 1979; Hohenwallner and Wimmer, 1973; Motomizu *et al*., 1983). Detection is achieved with a two step process, where ammonium molybdate reacts with inorganic phosphate under acidic conditions to produce a yellow phosphor-molybdate compound (Figure 3.1.3).

This phosphomolybdate compound then reacts with malachite green (yellow, Abs 446nm) under similar acidic conditions to generate a malachite green-molybdate product that is green, and absorbs at 640 nm. This reaction requires time for development, typically 10-12 minute duration, limiting its application to the end-point method, and creates a possible source of error i.e. when readings are taken before full development has occurred.

Being a phosphate detecting method, buffers used cannot contain any phosphate which is a common biological and physiological buffer. Being typically an end-point method, a large reaction volume or multiple reaction tubes have to be set up and the hydrolysis of ATP is halted at various time points in a quenching step, via precipitation or denaturation of the ATPase through chemical or thermal means, to determine ATPase activity. Precipitates or aggregates may affect the assay readout as well due to limited malachite green solubility.

The malachite green method is extremely sensitive, and is unaffected by chemical denaturants used to quench the ATP hydrolysis reaction, i.e. perchloric acid. This method can also be extended to determine the activities of other nucleotides. However malachite green is known to have a small

linearity range from nanomolar concentrations up to 40 µM so that detection of larger amounts of phosphates would require multiple dilutions which can complicate calculations and affect assay accuracy (Attin *et al*., 2005; Baykov *et al*., 1988). In addition, malachite green is also known to be a liver toxin, so that exposure should be reduced if possible (Srivastava *et al*., 2004).

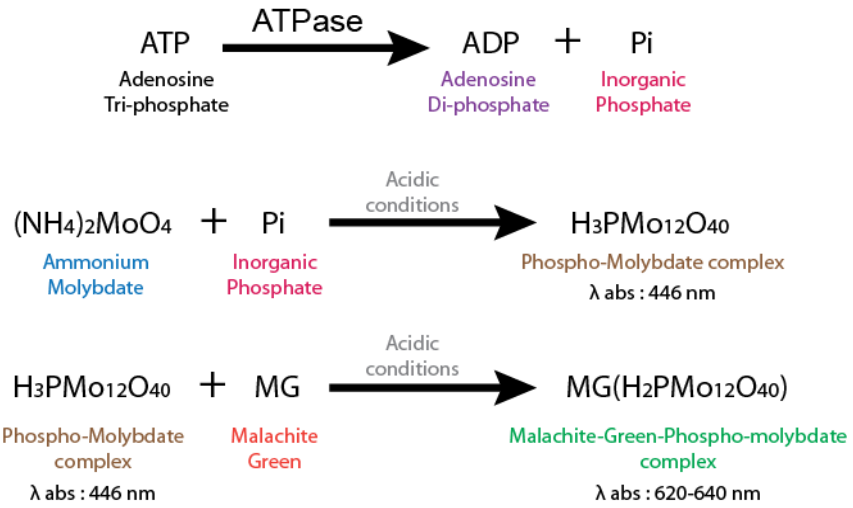

Figure 3.1.3 – Malachite Green ATPase assay. This method detects for inorganic phosphate in two steps, providing an optical absorbance readout at 620-640 nm.

3.1.2 Radioactive ATPase assays

The radioactive ATPase assay involves the use of phosphorus-32 labelled ATP, typically labelled on the γ phosphate (Schneider, 1969) or on the α-phosphate which allows for all species, ATP,ADP and even AMP to be detected. The method involves collection of samples at different time points, quenching the hydrolysis process by denaturation of the ATPase, clarification by centrifugation, and the supernatant spotted onto a cellulose base thin-layer chromatography plate for separation (Hammerstedt and Niehaus, 1975). Both the remaining ATP levels and the amount of free inorganic radioactive phosphate produced from hydrolysis can be detected via TLC & phosphor-imaging or using relevant tools such as Geiger counters or X-ray films to measure radioactive count rates (Figure 3.1.4). The method is highly sensitive, but in recent years it has been replaced by other assays due to the complexities involved in dealing with radioactive substances in the lab, with potential health hazards, and the need for licensing, certifications, trainings and appropriate safety precautions.

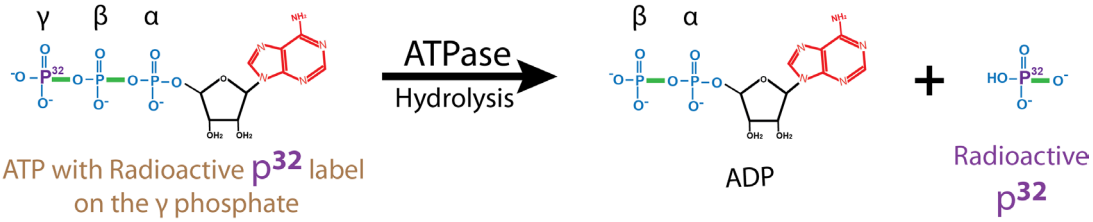

Figure 3.1.4 – Radioactive ATPase assay. A single step detection of either both substrate or product (radioactive inorganic phosphate).

3.1.3 HPLC based assays

This method detects ATP quantities via high performance liquid chromatography (HPLC) with the use of the appropriate columns and solvents (Figure 3.1.5). Both ATP and its product, ADP, can be observed within the same HPLC spectra. By integrating the areas under the respective peaks, the absolute quantities of ATP or ADP can be determined with appropriate standard curves using ATP/ADP of different known concentrations (Rao *et al*., 2010; Sudo *et al*., 2000).

Despite a good resolution of all molecular components present, enhancing accuracies of readouts, one major drawback of the method is the number of HPLC runs required, particularly as an end-point method where many samples from different time points have to be analysed. The method is typically unaffected by the presence of any other chemicals, thus allowing quenching of reactions with the use of chemical denaturants such as perchloric acid. By detecting both substrate and product, this method provides high accuracy.

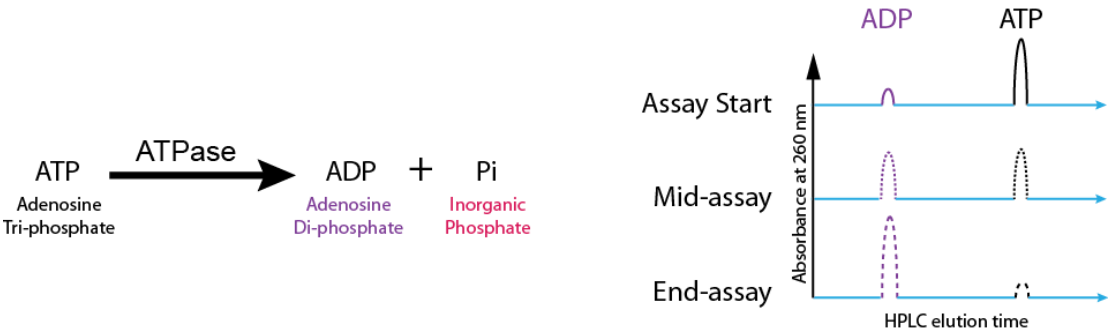

Figure 3.1.5 – HPLC based ATPase assay. By running samples through HPLC, only a single step is needed for detection of both substrate and products of a reaction.

3.1.4 MESG Phosphate detection

In this assay, free phosphate liberated from the hydrolysis of ATP is used to phosphorylate 2-amino-6-mercapto-7-methylpurine riboside (MESG), resulting in an optical absorbance increase at 360 nm (Webb, 1992). This reaction is catalysed by the enzyme purine nucleoside phosphorylase (PNP) (Figure 3.1.6). The advantage of this method is that it can be used in either real-time or end-point assays. However, the coupling of detection through an enzyme, i.e. PNP in this case, might result in readout complications due to PNP's own kinetics and reaction properties. In addition, due to the need to preserve PNP activity, it is not possible to utilize chemical denaturants to quench reactions or complex buffer conditions that may inhibit or denature PNP when this assay is used as an end-point method, resulting in poor or erroneous readouts.

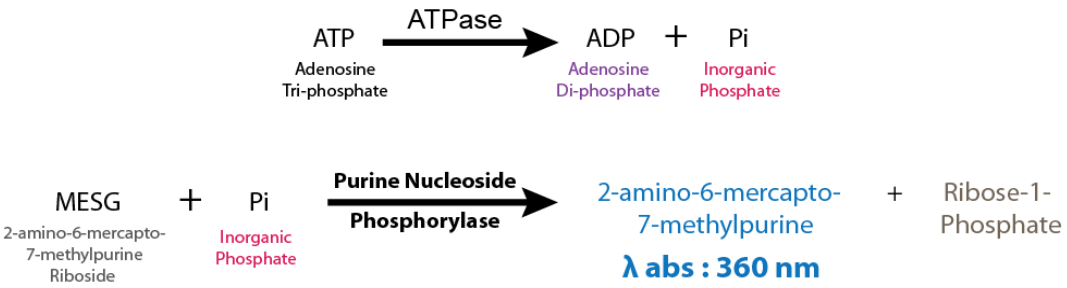

Figure 3.1.6 – MESG phosphate detection. An ATPase assay based on the detection of inorganic phosphate, coupled through another enzyme.

3.1.5 Luciferase Assay

The luciferase-ATP assay is an extremely well known ATP detection system. In this assay, ATP present in a sample is consumed when luciferase phosphorylates luciferin in the presence of oxygen, with the process emitting light at 490 nm (White *et al*., 1969) (Figure 3.1.7). By measuring and recording the light intensities emitted by the reaction, one can estimate the amount of ATP present in a sample (Denburg *et al*., 1969; Lee *et al*., 1970). The greatest advantage of this method is the extremely high sensitivity of the luciferase system in detecting ATP, even at concentrations as low as femtomolar (Praetorius and Leipziger, 2009). Due to its high sensitivity, if the reaction for the enzyme of study is carried out at a high ATP concentration, the luciferase reaction might reach saturation, and thus extra serial dilutions to bring ATP levels down might be needed (such as diluting millimolar ATP concentrations down to nanomolar concentrations resulting in possible inaccuracies). The method is used as an end-point method to determine the amount of ATP left in each sample after being quenched. The samples must not be quenched with chemical denaturants to prevent inactivation of luciferase. The reactions should also be carried out under aerobic conditions, since the lack of oxygen can be rate limiting.

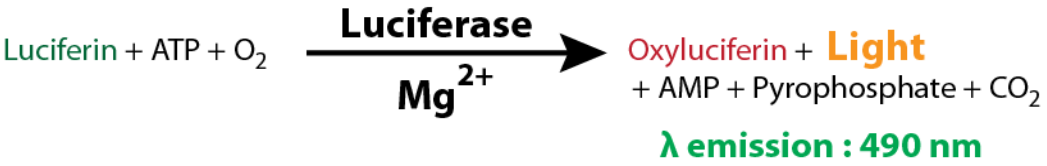

Figure 3.1.7 – Luciferase ATPase assay – A single step detection of substrate ATP by chemiluminiscence.

3.1.6 NADH based Assays

The nicotinamide adenine dinucleotide (NAD) system for the determination of ATPase activity is based on the detection of ADP formed from ATP hydrolysis by the ATPase (Figure 3.1.8). Pyruvate kinase transfers a phosphate from phosphoenolpyruvate (PEP) to ADP to regenerate ATP, producing pyruvate as a product. The pyruvate produced is then converted by lactate-dehydrogenase to lactate in a second reaction, during which NADH is oxidized to NAD+, resulting in a loss in absorbance at 340 nm (Lindsley, 2001).

The biggest advantage of this method is the regeneration of ATP which ensures that the ATPase is subjected to the presence of constant and excess substrate enabling the enzyme to perform at V max. However this multi-step coupling method may result in inconsistent or irregular readouts if any of the intermediary compounds becomes saturating or limiting (i.e. PEP levels), or if the activity of the coupling enzymes become rate limiting.

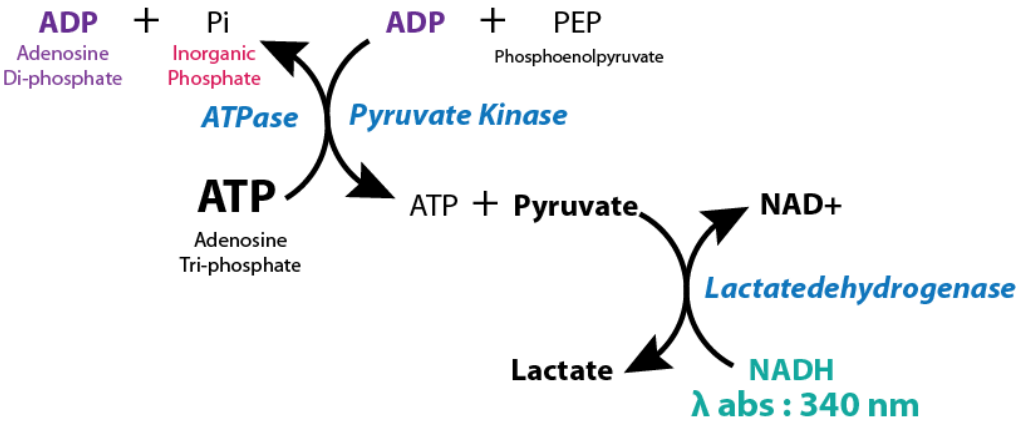

Figure 3.1.8 – NADH coupled ADP detection. This assay detects for reaction product of ATP hydrolysis, ADP by coupling through two other enzymes.

3.1.7 FRET Sensors

Fluorescence resonance energy transfer (FRET) ATP sensors are more commonly used in cell biology. They are transfected into cells to observe ATP gradients or ATP level changes within a cell (Ando *et al*., 2012; Imamura *et al*., 2009). FRET-sensors for ATP typically utilize a pair of fluorescent proteins with the emission wavelength of one overlapping with the excitation wavelength of the other, i.e. cyan fluorescent protein (CFP) and yellow fluorescent protein (YFP). An ATP sensing domain which responds to ATP by bringing the two fluorescent proteins into close proximity, is located in between the two proteins (Berg *et al*., 2009) resulting in fluorescence energy transfer (Figure 3.1.9).

The biggest complication with such an assay is the need to account for cross talk, where YFP can be, to a certain extent can be affected by the excitation of CFP. In addition, the recombinant FRET-ATP sensing protein may have variable activities, and may be subjected to photo-bleaching or inactivation.

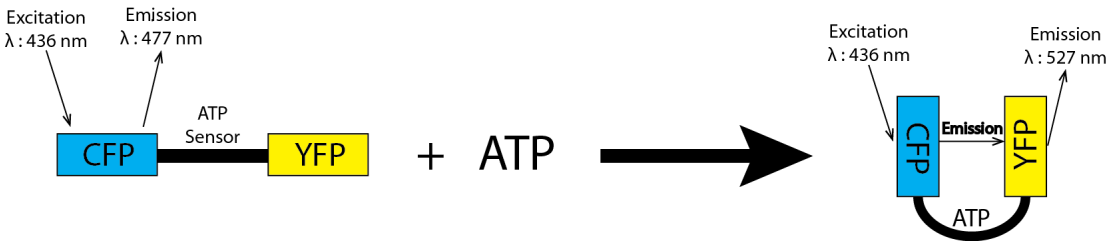

Figure 3.1.9 – ATP sensing through FRET. The cloning of an ATP binding domain of a protein that changes conformation upon ATP binding, between two fluorescent proteins allow for binding events to be monitored through fluorescence resonance energy transfers that occur only with the conformational change.

3.1.8 Polythiophenes – A new class of chemical ATP sensors

Polythiophene (PT) polymers are a novel class of synthetic fluorescent chemical sensors made by the oxidative polymerization of thiophene repeat units (Roncali, 1992; Ten Hoeve *et al*., 1991). Polythiophene polymers form linear chains with the heterocyclic thiofuran groups forming a backbone with overlapping π-orbitals, an essential feature that not only contributes to polythiophene's excellent electrical conductivities and usage in optoelectronics, but also to its optical properties as a chemical sensor (Thomas *et al*., 2007).

Due to its positively charged R groups such as cationic chemical moieties, these polythiopene (CPT) polymers can bind to molecules presenting complementary charges. In event of binding, the continuous π-backbone of the CPT polymer undergoes planarization in a collective response bringing about absorbance and fluorescence changes (Ho *et al*., 2008).

CPTs have been used for detection of nucleotide polymorphisms, or even proteins such as trypsin in extremely low concentrations (An *et al*., 2009; Nilsson and Inganas, 2003). Recently, it has been demonstrated that PT polymers can function biologically as an anti-prion agent (Margalith *et al*., 2012). In our application, we utilized the ability of ATP to quench the fluorescence of the CPT polymer, as a sensing parameter (Figure 3.1.10). We demonstrate for the first time, the possible use of a low concentration of CPT as a real-time reporter of ATP levels in an ATP hydrolysis assay. CPT, at a submicromolar concentration, is able to provide sensing of ATP concentration changes at millimolar levels. This allows for the majority of the ATP to be free, and not competed for by the presence of CPT bound.

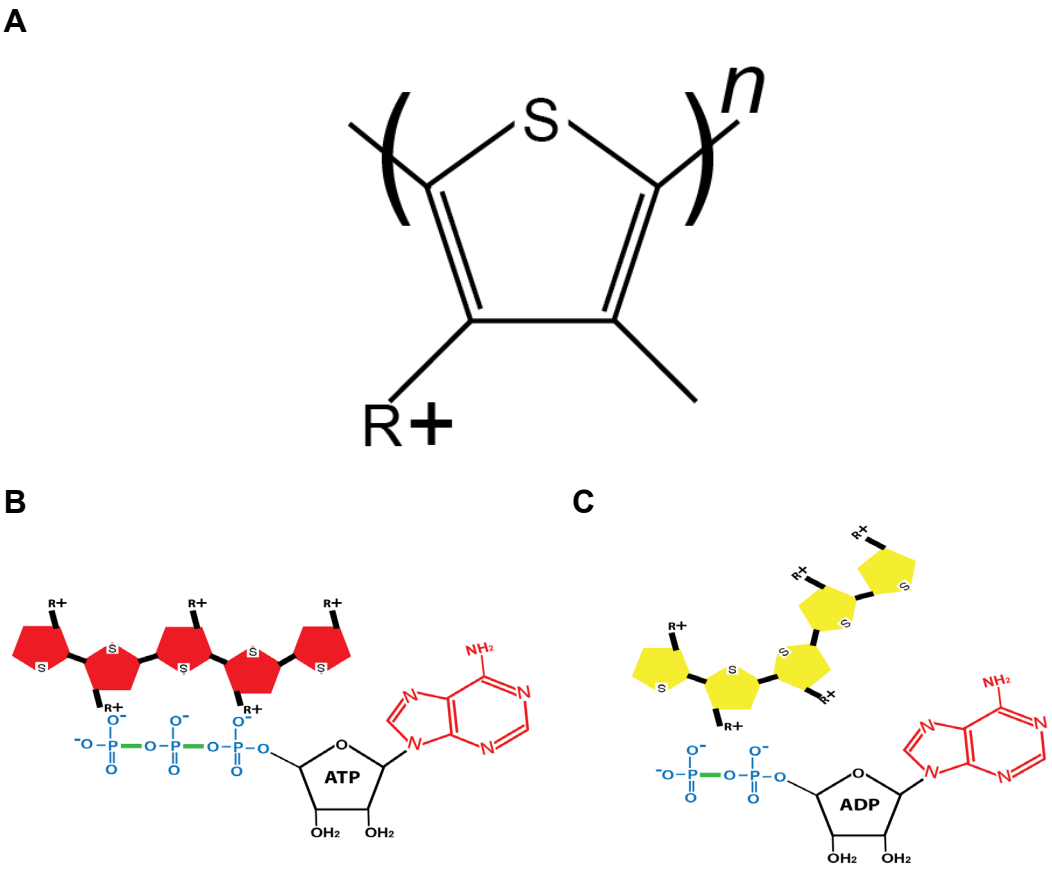

Figure 3.1.10 – Polythiophenes as ATP sensors – The structure of a single repeat unit of polythiophene with a positively charged R-group (A). Binding of the positively charged R-groups of a polythiophene polymer causes planarization of the hydrofuran backbone, resulting in fluorescence quenching (B). ADP does not re-order the hydrofuran backbone, allowing it to be disordered and thus does not cause any fluorescence quenching.

3.1.9 Aim

The aim of this project was to validate the use of polythiophenes in the sensing of ATP levels in real-time to potentially allow the development of polythiophenes for future use in intra-cellular imaging processes to visualize ATP fluxes in correlation to p97 localisation and activities.

3.2 Materials & Methods

3.2.1 PTQ synthesis and stock solution preparation

A cationic PT polymer, poly 1-(3-((4-methylthiophen-3-yl)oxy)propyl)quinuclidin-1-ium (PTQ), was synthesized by collaborator, Dr Umit Hakan. Solid PTQ polymer was dissolved in milli-Q water and stirred overnight with the bottle wrapped in aluminum foil to protect the contents from light. When necessary, the mixture was heated up to 60 °C to facilitate proper dissolution. Stock solutions were prepared at a concentration of 200 μM.

3.2.2 Nucleotides

All nucleotides utilized in the assays were purchased from Sigma Aldrich (A2383, A2647).

3.2.3 Purification of Proteins

p97/VCP was produced and purified as described in previous chapters (Chapter 1.2.5). Briefly, p97/VCP was recombinantly expressed in *E.coli* Rosetta DE3 transformed with pET-26B-p97, and purified through the C-terminus 6x-His tag via metal-cation-affinity chromatography, and further purified to homogeneity through size-exclusion chromatography. p97/VCP-N-D1 was expressed in *E.coli* Rosetta DE3 and purified in the same way as full length p97/VCP, except that prior to gel-filtration, it was subjected to ion-exchange chromatography using a Hi-Trap Q-sepharose 1 ml column and eluted with a 1 M NaCl gradient in 50 mM Phosphate pH 8. Both P97/VCP and p97/VCP-N-D1 were purified into reaction buffer (10 mM Phosphate pH 7.4,

1mM $MgCl_2$, 5% Glycerol) by gel filtration. All protein dilutions were performed using reaction buffer.

3.2.4 Protein concentration determination

Protein concentration was determined with the use of Bradford's assay (Pierce Coomassie). Standard curves were generated with serial dilutions of commercial BSA solutions (2mg/ml, Thermo Scientific) with reaction buffer and typical curves with regression above 0.95 were used for approximating the concentration of p97/VCP or p97/VCP-N-D1 used in our ATPase assay.

3.2.5 Fluorescence measurements

All fluorescence measurements were done in a Tecan Safire X^2 (Männedorf, Switzerland) spectrometer using 96 well black clear-bottom microplates (Greinier Bioscience – Cat-no. 655900).

3.2.6 ATPase Assay

Pre-quenched PTQ-ATP was prepared by mixing 100 mM ATP to 200 μM PTQ at a 1:15 volume ratio. 32μl of this pre-quenched mixture were then added to 168 μl of reaction buffer containing p97/VCP to initiate the hydrolysis reaction. The final concentration of ATP was1 mM, with 34 μM of PTQ in a total of volume of 200μl per well in the 96 well microplate. The microplate was incubated in the Tecan spectrometer where the fluorescence (excitation 420 nm) was read every two minutes with the emission between the range of 430

to 800 nm recorded. Non-hydrolysable ATP homologue, AMP-PNP was also used as an experimental control.

3.2.7 Standard curve generation

As ADP is the product of ATP hydrolysis, a standard curve was generated with the titration of ATP with ADP at various ratios ranging from 0% ADP-100% ATP to 100% ADP-0% ATP. Standard curves were generated from datasets from 1 mM, 1.5 mM, 2 mM and 2.5 mM total nucleotide concentrations. Solutions were prepared the same way for each reaction of the ATPase assay except that the ATPase was omitted. A Stern-Volmer plot was generated by integrating the area under the fluorescent emission curves of the various ATP:ADP ratios. Data analysis was performed with the help of Dr Umit Hakan Yildiz.

3.3 Results

3.3.1 Linear behavior of PTQ quenching in correlation to increasing ATP concentrations

We demonstrated that the PTQ polymer was responsive to variations in ATP concentrations by titrating 34 μM of PTQ with various concentrations of ATP/ADP. By collecting the full emission spectra up to 800 nm, and integrating the area under the curve for each ATP concentration in a Stern-Volmer plot, a good linear correlation obtained allowed the generation of a standard curve for the estimation of ATP concentrations at any point of time within a reaction (Figure 3.3.1).

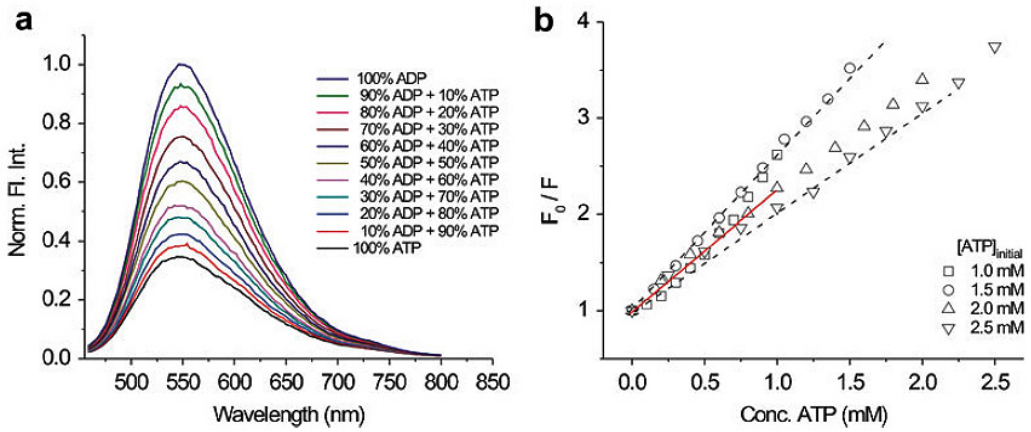

Figure 3.3.1 - Generation of a standard calibration curve for ATP concentration determination - Fluorescence emission of PTQ being quenched by different ratios of ATP/ADP (a). Stern-Volmer plot of PTQ quenching in correlation to ATP concentration (b).

3.3.2 ATP hydrolysis is necessary for the fluorescence recovery of the PTQ polymer

0.6 μM of p97/VCP was incubated with 1 mM ATP with ATP hydrolysis monitored through the unquenching of the PTQ polymer. AMP-PNP, a non-hydrolysable ATP homologue was used as a negative control, using the same experimental setup and same enzyme concentrations, to ensure that the fluorescence recovery of PTQ observed in our experiments was indeed a result of ATP hydrolysis. Little fluorescence recovery was observed with the use of AMP-PNP suggesting that unquenching of PTQ is specific, and can only achieved through ATP hydrolysis (Figure 3.3.2).

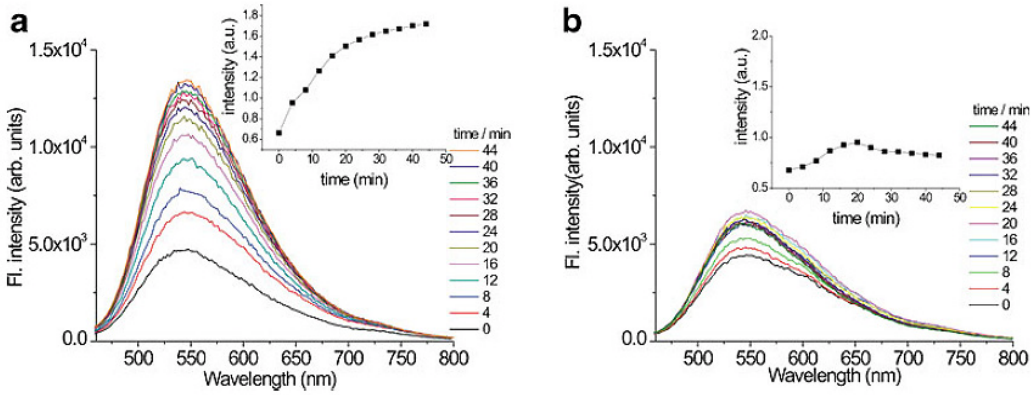

Figure 3.3.2 - ATP hydrolysis causes unquenching of PTQ polymer - Unquenching of the PTQ polymer observed over time with the incubation of 1 mM ATP with 0.6 μM of p97/VCP (a). Incubation of 1 mM AMP-PNP with 0.6 μM of p97/VCP over 44 minutes had little fluorescence unquenching (b).

3.3.3 K_m and V_{max} of ATP hydrolysis by p97/VCP obtained in our real-time ATPase assay is in agreement with published values in literature

To determine whether the assay was relevant for the generation of enzymatic kinetic data, we subjected various concentrations of ATP to hydrolysis by 0.6 µM of p97/VCP in kinetic experiments. By plotting the various initial rates obtained at different substrate concentrations into a Lineweaver-Burk plot, we determined the values of K_m and V_{max} of ATP hydrolysis by p97/VCP from the X and Y intercepts of the plot, to be 0.30 mM and 0.134 nmol ATP min^{-1} $µg^{-1}$ respectively (Figure 3.3.3). The values obtained were in range with published values in the literature.

A

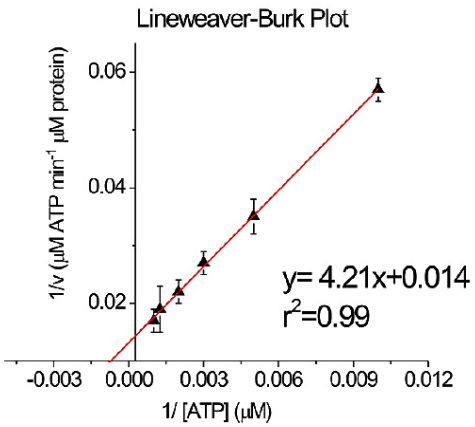

B

K_m	V_{max}	Reference
0.30 mM	0.134 nmol ATP min^{-1} $µg^{-1}$	Our assay method
0.33 mM	0.52 nmol ATP min^{-1} $µg^{-1}$	(Song, *et al.* 2003)
-	0.116 nmol ATP min^{-1} $µg^{-1}$	(Dalal, *et al.* 2004)

Figure 3.3.3 – Lineweaver-Burke Plot of ATP hydrolysis by p97/VCP.
A Lineweaver-Burke plot was used to estimate the K_m and V_{max} of ATP hydrolysis by p97/VCP (A). Values obtained were compared to published values in the literature (B).

3.3.4 p97/VCP-N-D1 possesses half the K_{cat} of full length p97/VCP

Hydrolysis of ATP by various concentrations of p97/VCP and p97/VCP-N-D1 was monitored in real-time by fluorescence of PTQ. By plotting the ATP concentration versus enzyme concentration we were able to determine the initial rates (V_o) of ATP hydrolysis at various enzyme concentrations allowing the approximation of the enzymatic K_{cat} values. The K_{cat} of both p97/VCP and p97/VCP-N-D1 was calculated to be 2.882 S^{-1} and 1.05 S^{-1} respectively (Figure 3.3.4).

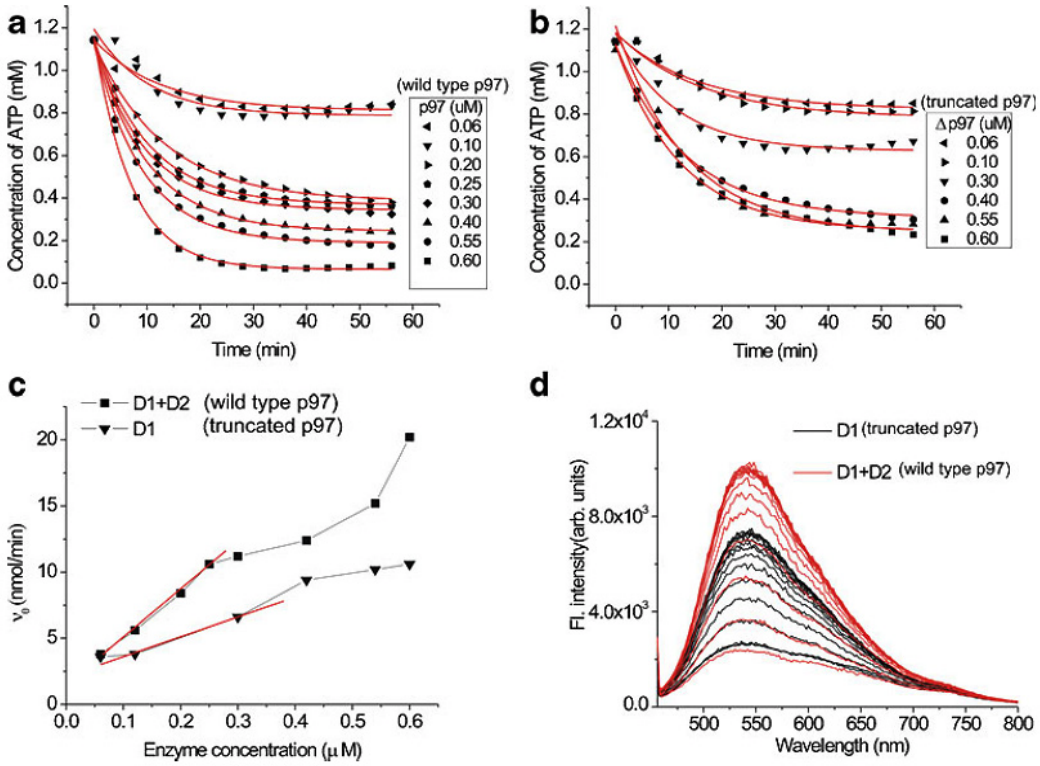

Figure 3.3.4 - Hydrolysis of ATP by various concentrations of p97/VCP (A) and p97-N-D1 (B). Plot of initial rates of ATP hydrolysis by p97/VCP and p97-N-D1 at various enzyme concentrations (C). Overlay of fluorescence unquenching curves of ATP hydrolysis by 0.6 μM of p97/VCP and p97-N-D1 respectively (D).

3.4 Discussion

In our experiments, we were able to demonstrate for the first time, the use of PTQ polymers in real-time ATP sensing using small reaction volumes. In this sensing method, ATP, the substrate, remained in excess and free to bind to the enzyme, while PTQ, at 30 fold lower concentration as compared to ATP, senses only changes in the equilibrium of ATP-ADP conversion. This prevents ATP being competed away from the enzyme, unlike FRET sensors which can act as a reservoir or a sink for ATP if used as a real-time assay.

The excellent linearity of PTQ's fluorescence quenching in correlation with increasing ATP concentration makes the method extremely reliable and easy to use without the need for complex mathematical approximations. As part of the method's validation, we have shown that we could obtain values for K_m and V_{max} for p97/VCP activity that are in agreement with values in the literature obtained using other methods.

Despite being a promising class of chemical sensors, we had observed several limitations of PTQ when developing our assays. PTQ has a tendency to aggregate and precipitate, but can be easily solubilized by strong agitation. Thus, mixing functions on micro-plate readers is important for consistent results. The fluorescence quenching of PTQ by ATP was also sensitive to ionic strengths, so that there is a need for optimization to prevent fluorescence recoveries.

Our method provides a key advantage in consistent measurements readouts by direct detection in real-time, and the avoidance of quenching steps, coupling steps and possible human error present in end-point methods. Apart from ATP sensing, PTQ can be extended to sensing other nucleotide tri-

phosphates, single stranded DNA or RNAs, potentially allowing other assay types to be developed, i.e. DNA hybridization studies, DNAse assays etc. Further applications of PTQ in molecular sensing can be extended to the development or creation of intra-cellular ATP sensors or reporters that may allow localizations and fluxes in concentration within a cell to be observed via confocal microscopy in real-time.

3.5 References for Chapter 3

An, L., Liu, L., Wang, S., 2009. Label-free, homogeneous, and fluorescence "turn-on" detection of protease using conjugated polyelectrolytes. Biomacromolecules 10, 454-457.

Ando, T., Imamura, H., Suzuki, R., Aizaki, H., Watanabe, T., Wakita, T., Suzuki, T., 2012. Visualization and measurement of ATP levels in living cells replicating hepatitis C virus genome RNA. PLoS pathogens 8, e1002561.

Attin, T., Becker, K., Hannig, C., Buchalla, W., Wiegand, A., 2005. Suitability of a malachite green procedure to detect minimal amounts of phosphate dissolved in acidic solutions. Clin Oral Investig 9, 203-207.

Baykov, A.A., Evtushenko, O.A., Avaeva, S.M., 1988. A malachite green procedure for orthophosphate determination and its use in alkaline phosphatase-based enzyme immunoassay. Anal Biochem 171, 266-270.

Berg, J., Hung, Y.P., Yellen, G., 2009. A genetically encoded fluorescent reporter of ATP:ADP ratio. Nat Methods 6, 161-166.

Boyer, P.D., Stokes, B.O., Wolcott, R.G., Degani, C., 1975. Coupling of "high-energy" phosphate bonds to energy transductions. Fed Proc 34, 1711-1717.

Dalal, S., M. F. N. Rosser, D. M. Cyr, and P. I. Hanson. 2004. Distinct Roles for the AAA ATPases NSF and p97 in the Secretory Pathway. Molecular Biology of the Cell 15:637-648.

Dean, M., Rzhetsky, A., Allikmets, R., 2001. The human ATP-binding cassette (ABC) transporter superfamily. Genome Res 11, 1156-1166.

Denburg, J.L., Lee, R.T., McElroy, W.D., 1969. Substrate-binding properties of firefly luciferase. I. Luciferin-binding site. Arch Biochem Biophys 134, 381-394.

Hammerstedt, R.H., Niehaus, W.G., Jr., 1975. A novel method for measurement of the specific radioactivity of gamma-32P ATP. Anal Biochem 63, 161-168.

Hirai, Y., Yoza, N., Ohashi, S., 1979. Flow Injection Analysis of Inorganic Polyphosphates. Abstracts of Papers of the American Chemical Society, 200-200.

Ho, H.A., Najari, A., Leclerc, M., 2008. Optical detection of DNA and proteins with cationic polythiophenes. Acc Chem Res 41, 168-178.

Hohenwallner, W., Wimmer, E., 1973. The Malachite green micromethod for the determination of inorganic phosphate. Clin Chim Acta 45, 169-175.

Imamura, H., Nhat, K.P., Togawa, H., Saito, K., Iino, R., Kato-Yamada, Y., Nagai, T., Noji, H., 2009. Visualization of ATP levels inside single living cells

with fluorescence resonance energy transfer-based genetically encoded indicators. Proc Natl Acad Sci U S A 106, 15651-15656.

Korn, E.D., Carlier, M.F., Pantaloni, D., 1987. Actin polymerization and ATP hydrolysis. Science 238, 638-644.

Kuznetsov, D.A., Musajev, P.I., 1988. Chemical-induced modulation of ATP and protein synthesis processed inside rat brain mitochondria. Int J Neurosci 38, 331-343.

Lecker, S.H., Goldberg, A.L., Mitch, W.E., 2006. Protein degradation by the ubiquitin-proteasome pathway in normal and disease states. J Am Soc Nephrol 17, 1807-1819.

Lee, R.T., Denburg, J.L., McElroy, W.D., 1970. Substrate-binding properties of firefly luciferase. II. ATP-binding site. Arch Biochem Biophys 141, 38-52.

Lindsley, J.E., 2001. Use of a real-time, coupled assay to measure the ATPase activity of DNA topoisomerase II. Methods Mol Biol 95, 57-64.
Majumdar, C., Frankel, F.R., 1973. Role of ATP in DNA replication. Nature 243, 33-36.

Margalith, I., Suter, C., Ballmer, B., Schwarz, P., Tiberi, C., Sonati, T., Falsig, J., Nystrom, S., Hammarstrom, P., Aslund, A., Nilsson, K.P., Yam, A., Whitters, E., Hornemann, S., Aguzzi, A., 2012. Polythiophenes inhibit prion propagation by stabilizing prion protein (PrP) aggregates. J Biol Chem 287, 18872-18887.

Motomizu, S., Wakimoto, T., Toei, Y., 1983. Determination of trace amounts of phosphate in river water by flow-injection analysis. Talanta 30, 333-338.

Nilsson, K.P., Inganas, O., 2003. Chip and solution detection of DNA hybridization using a luminescent zwitterionic polythiophene derivative. Nat Mater 2, 419-424.

Praetorius, H.A., Leipziger, J., 2009. ATP release from non-excitable cells. Purinergic Signal 5, 433-446.

Rao, F., See, R.Y., Zhang, D., Toh, D.C., Ji, Q., Liang, Z.X., 2010. YybT is a signaling protein that contains a cyclic dinucleotide phosphodiesterase domain and a GGDEF domain with ATPase activity. J Biol Chem 285, 473-482.

Rolfe, D.F., Brown, G.C., 1997. Cellular energy utilization and molecular origin of standard metabolic rate in mammals. Physiol Rev 77, 731-758.

Roncali, J., 1992. Conjugated poly(thiophenes): synthesis, functionalization, and
applications. Chemical Reviews 92, 711-738.

Schneider, P.B., 1969. An enzymatic assay for adenosine 5'-triphosphate (ATP) and other nucleoside triphosphates and determination of the specific radioactivity of the terminal P. Anal Biochem 28, 76-84.

Song, C., Q. Wang, and C.-C. H. Li. 2003. ATPase Activity of p97-Valosin-containing Protein (VCP): D2 MEDIATES THE MAJOR ENZYME ACTIVITY, AND D1 CONTRIBUTES TO THE HEAT-INDUCED ACTIVITY. Journal of Biological Chemistry 278:3648-3655.

Srivastava, S., Sinha, R., Roy, D., 2004. Toxicological effects of malachite green. Aquat Toxicol 66, 319-329.

Sudo, J., Terui, J., Iwase, H., Kakuno, K., 2000. Assay of ATPase and Na,K-ATPase activity using high-performance liquid chromatographic determination of ADP derived from ATP. J Chromatogr B Biomed Sci Appl 744, 19-23.

Tanaka, K., Waxman, L., Goldberg, A.L., 1983. ATP serves two distinct roles in protein degradation in reticulocytes, one requiring and one independent of ubiquitin. J Cell Biol 96, 1580-1585.

Ten Hoeve, W., Wynberg, H., Havinga, E.E., Meijer, E.W., 1991. Substituted 2,2':5',2":5",2"':5"',2"":5"",2""':
5"",2"""":5"""",2""":5""",2"""":5""",2""":5""",2""":5""",2""":5"""-undecithiophenes, the longest characterized oligothiophenes. Journal of the American Chemical Society 113, 5887-5889.

Thomas, S.W., 3rd, Joly, G.D., Swager, T.M., 2007. Chemical sensors based on amplifying fluorescent conjugated polymers. Chem Rev 107, 1339-1386.

Webb, M.R., 1992. A continuous spectrophotometric assay for inorganic phosphate and for measuring phosphate release kinetics in biological systems. Proc Natl Acad Sci U S A 89, 4884-4887.

White, E.H., Rapaport, E., Hopkins, T.A., Seliger, H.H., 1969. Chemi- and bioluminescence of firefly luciferin. J Am Chem Soc 91, 2178-2180.

Zerangue, N., Malan, M.J., Fried, S.R., Dazin, P.F., Jan, Y.N., Jan, L.Y., Schwappach, B., 2001. Analysis of endoplasmic reticulum trafficking signals by combinatorial screening in mammalian cells. Proc Natl Acad Sci U S A 98, 2431-2436.

Chapter 4

The roles of p97/VCP in human health and disease

4.1 Introduction

p97/VCP, which has been extensively characterized both biochemically and structurally over the past two decades, is now increasingly implicated in molecular mechanisms that are involved in human health and diseases. Despite the recent overshadowing interest in a group of neuro- and musculo-degenerative diseases known as Inclusion body myopathy and Paget's disease of the bone (IBMPFD), p97/VCP is also central to many other major diseases, from cancer, muscular atrophy, neurodegenerative diseases such as Huntington's disease, amyotrophic lateral sclerosis, cystic fibrosis and inflammation, and is implicated in other lesser known minor diseases.

This chapter, as a summary to the thesis, aims to present an overview on p97/VCP in human disease, identifying new research gaps and formulating hypotheses based on current existing understandings in the field, including our experimental results and our unpublished data.

4.2. Major diseases implicating p97/VCP

The mechanism through which p97/VCP can be implicated in the onset or pathology of a disease is a plethora of different adaptor proteins associations, each directing p97/VCP to function in different molecular pathways and biological processes. Perturbations and/or loss of the usual cellular homeostasis of different p97-adaptor interactions may result in either gain of

function or loss of function of certain biological processes leading to disease over time. Figure 4.1 presents the various imbalances in p97/VCP functions associated with various diseases, and Table 4.1 summarizes the adaptor proteins interactions and the respective cellular processes in which they are implicated.

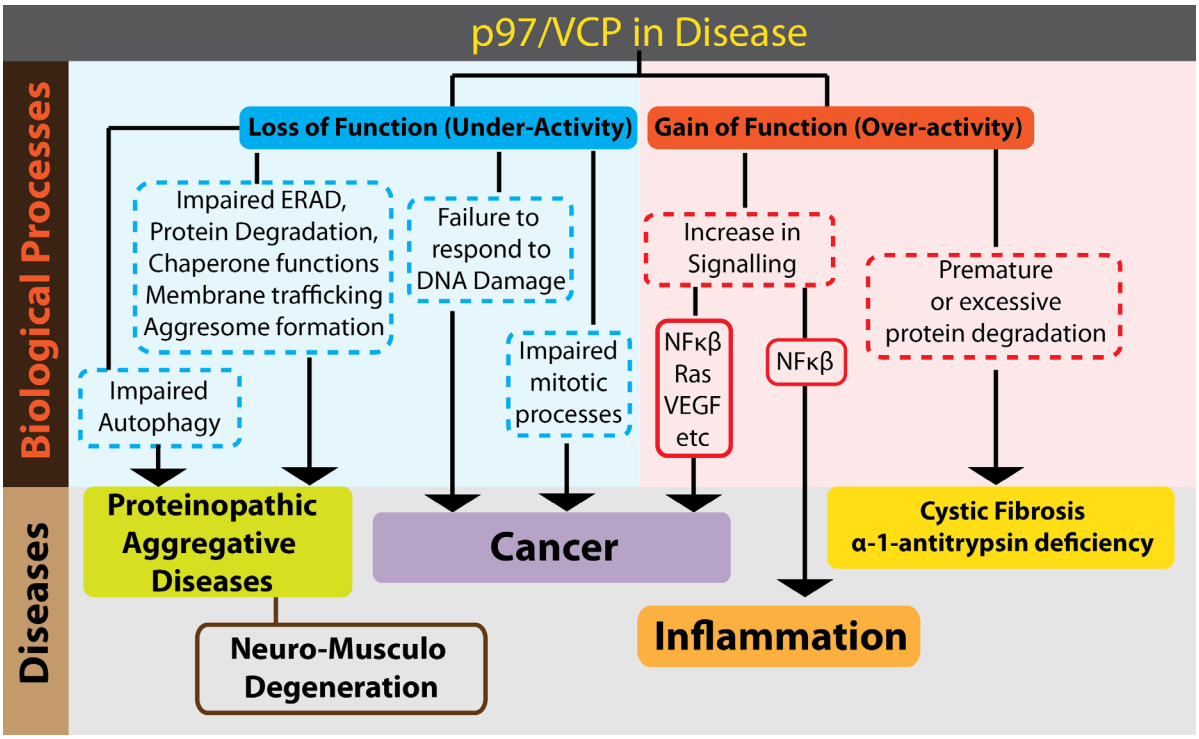

Figure 4.1 - p97/VCP in disease – p97/VCP-related diseases can be broadly classified into gain of function or loss of function diseases. With insufficient or reduced p97/VCP activities, impaired biological processes lead to diseases such as cancer and neuro-musculo-degenerations. Over-activity of p97/VCP results in inflammation, cancer or protein deficiency

Cofactors directing p97's biological functions		
Function	**Cofactors**	**Implication(s)**
Protein degradation (ERAD, chaperone functions, Ubiquitin proteasome system)	**gp78** (Zhong, Shen et al. 2004) **Hrd1** (Ballar, Pabuccuoglu et al. 2011) **Ufd1-Npl4** (Pye, Beuron et al. 2007) **Ufd2**(Richly, Rape et al. 2005) **Ufd3** (Johnson, Ma et al. 1995) **UBX2,3** (Hartmann-Petersen, Wallace et al. 2004)	Cystic Fibrosis, alpha-1-trypsin deficiency, Alzheimer's disease, Parkinson's disease, IBMPFD,
Membrane trafficking	**Clathrin** (Pleasure, Black et al. 1993) **Synaptotagmin I, II** (Shin, Maximov et al. 2004) **SVIP** (Wang, Ballar et al. 2011) **UBXD9** (Orme and Bogan 2012)	Autophagic processes, Membrane trafficking disorders
Mitosis-related processes (chromatin condensation, nuclear envelope, golgi and ER fragmentation and re-assembly, spindle checkpoint, spindle dynamics)	**Ase1**(Cao, Nakajima et al. 2003) **Aurora B kinase** (Dobrynin, Popp et al. 2011) **Cdc5** (Cao, Nakajima et al. 2003) **p47** (Meyer 2005) **p37** (Uchiyama, Totsukawa et al. 2006) **Ufd1-Npl4** (Pye, Beuron et al. 2007) **VCIP** (LeBrasseur 2004)	Cell cycle arrest, aneuploidy, cancer metastasis
Aggresome formation	**Ataxin-3** (Zhong and Pittman 2006); **HDAC6** (Yao 2010)	Excessive inclusion body formation, neurodegenerative disorders such as Machado-Joseph disease, spinocerebral ataxias
DNA damage repair	**BRCA1** (Zhang, Wang et al. 2000) **DUF** (Yamada, Okuhara et al. 2000) **TB-RBP** (Wu, Lefrancois et al. 1999) **Ufd1-Npl4** (Meerang, Ritz et al. 2011)	Cancer metastasis
Inflammation	**IκBα-NFκB** (Bodas, Min et al. 2010) **Akt** (Klein, Barati et al. 2005)	Chronic inflammation, toxin insensitivity, cancer metastasis
Autophagy	**HDAC6** (Yao 2010) **Ufd1-Npl4** (Badadani, Nalbandian et al. 2010)	Inefficient aggresome clearance

Table 4.1 - p97/VCP in various cellular processes – p97/VCP is directed to various cellular processes by binding different adaptor proteins. Summarized are the major adaptor proteins that are known to bind p97/VCP.

4.3. p97/VCP gain of function diseases

The gain of function category, where over-activity of certain biological processes involving p97/VCP can cause diseases, includes cancer, inflammation and protein deficiencies.

4.3.1. p97/VCP gain of function in cancer

At the cellular level, p97/VCP is involved in the turnover of inhibitory proteins that down-regulate cellular proliferation, such as neurofibrinomin-1 (NF1), or Iκβα, the inhibitor alpha of nuclear factor kappa-light-chain-enhancer of activated B cells (Nfκβ) (Dai *et al.,* 1998; Phan *et al.,* 2010). NF1, a stimulator of synaptogenesis and neuronal tissue differentiation, inhibits cell division through the blocking of the Ras signaling pathway that induces proliferation (Hannan *et al.,* 2006; Trovo-Marqui and Tajara, 2006). Iκβα is a negative regulator of Nfκβ, a transcription factor that promotes cellular proliferation and cell survival in cancer (Escarcega *et al.,* 2007). Polyubiquitinated Iκβα is segregated from Nfκβ by p97/VCP and handed over to the 26S proteasome for degradation (Dai *et al.,* 1998). With excess p97/VCP activity in degrading Iκβα and NF1, increase in cell division may promote cancer growth.

Clinical studies have shown elevation of p97/VCP levels in many cancers such as prostate, liver, thyroidal, pancreatic and lung cancers in positive correlation with increased cancer recurrence and prognosis of metastasis (Asai *et al.,* 2002; Tsujimoto *et al.,* 2004; Valle *et al.,* 2011; Yamamoto *et al.,* 2005; Yamamoto *et al.,* 2003; Yamamoto et al., 2004). Inhibition of p97/VCP via chemical inhibitors or p97/VCP knockdown using

micro-RNAs show promise in cancer therapy at the cell culture level, where p97/VCP inhibition or down-regulation suppresses cell growth and induces apoptosis (Chou and Deshaies, 2011b; Liu *et al.,* 2012).

4.3.2. p97/VCP gain of function proteinopathies

p97/VCP functions in endoplasmic reticulum (ER)-associated degradation (ERAD) in the process of retro-translocating misfolded proteins from the ER and shuttling them to the 26S proteasome for degradation (Vembar and Brodsky, 2008). With enhanced p97/VCP activities, half-lives and retention times of proteins in the ER may decrease, potentially reducing the propensity for refolding processes to occur. As a consequence of insufficient functional proteins, diseases such as cystic fibrosis or α-1-antitrypsin deficiency occur.

The cystic fibrosis transmembrane conductance regulator protein (CFTR) is an ion channel that spans the plasma membrane 12 times and is responsible for the export and regulation of chloride and thiocynate ions in cells and the extra-cellular environment (Linsdell, 2001). A protein with difficulties to fold, the majority (~ 80%) of the wild-type CFTR is targetted for degradation by ERAD, with only 20% making it to the cell surface (Cheng *et al.,* 1990; Ward *et al.,* 1995). In cystic fibrosis disease, a mutation resulting in deletion of phenyalanine 508 (Δ508), shifts the equilibrium to almost all CFTR being degraded by ERAD, despite being partially functional and active (Farinha and Amaral, 2005). The lack of CFTR at the cell surface membrane causes cystic fibrosis, a debilitating and potentially lethal ailment, where the lack of secreted chloride and thiocyanate ions causes severe phlegm congestions leading to bacterial infections that can cause mortality when

airways are blocked. Modulation in the rate of ERAD, by interfering with p97/VCP function and levels using siRNA/shRNA have been shown to be effective in the rescue of Δ508 CFTR (Vij *et al.,* 2006).

Similarly, α-1-antitrypsin is a protein produced by the liver and secreted into the blood stream and when mutated, there is an equilibrium shift where all the protein is degraded with little being secreted (Stoller and Aboussouan, 2005). Since α-1-antitrypsin is essential for the protection of lung tissue against damaging effects of elastase enzymes produced by neutrophils in the lung, the lack of this α-1-antitrypsin can result in emphysema or liver damage (Heresi and Stoller, 2008). Silencing SVIP, the small VCP-interacting protein and an inhibitor of ERAD, results in increased degradation of mutant α-1-antitrypsin (Ballar *et al.,* 2007). This suggests that modulating ERAD processes, i.e. via p97/VCP inhibition, may rescue α-1-antitrypsin deficiency.

4.4. p97/VCP loss of function diseases

Loss of function diseases dominate p97/VCP-related human ailments. Reduction or malfunction in p97/VCP activities can lead to cancer and various neuro-musculo-degenerative diseases.

4.4.1. p97/VCP loss of function in cancer

The link between p97/VCP's loss of function and cancer is not clearly defined at the moment, although p97/VCP is involved in processes that are essential to cellular proliferation. In cancer, p97/VCP can be implicated by its essential function in DNA repair or mitotic processes, as explained in Chapter 1, above.

p97/VCP plays an integral role in DNA damage repair when double stranded DNA breaks occur. p97/VCP with its adaptor proteins Ufd1/Npl4 extracts ubiquitinated proteins at the site of DNA damage to facilitate the binding of DNA repair proteins such as 53BP1, BRCA1 etc. (Meerang *et al.,* 2011). In mitosis, p97/VCP's function is essential at many different steps, from interphase, to metaphase alignment of chromosomes, to the regulation of anaphase onset and microtubule dynamics (Cao *et al.,* 2003; Dobrynin *et al.,* 2011; Meyer *et al.,* 2010). In either DNA damage repair or mitosis, when p97/VCP malfunctions or its activities decline, genetic damage and mutations, or chromosomal aneuploidy can lead to cancer.

p97/VCP loss of function may also be involved in cancer development through hypoxia inducible factor 1 alpha (HIF1α). HIF1α promotes cancer cell survival through its role in angiogenesis and in helping cells to cope with hypoxic conditions that are commonly seen in tumours. p97/VCP mediates the cytoplasmic degradation of HIF1α through an adaptor protein, Ubxd7, whereby the p97-Ubxd7 complex shuttles ubiquitinated HIF1α to the 26S proteasome (Alexandru *et al.,* 2008). Diminished p97/VCP activity resulting in accumulation in HIF1α may support tumor growth.

4.4.2. p97/VCP in inclusion body myopathy and Paget's disease of the bone and frontal-temporal dementia (IBMPFD)

In pathological proteinopathies, most recently p97/VCP was in the limelight with strong attention on a disease known as inclusion body myopathy and Paget's disease of the bone and frontal-temporal dementia (IBMPFD). IBMPFD is a rare autosomal dominant genetic disease with late onset,

typically in adulthood (Kimonis *et al.,* 1993). Patients with the disease suffer varying degrees of degeneration in three tissue types, bone, muscle, and the nervous system, resulting in muscle weakness, loss of muscle function, and dementia (Kimonis *et al.,* 1993).

The disease is associated with a single point mutation in each patient, resulting in an amino acid substitution, generally in the N-domain and N-D1 linker of p97/VCP (Nalbandian *et al.,* 2012). There are 20 known point mutations, with a total of 13 known amino acid substitutions in IBMPFD. While many studies have attempted to elucidate a biochemical cause for the disease, there is still neither general consensus nor general mechanism for IBMPFD.

As mutations are located to the N-domain and the N-D1 linker of p97/VCP, it has been speculated that these IBMPFD related mutations can have an effect on the turnover of ATP by mutant p97/VCP and thus may eventually result in disease. However, not all IBMPFD mutations appear to have dramatically elevated ATPase activities, as only A232E reportedly has an ATPase activity several fold above that of wild-type p97/VCP, while only slight elevations above wild type is found in other mutants (Halawani *et al.,* 2009; Niwa *et al.,* 2012). The ATPase activity of the R155H mutant, the most common IBMPFD mutation, is similar to that of wild-type p97/VCP, thus suggesting that ATPase activity alone may not be the common mechanism in IBMPFD (Watts *et al.,* 2004; Weihl *et al.,* 2006).

Currently, imbalanced adaptor protein interactions is believed to be a possible cause of IBMPFD, where IBMPFD mutant proteins appear to bind more Ataxin-3 and less ubiquitin ligase E4B(Fernandez-Saiz and Buchberger,

2010). Biochemical and biophysical data seem to suggest that changes in ATP affinity, ATP binding stoichiometry and dysregulated transitions between an ADP-bound to ADP-permissible to ATP-bound state to be a possible disease mechanism (Tang *et al.,* 2010a). Cell lines over-expressing IBMPFD mutant p97/VCP proteins such as R155H or A232E were observed to have defects in autophagosome maturation (Ju *et al.,* 2009; Tresse *et al.,* 2010) and in addition to disrupted autophagosome and endosome maturation in various IBMPFD mutations, autophagosome biogenesis was increased, mTOR signaling was also disrupted and global protein translation was diminished in such p97/VCP mutants (Ching *et al.,* 2013).

Whether ERAD is impaired in IBMPFD remains contentious. One group presented evidence for normal ERAD in IBMPFD mutants R155H and A232E using fluorescent CD3δ-YFP, a sensitive reporter of ERAD function, while another group reported ERAD to be impaired in R155H and R95G mutants as revealed by accumulation of CFTR, a natural ERAD substrate (Tresse *et al.,* 2010; Weihl *et al.,* 2006). Since CFTR can also be degraded by autophagy, it could be possible that impaired autophagy in IBMPFD mutants resulted in CFTR accumulations thus misleading one to believe that ERAD was also compromised (Luciani *et al.,* 2011). Another possibility would be that ERAD is compromised for only certain types of substrates, but not for others.

Another aspect of IBMPFD that remains baffling is the late onset of the disease, typically in adulthood and beyond. Personal communication with Dr. Virginia Kimonis, a clinician & researcher who first defined and characterized IBMPFD as a disease, indicated that there are siblings harbouring identical

mutations in p97/VCP, yet one has succumbed to the disease, while the elder sibling appears to show no symptoms at all. Low penetrance has similarly been observed in clinical studies of families with recurring IBMPFD mutations, where not all carriers of the gene mutation show symptoms of or suffer from a disease (Fanganiello *et al.,* 2011; Gidaro *et al.,* 2008; Viassolo *et al.,* 2008).

An additional rational speculation for IBMPFD's disease mechanism is to address metabolism. Can IBMPFD be a metabolic disorder? Indeed, in Chapter 1 above I have demonstrated that ATP levels can regulate p97-adaptor protein competition and preference. In a *drosophila* IBMPFD model, where the *drosophila* p97/VCP homogue TER94 harboring corresponding IBMPFD mutations was over-expressed, reduced cellular ATP levels were observed. The neurodegeneration caused by the TER94 IBMPFD mutants was partially alleviated when the mutant flies were fed on a high energy diet to improve cellular ATP levels (Chang *et al.,* 2011). In generating the R155H homozygous IBMPFD mouse model, a high fat diet appeared to reduce the embryonic lethality of mouse homozygotes and enhance post-natal survival to over 10 weeks (personal communication with Dr. Kimonis at AAA-ATPase meeting in Kumamoto 2011). These studies provide a metabolic link and a possible role of cellular energetics in IBMPFD late onset and disease pathology, as hormonal changes and metabolism declines in aging (Barzilai *et al.,* 2012).

Another hypothesis would be whether p97/VCP is involved in cellular stemness, as it is involved in the regulation of factors that regulate cell proliferation. Tissues such as muscle, bone marrow, and the nervous system contain regenerative stem cells (McKay, 1997; Qu-Petersen *et al.,* 2002). Over

time or with aging, mutant p97/VCP may affect the proliferative potential of these stem cells and impede regenerative repair to these tissues. In a similar muscle atrophy disease known as Duchenne muscular dystrophy, the delay in onset of the disease is due to the regenerative potential of muscle stem cells, known as satellite cells that constantly repair muscle damage to maintain function (Ishimoto *et al.,* 1983; Morgan and Zammit, 2010). The finite nature of stem cell renewal results in depletion or exhaustion over time, and thus allowing the onset of atrophy (Sacco *et al.,* 2010). Apart from depletion of muscle stem cells, neuronal cell death and de-nervation is also known to cause muscle atrophy (Kohn, 1965; Rowan *et al.,* 2012). It would be interesting to determine whether muscle weakness and atrophy in IBMPFD is indirectly caused by preceding neuronal cell loss or independent of this mechanism.

4.4.2.1. No Impaired hexamerization rate in the R155H IBMPFD mutant

Based on the hexamerization assay of Wang *et .,* 2003, we monitored the hexamerization kinetics of both wild-type p97/VCP and its R155H IBMPFD mutant, in the absence or presence of ATP. We wanted to test if any discernable hexamerization rates could be a cause for the disease. We observed no significant difference in the hexamerization rates of wild-type p97/VCP or R155H and ATP accelerated the hexamerization of both proteins (Figure 4.2).

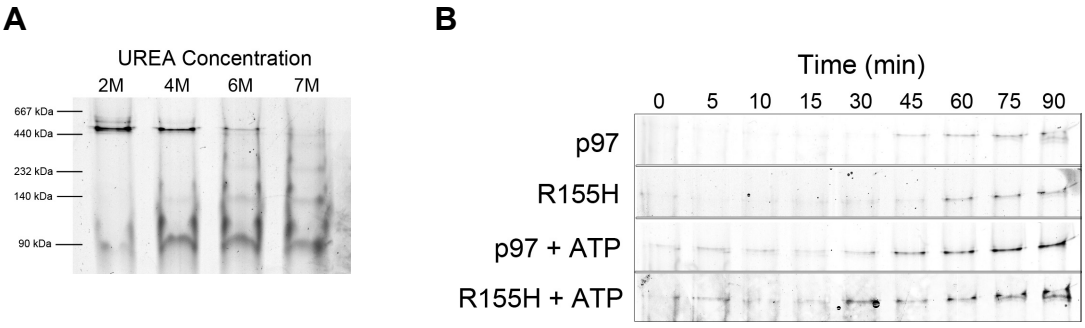

Figure 4.2 - Hexamerization kinetic assay of wild-type p97/VCP and its R155H IBMPFD mutant – Determination of the optimal urea concentration for the dissociation of p97/VCP into its monomers indicated that 7M Urea was required **(A).** p97/VCP and R155H hexamerization was monitored over time after urea removal in the presence or absence of 1 mM ATP **(B).**

4.4.2.2. The R155H IBMPFD mutant shows perturbed adaptor protein preference in the presence of ATP

Using the competition assay between p97/VCP adaptors monitored by SPR biosensor technology (see Chapter 1, above), we tested whether the R155H IBMPFD mutant of p97/VCP exhibits competition differences as compared to the wild-type p97/VCP. In the absence of ATP, no difference was observed in the ability of UN to compete p47 for binding to either wild-type p97/VCP or the R155H mutant (Figure 4.3 A). On the other hand, in the presence of 2 mM ATP, UN at both 0.5 µM or 5 µM appeared to compete R155H away from p47 more efficiently than with wild-type p97/VCP (Figure 4.3 B). This is not surprising given the reported higher affinity of ATP to the D1 site in the R155H mutant as compared to wild-type p97/VCP. (Tang *et al.,* 2010b). Our experiments suggest that cellular ATP levels can further contribute to the

imbalanced adaptor protein preference by perturbing the proportions of R155H-UN and R155-p47 complexes.

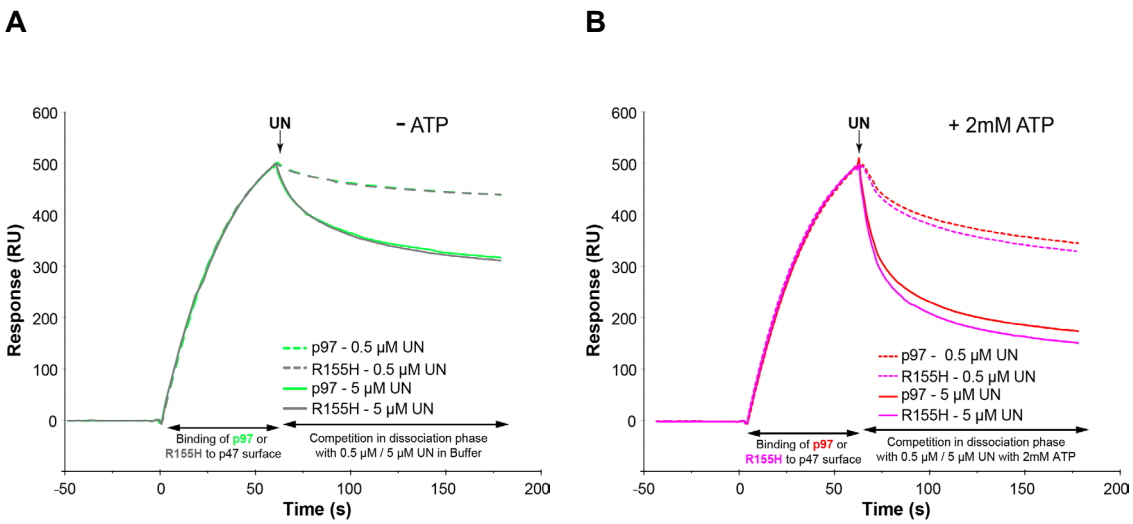

Figure 4.3 - ATP reveals minor differences in the competition between Ufd1/Npl4 and p47 for either R155H IBMPFD mutant or wild-type p97/VCP . Approximately 500 response units of p97/VCP or R155H were captured by immobilized p47, to be competed off with 0.5 μM or 5 μM UN in a dissociation phase conducted in the absence **(A)** or presence **(B)** of 2 mM ATP.

4.4.3. p97/VCP in Huntington's disease

Apart from IBMPFD, p97/VCP is also involved in other neurodegenerative diseases such as Huntington's, Alzheimer's and Parkinson's diseases. This involvement is observed by the presence of p97/VCP in protein aggregates or inclusions characteristic of these diseases. Huntington's disease is caused by expansion of poly-glutamine repeats within endogenously expressed huntingtin protein (Htt) (Walker, 2007). Htt is coded by the IT15 gene located on chromosome 4, whose exact functions in biological processes remain unclear. Nevertheless, Htt has been shown to be essential to life, as embryo lethality was observed in Htt knockout mice (Nasir *et al.,* 1995). Htt has been shown to be a transcriptional regulator of BDNF, a neurotrophin important for

the proliferation and survival of neurons both in the central and peripheral nervous systems (Zuccato *et al.,* 2001).

At a genetic level, the regular Htt protein contains only six glutamine residues or less, with increasing number of glutamine repeats positively correlated with disease onset, typically with a threshold of 36 repeats. Patients with adult onset Huntington's disease suffer from neurodegeneration caused by gradual death of specific neuron subpopulations in the brain, such as the striatal neurons, affecting motor function and cognitive abilities (Slow *et al.,* 2003). This is due to the cytotoxicity of mutant htt protein that forms insoluble aggregates in both the nucleus and cytoplasm of cells. Although the actual cause of cytotoxicity is not obvious, aggregates may affect cellular functions leading to cell death by causing aggregation, sequestration or misfolding of other vital proteins or dysregulation of transcription processes (Paulson *et al.,* 2000).

p97/VCP is implicated in Huntington's disease in several ways, possibly functioning as a chaperone. p97/VCP co-localizes with mutant htt protein (Hirabayashi *et al.,* 2001) and over-expression of p97/VCP homologues has been shown to partially solubilize and decrease the toxicity of mutant htt aggregates in a *C. elegans* model (Yamanaka *et al.,* 2004). Htt protein has also been postulated to be a modulator of ERAD via its binding to the CUE domains of gp78, a membrane-bound ERAD-related ubiquitin E3 ligase. This Htt association blocks the binding of p97/VCP to gp78 and thus downregulating the cytoplasmic events of ERAD, i.e. binding of p97/VCP to the ER membrane is necessary for the retro-translocation of misfolded proteins from the ER (Yang *et al.,* 2010). Furthermore, the cytoplasmic

aggregates of mutant htt appear to sequester p97/VCP irreversibly, depleting p97/VCP from the cellular pool.

4.5. p97/VCP therapeutics

4.5.1. p97/VCP inhibitors

There are currently four known p97/VCP inhibitors (Table 4.2; (Chou and Deshaies, 2011a; Chou *et al.,* 2011; Wang *et al.,* 2008). All four inhibitors have been shown to posess anti-cancer properties *in vitro*. The use of these inhibitors can possibly be extended to the treatment of diseases caused by p97/VCP over-activity, with the need for more research to validate the therapeutic potentials of these drugs.

Inhibitors of p97/VCP	
Compound name	**Activity**
Eeyarestatin I	Possesses anticancer properties by preferential association with VCP/p97 (without altering its ATPase activity) and inhibits deubiquitinating enzymes that associate with VCP/p97
2-Anilino-4-aryl-1,3-thiazole	Potent small molecule VCP/p97 inhibitor that targets VCP/p97 ATPase activity and VCP/p97-associated protein degradation
Syk inhibitor III	Irreversible VCP/p97 ATPase inhibitor that has high affinity to Cys522 residue located in the D2 domain
N2,N4-dibenzylquinazoline-2,4-diamine (DBeQ)	Potent reversible ERAD and autophagy inhibitor that selectively competes with ATP in the ATPase domains of VCP/p97; Shown anti-proliferative properties in human cancer cells

Table 4.2 –Known inhibitors of p97/VCP. There are currently four known inhibitors of p97/VCP with many others in development. Eeyarestatin I may be non specific to p97/VCP, being highly reactive and may inhibit Sec61 as well. **(**Chou and Deshaies, 2011a; Chou *et al.,* 2011; Wang *et al.,* 2008)

4.5.2. Where are the p97/VCP enhancers?

Currently there are no activating drugs that are specifically designed to improve or enhance p97/VCP function. In Huntington's disease, over-expression of the proteasome activating protein PA28γ increased the survival of striatal neuronal cells expressing the mutant htt when exposed to toxic challenges (Seo *et al.,* 2007). In principle, enhancing p97/VCP's activities can also prove to be therapeutic, i.e. improved chaperone function. This is one potential research niches that has not been explored. Strategies to enhance p97/VCP's function may include increasing its expression in cells and tissues or to enhance its activity, possibly by providing more energy in the form of ATP as p97/VCP depends on ATP for executing its functions.

4.6. Understanding p97/VCP population demographics

As p97/VCP is an extremely abundant protein that is constantly involved in many different processes, and because some adaptor proteins are mutually exclusive while others are not, elucidating the p97/VCP interactome is a timely challenge. It has not been yet done and is probably demanding due to technological limitations at this point of time, but there is an immense value in determining the proportion of p97/VCP activities dedicated to different cellular pathways. As a first approach, this can be done by determining the various types of adaptor proteins that complex with p97/VCP. With an established interactome, one can analyse different tissue types, vary conditions such as metabolic fluxes, and work with mutant p97/VCP to have a clearer understanding of how the interactions of p97/VCP contribute to diseases.

This task can be possibly achieved with the use of proximity ligation assays. In this method, two proximity probes, i.e. antibodies, are tagged with DNA oligonucleotides. When in close proximity, the DNAs on both antibodies are allowed to bind to each other, providing a readout using polymerase chain reaction (Weibrecht *et al.,* 2010). Potential probes are anti-p97 antibodies and respective adaptor protein antibodies in cellular or tissue samples, and the method allows for the quantitation of interactions. Using different antibodies for different adaptor proteins, one can determine the proportion of p97/VCP bound to each different adaptor protein and thus extrapolate to the proportion of p97/VCP engaged in the respective cellular activities.

Based on the imbalanced adaptor protein recruitments by p97/VCP IBMPFD mutants, or the blockade of p97/VCP's interaction with gp78 by mutant htt, it appears that these diseases cannot be cured by targetting p97/VCP's enzymatic activities. Perhaps the optimal approach for p97/VCP therapy lies not solely in the enhancing or inhibiting p97's enzymatic activities, but instead, to rebalance p97/VCP-adaptor protein interactions. This can be achieved by preventing some adaptor protein interactions an/or improving another, re-directing p97/VCP-related processes. If the p97/VCP interactome is constructed, novel strategies can then be developed to re-balance p97/VCP adaptor proteins dynamics.

4.6.1. p97/VCP levels in mammalian tissue and cultured cell lines

As reported in the literature, p97/VCP is often described as a protein so abundant that it constitutes 1 % of the total protein quantity in cells (Woodman, 2003). In order to validate this, we used recombinant p97/VCP of known

quantities to generate a standard curve by immuno-blotting the recombinant protein onto the exact same PVDF membrane with the total cell lysate samples from various mouse tissues and cell lines. Blotting at least five concentrations of recombinant p97/VCP allowed us to generate a standard curve with >0.95 regressions to be used for approximating p97/VCP quantities in unknown samples (Figure 4.4). Mouse Anti-p97/VCP antibody (Santa Cruz) was used to probe for p97/VCP, and visualization on x-ray film was accomplished by using horse-radish peroxidase-conjugated goat anti-mouse secondary antibody and chemiluminiscence substrates. Densitometry was carried out with the use of a Biorad GS800 densitometer, and the analysis was done in the Biorad Quantity One software.

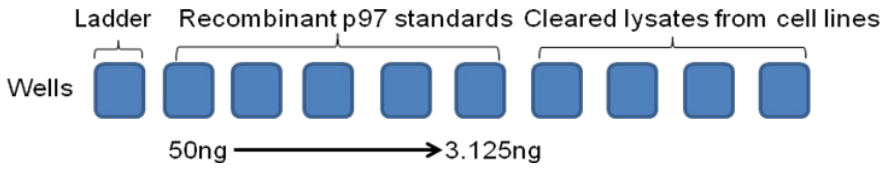

Figure 4.4 - Typical sample loading in a 10-well SDS-PAGE for quantifying p97/VCP by immuno-blotting. Recombinant p97/VCP at known amounts is loaded into the same gel where clarified cell lysates are loaded in replicates. By blotting the standards with the samples onto the same membrane, one can utilize densitometry to quantify and determine p97/VCP quantities.

As shown in Figure 4.5, all cell lines tested, ranging from 293T human embryonic kidney cells, to C2C12 myoblasts, breast cancer cell line MCF7 and SY5Y neuroblastoma cells, consistently expressed p97/VCP at a high level. The levels of p97/VCP seen ranged from 0.42 % to 0.92 % of total protein, which is higher than the usual percent of total protein seen in the corresponding mouse tissues we tested (Figure 4.5 D). It should be determined if these high levels of p97/VCP in cell line are integral for the

proliferative properties and survival of these cells in culture, while in tissues, where many cells have been differentiated and no longer mitotic, p97/VCP can be down regulated.

Our experiments for determining p97/VCP levels in various mouse tissues revealed the highest levels of p97/VCP in testis at 0.594 %, followed by the pancreas, small intestine and thymus at 0.424 %, 0.367 % and 0.349 %, respectively. Interestingly, there is little evidence on these tissues as being involved or degenerated in p97/VCP-related diseases i.e. IBMPFD, etc. Hence, one wonders about the possibility of any correlation between tissue susceptibility and disease state. Comparatively, tissues such as brain and muscle that degenerate in disease states, have only moderate amounts of p97/VCP. Similarly, p97/VCP's essential functions in cellular proliferation could be a reason for the high levels of p97/VCP seen in testis, where active cell divisions in spermatogenesis take place.

A

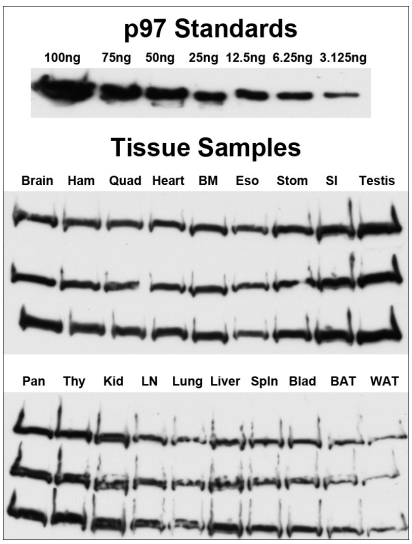

B

Tissue types	p97 bands intensities (OD)	p97 quantity (ng)	% p97
Brain	3577.02 ± 370.83	69.11	**0.346**
Hamstring	2504.30 ± 273.93	41.03	**0.205**
Quadriceps	1770.34 ± 78.28	21.81	**0.109**
Heart	2297.83 ± 285.02	35.62	**0.178**
Bone marrow	2273.62 ± 155.51	34.99	**0.175**
Esophagus	1421.15 ± 81.01	12.67	**0.063**
Stomach	2808.15 ± 282.64	48.98	**0.245**
Small intestine*	3737.88 ± 666.92	73.32	**0.367**
Testis	5475.34 ± 119.31	118.81	**0.594**
Pancreas	4661.56 ± 314.70	84.85	**0.424**
Thymus*	3986.76 ± 859.83	69.74	**0.349**
Kidney	2516.64 ± 53.78	36.83	**0.184**
Lymph node	2076.56 ± 192.60	26.98	**0.135**
Lung*	1065.36 ± 157.18	4.35	**0.022**
Liver*	2664.73 ± 611.07	40.15	**0.201**
Spleen*	1797.60 ± 265.84	20.73	**0.104**
Bladder	1624.41 ± 188.29	16.86	**0.084**
Brown adipose	1150.78 ± 233.26	6.26	**0.031**
White adipose	650.72 ± 214.04	null	null

C

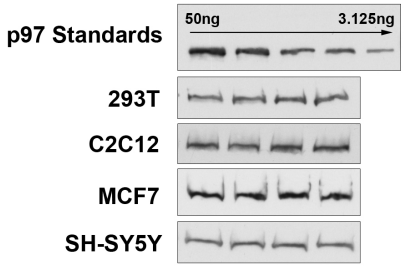

Cell lines	Percentage of cellular p97 (%)
293T	**0.924**
C2C12	**0.682**
MCF7	**0.436**
SH-SY5Y	**0.422**

D

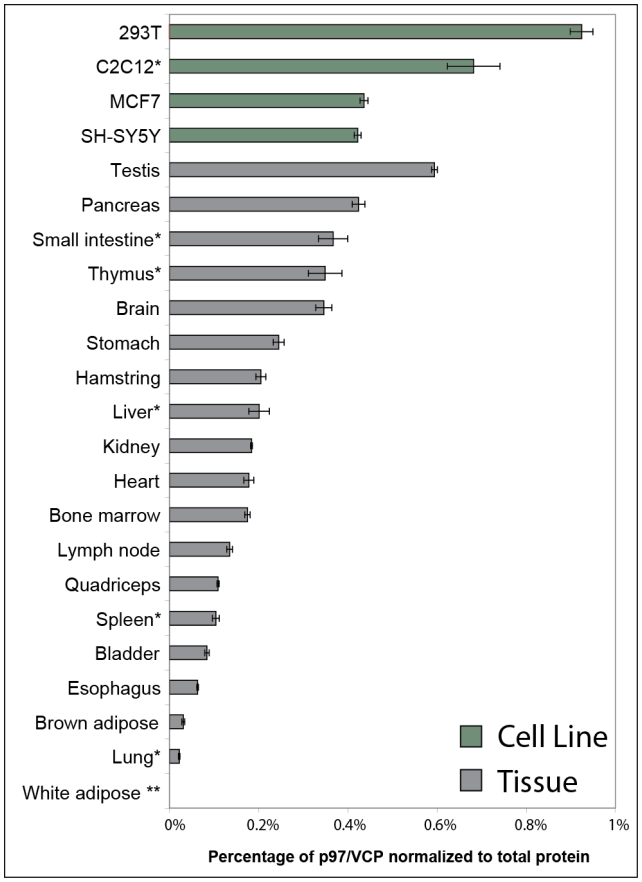

Figure 4.5 - Quantification of p97/VCP levels in cell lines and tissues – Immuno-blots of p97/VCP from various mouse tissues were performed in triplicates and compared to the standard amounts of the recombinant p97/VCP **(A)**. Densitometry was used to determine p97/VCP quantities in the various mouse tissues **(B)**. Tissues marked with * had > 10 % standard deviation Quantification of p97/VCP in white adipose tissue was not carried out as it was not within the regression range of our p97/VCP standard curves. p97/VCP levels were also determined for 4 commonly used cell lines **(C)**. A plot of p97/VCP levels within various cell lines and mouse tissues **(D)**.

4.7 Conclusion

Building on all of p97/VCP's biochemical and biological properties, p97/VCP should be now looked upon within a broader perspective as this essential AAA-ATPase appears to become increasingly implicated in important cellular processes and in diseases. The identification and characterization of the dynamics of p97/VCP interactions in both cellular and whole animal context will permit the design of novel therapeutics to either regulate or perturb p97/VCP adaptor protein interactions as an alternative approach to treat diseases. The capability to influence the equilibrium between the various activities of p97/VCP may become the front line in combating p97/VCP-related diseases.

4.8 References to Chapter 4

Alexandru, G., Graumann, J., Smith, G.T., Kolawa, N.J., Fang, R., Deshaies, R.J., 2008. UBXD7 binds multiple ubiquitin ligases and implicates p97 in HIF1alpha turnover. Cell 134, 804-816.

Asai, T., Tomita, Y., Nakatsuka, S., Hoshida, Y., Myoui, A., Yoshikawa, H., Aozasa, K., 2002. VCP (p97) regulates NFkappaB signaling pathway, which is important for metastasis of osteosarcoma cell line. Jpn J Cancer Res 93, 296-304.

Ballar, P., Zhong, Y., Nagahama, M., Tagaya, M., Shen, Y., Fang, S., 2007. Identification of SVIP as an endogenous inhibitor of endoplasmic reticulum-associated degradation. J Biol Chem 282, 33908-33914.

Barzilai, N., Huffman, D.M., Muzumdar, R.H., Bartke, A., 2012. The critical role of metabolic pathways in aging. Diabetes 61, 1315-1322.

Cao, K., Nakajima, R., Meyer, H.H., Zheng, Y., 2003. The AAA-ATPase Cdc48/p97 regulates spindle disassembly at the end of mitosis. Cell 115, 355-367.

Chang, Y.C., Hung, W.T., Chang, H.C., Wu, C.L., Chiang, A.S., Jackson, G.R., Sang, T.K., 2011. Pathogenic VCP/TER94 alleles are dominant actives and contribute to neurodegeneration by altering cellular ATP level in a Drosophila IBMPFD model. PLoS Genet 7, e1001288.

Cheng, S.H., Gregory, R.J., Marshall, J., Paul, S., Souza, D.W., White, G.A., O'Riordan, C.R., Smith, A.E., 1990. Defective intracellular transport and processing of CFTR is the molecular basis of most cystic fibrosis. Cell 63, 827-834.

Ching, J.K., Elizabeth, S.V., Ju, J.-S., Lusk, C., Pittman, S.K., Weihl, C.C., 2013. mTOR dysfunction contributes to vacuolar pathology and weakness in valosin-containing protein associated inclusion body myopathy. Human Molecular Genetics.

Chou, T.F., Deshaies, R.J., 2011a. Quantitative cell-based protein degradation assays to identify and classify drugs that target the ubiquitin-proteasome system. J Biol Chem 286, 16546-16554.

Chou, T.F., Deshaies, R.J., 2011b. Development of p97 AAA ATPase inhibitors. Autophagy 7, 1091-1092.

Chou, T.F., Brown, S.J., Minond, D., Nordin, B.E., Li, K., Jones, A.C., Chase, P., Porubsky, P.R.,
Stoltz, B.M., Schoenen, F.J., Patricelli, M.P., Hodder, P., Rosen, H., Deshaies, R.J., 2011. Reversible inhibitor of p97, DBeQ, impairs both ubiquitin-

dependent and autophagic protein clearance pathways. Proc Natl Acad Sci U S A 108, 4834-4839.

Dai, R.M., Chen, E., Longo, D.L., Gorbea, C.M., Li, C.C., 1998. Involvement of valosin-containing protein, an ATPase Co-purified with IkappaBalpha and 26 S proteasome, in ubiquitin-proteasome-mediated degradation of IkappaBalpha. J Biol Chem 273, 3562-3573.

Dobrynin, G., Popp, O., Romer, T., Bremer, S., Schmitz, M.H., Gerlich, D.W., Meyer, H., 2011. Cdc48/p97-Ufd1-Npl4 antagonizes Aurora B during chromosome segregation in HeLa cells. J Cell Sci 124, 1571-1580.

Escarcega, R.O., Fuentes-Alexandro, S., Garcia-Carrasco, M., Gatica, A., Zamora, A., 2007. The transcription factor nuclear factor-kappa B and cancer. Clin Oncol (R Coll Radiol) 19, 154-161.

Fanganiello, R.D., Kimonis, V.E., Corte, C.C., Nitrini, R., Passos-Bueno, M.R., 2011. A Brazilian family with hereditary inclusion body myopathy associated with Paget disease of bone and frontotemporal dementia. Braz J Med Biol Res 44, 374-380.

Farinha, C.M., Amaral, M.D., 2005. Most F508del-CFTR is targeted to degradation at an early folding checkpoint and independently of calnexin. Mol Cell Biol 25, 5242-5252.

Fernandez-Saiz, V., Buchberger, A., 2010. Imbalances in p97 co-factor interactions in human proteinopathy. EMBO Rep 11, 479-485.

Gidaro, T., Modoni, A., Sabatelli, M., Tasca, G., Broccolini, A., Mirabella, M., 2008. An Italian family with inclusion-body myopathy and frontotemporal dementia due to mutation in the VCP gene. Muscle Nerve 37, 111-114.

Halawani, D., LeBlanc, A.C., Rouiller, I., Michnick, S.W., Servant, M.J., Latterich, M., 2009. Hereditary inclusion body myopathy-linked p97/VCP mutations in the NH2 domain and the D1 ring modulate p97/VCP ATPase activity and D2 ring conformation. Mol Cell Biol 29, 4484-4494.

Hannan, F., Ho, I., Tong, J.J., Zhu, Y., Nurnberg, P., Zhong, Y., 2006. Effect of neurofibromatosis type I mutations on a novel pathway for adenylyl cyclase activation requiring neurofibromin and Ras. Hum Mol Genet 15, 1087-1098.

Heresi, G.A., Stoller, J.K., 2008. Augmentation therapy in alpha-1 antitrypsin deficiency. Expert Opin Biol Ther 8, 515-526.

Hirabayashi, M., Inoue, K., Tanaka, K., Nakadate, K., Ohsawa, Y., Kamei, Y., Popiel, A.H., Sinohara, A., Iwamatsu, A., Kimura, Y., Uchiyama, Y., Hori, S., Kakizuka, A., 2001. VCP/p97 in abnormal protein aggregates, cytoplasmic vacuoles, and cell death, phenotypes relevant to neurodegeneration. Cell Death Differ 8, 977-984.

Ishimoto, S., Goto, I., Ohta, M., Kuroiwa, Y., 1983. A quantitative study of the muscle satellite cells in various neuromuscular disorders. J Neurol Sci 62, 303-314.

Ju, J.S., Fuentealba, R.A., Miller, S.E., Jackson, E., Piwnica-Worms, D., Baloh, R.H., Weihl, C.C., 2009. Valosin-containing protein (VCP) is required for autophagy and is disrupted in VCP disease. J Cell Biol 187, 875-888.

Kimonis, V., Donkervoort, S., Watts, G., 1993. Inclusion Body Myopathy with Paget Disease of Bone and/or Frontotemporal Dementia. In: Pagon, R.A., Bird, T.D., Dolan, C.R., Stephens, K., Adam, M.P. (Eds.), GeneReviews, Seattle (WA).

Kohn, R.R., 1965. Denervation Muscle Atrophy: An Autolytic System in Vitro. Am J Pathol 47, 315-323.

Linsdell, P., 2001. Thiocyanate as a probe of the cystic fibrosis transmembrane conductance regulator chloride channel pore. Can J Physiol Pharmacol 79, 573-579.

Liu, Y., Hei, Y., Shu, Q., Dong, J., Gao, Y., Fu, H., Zheng, X., Yang, G., 2012. VCP/p97, down-regulated by microRNA-129-5p, could regulate the progression of hepatocellular carcinoma. PLoS One 7, e35800.

Luciani, A., Villella, V.R., Esposito, S., Brunetti-Pierri, N., Medina, D.L., Settembre, C., Gavina,
M., Raia, V., Ballabio, A., Maiuri, L., 2011. Cystic fibrosis: a disorder with defective autophagy. Autophagy 7, 104-106.

McKay, R., 1997. Stem cells in the central nervous system. Science 276, 66-71.

Meerang, M., Ritz, D., Paliwal, S., Garajova, Z., Bosshard, M., Mailand, N., Janscak, P., Hubscher, U., Meyer, H., Ramadan, K., 2011. The ubiquitin-selective segregase VCP/p97 orchestrates the response to DNA double-strand breaks. Nat Cell Biol 13, 1376-1382.

Meyer, H., Drozdowska, A., Dobrynin, G., 2010. A role for Cdc48/p97 and Aurora B in controlling chromatin condensation during exit from mitosis. Biochem Cell Biol 88, 23-28.

Morgan, J.E., Zammit, P.S., 2010. Direct effects of the pathogenic mutation on satellite cell function in muscular dystrophy. Exp Cell Res 316, 3100-3108.

Nalbandian, A., Ghimbovschi, S., Radom-Aizik, S., Dec, E., Vesa, J., Martin, B., Knoblach, S., Smith, C., Hoffman, E., Kimonis, V.E., 2012. Global gene profiling of VCP-associated inclusion body myopathy. Clin Transl Sci 5, 226-234.

Nasir, J., Floresco, S.B., O'Kusky, J.R., Diewert, V.M., Richman, J.M., Zeisler, J., Borowski, A., Marth, J.D., Phillips, A.G., Hayden, M.R., 1995. Targeted disruption of the Huntington's disease gene results in embryonic lethality and behavioral and morphological changes in heterozygotes. Cell 81, 811-823.

Niwa, H., Ewens, C.A., Tsang, C., Yeung, H.O., Zhang, X., Freemont, P.S., 2012. The role of the N-domain in the ATPase activity of the mammalian AAA ATPase p97/VCP. J Biol Chem 287, 8561-8570.

Paulson, H.L., Bonini, N.M., Roth, K.A., 2000. Polyglutamine disease and neuronal cell death. Proc Natl Acad Sci U S A 97, 12957-12958.

Phan, V.T., Ding, V.W., Li, F., Chalkley, R.J., Burlingame, A., McCormick, F., 2010. The RasGAP proteins Ira2 and neurofibromin are negatively regulated by Gpb1 in yeast and ETEA in humans. Mol Cell Biol 30, 2264-2279.

Qu-Petersen, Z., Deasy, B., Jankowski, R., Ikezawa, M., Cummins, J., Pruchnic, R., Mytinger, J., Cao, B., Gates, C., Wernig, A., Huard, J., 2002. Identification of a novel population of muscle stem cells in mice: potential for muscle regeneration. J Cell Biol 157, 851-864.

Rowan, S.L., Rygiel, K., Purves-Smith, F.M., Solbak, N.M., Turnbull, D.M., Hepple, R.T., 2012. Denervation causes fiber atrophy and myosin heavy chain co-expression in senescent skeletal muscle. PLoS One 7, e29082.

Sacco, A., Mourkioti, F., Tran, R., Choi, J., Llewellyn, M., Kraft, P., Shkreli, M., Delp, S., Pomerantz, J.H., Artandi, S.E., Blau, H.M., 2010. Short telomeres and stem cell exhaustion model Duchenne muscular dystrophy in mdx/mTR mice. Cell 143, 1059-1071.

Seo, H., Sonntag, K.C., Kim, W., Cattaneo, E., Isacson, O., 2007. Proteasome activator enhances survival of Huntington's disease neuronal model cells. PLoS One 2, e238.

Slow, E.J., van Raamsdonk, J., Rogers, D., Coleman, S.H., Graham, R.K., Deng, Y., Oh, R., Bissada, N., Hossain, S.M., Yang, Y.Z., Li, X.J., Simpson, E.M., Gutekunst, C.A., Leavitt, B.R.,
Hayden, M.R., 2003. Selective striatal neuronal loss in a YAC128 mouse model of Huntington disease. Hum Mol Genet 12, 1555-1567.

Stoller, J.K., Aboussouan, L.S., 2005. Alpha1-antitrypsin deficiency. Lancet 365, 2225-2236.

Tang, W.K., Li, D., Li, C.C., Esser, L., Dai, R., Guo, L., Xia, D., 2010a. A novel ATP-dependent conformation in p97 N-D1 fragment revealed by crystal structures of disease-related mutants. Embo J 29, 2217-2229.

Tang, W.K., Li, D., Li, C.C., Esser, L., Dai, R., Guo, L., Xia, D., 2010b. A novel ATP-dependent conformation in p97 N-D1 fragment revealed by crystal structures of disease-related mutants. EMBO J 29, 2217-2229.

Tresse, E., Salomons, F.A., Vesa, J., Bott, L.C., Kimonis, V., Yao, T.P., Dantuma, N.P., Taylor, J.P., 2010. VCP/p97 is essential for maturation of ubiquitin-containing autophagosomes and this function is impaired by mutations that cause IBMPFD. Autophagy 6, 217-227.

Trovo-Marqui, A.B., Tajara, E.H., 2006. Neurofibromin: a general outlook. Clin Genet 70, 1-13.

Tsujimoto, Y., Tomita, Y., Hoshida, Y., Kono, T., Oka, T., Yamamoto, S., Nonomura, N., Okuyama, A., Aozasa, K., 2004. Elevated expression of valosin-containing protein (p97) is associated with poor prognosis of prostate cancer. Clin Cancer Res 10, 3007-3012.

Valle, C.W., Min, T., Bodas, M., Mazur, S., Begum, S., Tang, D., Vij, N., 2011. Critical role of VCP/p97 in the pathogenesis and progression of non-small cell lung carcinoma. PLoS One 6, e29073.

Vembar, S.S., Brodsky, J.L., 2008. One step at a time: endoplasmic reticulum-associated degradation. Nat Rev Mol Cell Biol 9, 944-957.

Viassolo, V., Previtali, S.C., Schiatti, E., Magnani, G., Minetti, C., Zara, F., Grasso, M., Dagna-Bricarelli, F., Di Maria, E., 2008. Inclusion body myopathy, Paget's disease of the bone and frontotemporal dementia: recurrence of the VCP R155H mutation in an Italian family and implications for genetic counselling. Clin Genet 74, 54-60.

Vij, N., Fang, S., Zeitlin, P.L., 2006. Selective inhibition of endoplasmic reticulum-associated degradation rescues DeltaF508-cystic fibrosis transmembrane regulator and suppresses interleukin-8 levels: therapeutic implications. J Biol Chem 281, 17369-17378.

Walker, F.O., 2007. Huntington's disease. Lancet 369, 218-228.

Wang, Q., Song, C., Li, C.C., 2003. Hexamerization of p97-VCP is promoted by ATP binding to the D1 domain and required for ATPase and biological activities. Biochem Biophys Res Commun 300, 253-260.

Wang, Q., Li, L., Ye, Y., 2008. Inhibition of p97-dependent protein degradation by Eeyarestatin I. J Biol Chem 283, 7445-7454.

Ward, C.L., Omura, S., Kopito, R.R., 1995. Degradation of CFTR by the ubiquitin-proteasome pathway. Cell 83, 121-127.

Watts, G.D., Wymer, J., Kovach, M.J., Mehta, S.G., Mumm, S., Darvish, D., Pestronk, A., Whyte, M.P., Kimonis, V.E., 2004. Inclusion body myopathy associated with Paget disease of bone and frontotemporal dementia is caused by mutant valosin-containing protein. Nat Genet 36, 377-381.

Weibrecht, I., Leuchowius, K.J., Clausson, C.M., Conze, T., Jarvius, M., Howell, W.M., Kamali-Moghaddam, M., Soderberg, O., 2010. Proximity ligation

assays: a recent addition to the proteomics toolbox. Expert Rev Proteomics 7, 401-409.

Weihl, C.C., Dalal, S., Pestronk, A., Hanson, P.I., 2006. Inclusion body myopathy-associated mutations in p97/VCP impair endoplasmic reticulum-associated degradation. Hum Mol Genet 15, 189-199.

Woodman, P.G., 2003. p97, a protein coping with multiple identities. J Cell Sci 116, 4283-4290.

Yamamoto, S., Tomita, Y., Uruno, T., Hoshida, Y., Qiu, Y., Iizuka, N., Nakamichi, I., Miyauchi, A., Aozasa, K., 2005. Increased expression of valosin-containing protein (p97) is correlated with disease recurrence in follicular thyroid cancer. Ann Surg Oncol 12, 925-934.

Yamamoto, S., Tomita, Y., Nakamori, S., Hoshida, Y., Nagano, H., Dono, K., Umeshita, K., Sakon, M., Monden, M., Aozasa, K., 2003. Elevated expression of valosin-containing protein (p97) in hepatocellular carcinoma is correlated with increased incidence of tumor recurrence. J Clin Oncol 21, 447-452.

Yamamoto, S., Tomita, Y., Hoshida, Y., Nagano, H., Dono, K., Umeshita, K., Sakon, M., Ishikawa, O., Ohigashi, H., Nakamori, S., Monden, M., Aozasa, K., 2004. Increased expression of valosin-containing protein (p97) is associated with lymph node metastasis and prognosis of pancreatic ductal adenocarcinoma. Ann Surg Oncol 11, 165-172.

Yamanaka, K., Okubo, Y., Suzaki, T., Ogura, T., 2004. Analysis of the two p97/VCP/Cdc48p proteins of Caenorhabditis elegans and their suppression of polyglutamine-induced protein aggregation. J Struct Biol 146, 242-250.

Yang, H., Liu, C., Zhong, Y., Luo, S., Monteiro, M.J., Fang, S., 2010. Huntingtin interacts with the cue domain of gp78 and inhibits gp78 binding to ubiquitin and p97/VCP. PLoS One 5, e8905.

Zuccato, C., Ciammola, A., Rigamonti, D., Leavitt, B.R., Goffredo, D., Conti, L., MacDonald, M.E., Friedlander, R.M., Silani, V., Hayden, M.R., Timmusk, T., Sipione, S., Cattaneo, E., 2001. Loss of huntingtin-mediated BDNF gene transcription in Huntington's disease. Science 293, 493-498.

5. List of Author's Publications

Data and results of Chapter 1 is published in :

Chia, W.S., Chia, D.X., Rao, F., Bar Nun, S., Geifman Shochat, S., 2012. ATP Binding to p97/VCP D1 Domain Regulates Selective Recruitment of Adaptors to Its Proximal N-Domain. PLoS One 7, e50490.

Part of data and results of Chapter 2 is currently in manuscript with collaborator Dr Ariel Stanhill, Technion, Israel.

Data and results of Chapter 3 is published in :

Yildiz, U.H., Chia, W.S., Mailepessov, Chia, D.X., Geifman Shochat S., Liedberg, B., 2012. Real-time determination of the activity of ATPase by use of a water-soluble polythiophene. Anal Bioanal Chem 404, 2369-2375.

SPRINGER LICENSE
TERMS AND CONDITIONS

Nov 27, 2012

This is a License Agreement between Chia Weisheng ("You") and Springer ("Springer") provided by Copyright Clearance Center ("CCC"). The license consists of your order details, the terms and conditions provided by Springer, and the payment terms and conditions.

All payments must be made in full to CCC. For payment instructions, please see information listed at the bottom of this form.

License Number	3036881097832
License date	Nov 27, 2012
Licensed content publisher	Springer
Licensed content publication	Analytical and Bioanalytical Chemistry
Licensed content title	Real-time determination of the activity of ATPase by use of a water-soluble polythiophene
Licensed content author	Umit Hakan Yildiz
Licensed content date	Jan 1, 2012
Volume number	404
Issue number	8
Type of Use	Thesis/Dissertation
Portion	Figures
Author of this Springer article	Yes and you are a contributor of the new work
Order reference number	
Title of your thesis / dissertation	Protein-protein Interactions that mediate the role of p97/VCP in Endoplasmic Reticulum Associated Degradation
Expected completion date	Jan 2013
Estimated size(pages)	100
Total	0.00 USD
Terms and Conditions	

Introduction

The publisher for this copyrighted material is Springer Science + Business Media. By clicking "accept" in connection with completing this licensing transaction, you agree that the following terms and conditions apply to this transaction (along with the Billing and Payment terms and conditions established by Copyright Clearance Center, Inc. ("CCC"), at the time that you opened your Rightslink account and that are available at any time at http://myaccount.copyright.com).

Limited License

With reference to your request to reprint in your thesis material on which Springer Science and Business Media control the copyright, permission is granted, free of charge, for the use indicated in your enquiry.

Licenses are for one-time use only with a maximum distribution equal to the number that you identified in the licensing process.

This License includes use in an electronic form, provided its password protected or on the university's intranet or repository, including UMI (according to the definition at the Sherpa website: http://www.sherpa.ac.uk/romeo/). For any other electronic use, please contact Springer at (permissions.dordrecht@springer.com or permissions.heidelberg@springer.com).

The material can only be used for the purpose of defending your thesis, and with a maximum of 100 extra copies in paper.

Although Springer holds copyright to the material and is entitled to negotiate on rights, this license is only valid, provided permission is also obtained from the (co) author (address is given with the article/chapter) and provided it concerns original material which does not carry references to other sources (if material in question appears with credit to another source, authorization from that source is required as well).

Permission free of charge on this occasion does not prejudice any rights we might have to charge for reproduction of our copyrighted material in the future.

Altering/Modifying Material: Not Permitted
You may not alter or modify the material in any manner. Abbreviations, additions, deletions and/or any other alterations shall be made only with prior written authorization of the author(s) and/or Springer Science + Business Media. (Please contact Springer at (permissions.dordrecht@springer.com or permissions.heidelberg@springer.com)

Reservation of Rights
Springer Science + Business Media reserves all rights not specifically granted in the combination of (i) the license details provided by you and accepted in the course of this licensing transaction, (ii) these terms and conditions and (iii) CCC's Billing and Payment terms and conditions.

Copyright Notice:Disclaimer
You must include the following copyright and permission notice in connection with any reproduction of the licensed material: "Springer and the original publisher /journal title, volume, year of publication, page, chapter/article title, name(s) of author(s), figure number(s), original copyright notice) is given to the publication in which the material was originally published, by adding; with kind permission from Springer Science and Business Media"

Warranties: None

Example 1: Springer Science + Business Media makes no representations or warranties with respect to the licensed material.

Example 2: Springer Science + Business Media makes no representations or warranties with respect to the licensed material and adopts on its own behalf the limitations and disclaimers established by CCC on its behalf in its Billing and Payment terms and conditions for this licensing transaction.

Indemnity

You hereby indemnify and agree to hold harmless Springer Science + Business Media and CCC, and their respective officers, directors, employees and agents, from and against any and all claims arising out of your use of the licensed material other than as specifically authorized pursuant to this license.

No Transfer of License
This license is personal to you and may not be sublicensed, assigned, or transferred by you to any other person without Springer Science + Business Media's written permission.

No Amendment Except in Writing
This license may not be amended except in a writing signed by both parties (or, in the case of Springer Science + Business Media, by CCC on Springer Science + Business Media's behalf).

Objection to Contrary Terms
Springer Science + Business Media hereby objects to any terms contained in any purchase order, acknowledgment, check endorsement or other writing prepared by you, which terms are inconsistent with these terms and conditions or CCC's Billing and Payment terms and conditions. These terms and conditions, together with CCC's Billing and Payment terms and conditions (which are incorporated herein), comprise the entire agreement between you and Springer Science + Business Media (and CCC) concerning this licensing transaction. In the event of any conflict between your obligations established by these terms and conditions and those established by CCC's Billing and Payment terms and conditions, these terms and conditions shall control.

Jurisdiction
All disputes that may arise in connection with this present License, or the breach thereof, shall be settled exclusively by arbitration, to be held in The Netherlands, in accordance with Dutch law, and to be conducted under the Rules of the 'Netherlands Arbitrage Instituut' (Netherlands Institute of Arbitration).***OR:***

All disputes that may arise in connection with this present License, or the breach thereof, shall be settled exclusively by arbitration, to be held in the Federal Republic of Germany, in accordance with German law.

Other terms and conditions:

v1.3

If you would like to pay for this license now, please remit this license along with your payment made payable to "COPYRIGHT CLEARANCE CENTER" otherwise you will be invoiced within 48 hours of the license date. Payment should be in the form of a check or money order referencing your account number and this invoice number RLNK500905047.
Once you receive your invoice for this order, you may pay your invoice by credit card. Please follow instructions provided at that time.

Make Payment To:
Copyright Clearance Center
Dept 001
P.O. Box 843006
Boston, MA 02284-3006

For suggestions or comments regarding this order, contact RightsLink Customer Support: customercare@copyright.com or +1-877-622-5543 (toll free in the US) or

+1-978-646-2777.

Gratis licenses (referencing $0 in the Total field) are free. Please retain this printable license for your reference. No payment is required.